177
4-22-81
JWO

(2)

D.2545

R-3724

ORNL-5756

MASTER

ornl

OAK
RIDGE
NATIONAL
LABORATORY

UNION
CARBIDE

Final Analysis of the GCFR Radial Blanket and Shield Integral Experiment

D. T. Ingersoll
L. R. Williams

OPERATED BY
UNION CARBIDE CORPORATION
FOR THE UNITED STATES
DEPARTMENT OF ENERGY

ORNL-5756
Distribution Category UC-77
Gas-Cooled Reactor Technology

Contract No. W-7405-eng-26

ENGINEERING PHYSICS DIVISION

Gas-Cooled Fast Reactor Program
FTP/A 01351

FINAL ANALYSIS OF THE GCFR RADIAL BLANKET AND SHIELD INTEGRAL EXPERIMENT

D. T. Ingersoll
L. R. Williams

Date Published - April 1981

This Work Sponsored by
U.S. Department of Energy
Office of Advanced Nuclear Systems
and Projects

OAK RIDGE NATIONAL LABORATORY
Oak Ridge, Tennessee 37830
operated by
UNION CARBIDE CORPORATION
for the
U.S. DEPARTMENT OF ENERGY

TABLE OF CONTENTS

ABSTRACT

An integral experiment has been performed for verification of radiation transport methods and nuclear data used in the design of the radial shield for the proposed gas-cooled fast breeder reactor demonstration plant. The experiment was conducted at the ORNL Tower Shielding Facility and consisted of integral and spectral measurements of the neutron and gamma-ray flux transmitted through slabs of materials which modeled a GCFR-type radial blanket and radial shield. Both UO_2 and ThO_2 blankets were investigated as well as several shield designs comprising stainless steel, graphite, and boronated graphite.

The analysis was performed using existing discrete-ordinates methods and cross section data which are currently used for fast reactor shield design. Neutron transmission through the blankets was predicted within 20-30% while gamma-ray heating between the blanket rows was predicted within 10%. ENDF/B-V thorium data appeared better than ENDF/B-IV for predicting neutron transmission and gamma-ray heating. Neutron attenuation in the shield assemblies was generally predicted within 15% which corresponds to the estimated experimental and analytical uncertainties. Several other conclusions regarding the performance of laminated shields were obtained.

ACKNOWLEDGEMENTS

The authors wish to thank C. O. Slater and R. L. Childs for their assistance with the analysis, D. E. Bartine for his guidance and management of the project, and F. J. Muckenthaler for his thoughtful ideas and cooperation in supplying data. The authors also wish to especially thank R. G. Perkins, formally of General Atomic Company, for his numerous ideas and contributions toward the design of the Radial Blanket and Shield Experiment.

1. INTRODUCTION

Designing a reactor shield is a complex effort involving intimate relationships between radiation transport, thermal-mechanical forces, material properties, and economics. The shield designer is challenged with designing an adequate shield which satisfies licensing requirements, but which also minimizes costly design conservatisms. Several analytic tools have been developed which aid the shield designer in achieving the optimum compromise of these considerations. However, verification of these design methods and the relevant nuclear data is essential, especially for advanced reactors since little operating experience is available. Integral experiments provide the means for this verification by (1) providing measured data against which analytic predictions based on specific methods and nuclear data can be judged, and (2) providing a direct measurement of the effectiveness of the final shield design.

An integral experiment was designed and executed for the verification of radiation transport methods and nuclear data used for the design of the radial shield for the proposed 300 MW(e) gas-cooled fast breeder reactor (GCFR).[1] The experiment was part of a five-year integral testing program[2] which was designed to systematically

identify and resolve significant questions regarding the adequacy of the GCFR shield design. Whereas most of the experiments dealt with problems resulting from neutron streaming in the myriad of open coolant channels and shield heterogeneities, the Radial Blanket and Shield Experiment addressed potential difficulties in calculating deep penetration of neutrons and gamma rays through the thick laminated radial shield. Also, the experiment addressed uncertainties associated with the radial blanket since the particular design of the blanket affects the source term incident on the radial shield and hence affects the overall attenuation characteristics of the shield.

The need for such an experiment was provided by the GCFR shield designer, General Atomic Company (GAC), in a document[3] which described the reactor shield concept, the design criteria, the types of data desired from the experiment, and specific test requirements. In accordance with those goals and requirements, the experiment was designed and preanalyzed[4] at ORNL with the active cooperation of GAC.

The experiment was conducted in 1979 at the ORNL Tower Shielding Facility (TSF) and consisted of integral and spectral measurements of the neutron and gamma-ray flux transmitted through slabs of materials which modeled a GCFR-type radial blanket and radial shield. Both

uranium-oxide and thorium-oxide blankets were investigated as well as several shield designs comprising stainless steel, graphite, and boronated graphite. The measurements,[5] combined with the subsequent analysis described herein, provide significant information regarding the adequacy of the important nuclear data and provide valuable insight into the performance characteristics of not only the reference shield design but also alternate design concepts.

The demise of the GCFR program in the United States places an apparent handicap on the usefulness of results and conclusions gained from the Radial Blanket and Shield Experiment. This handicap is primarily manifested in the fact that the experiment was not a parametric study of blanket and shield materials, but was instead directed toward determining the characteristics of specific shield designs employed in the GCFR. Nevertheless, much of the data has value independent of the GCFR. Specifically, comparisons of the UO_2 and ThO_2 blanket mockups and the resulting conclusions regarding the adequacy of thorium nuclear data are of generic interest. Also, the thorough investigation of laminated shields containing graphite, boronated graphite, and steel has considerable potential value for LMFBR concepts which permit such materials in the shield design. Finally, the difficulties encountered in obtaining certain types of data in even this geometrically simple experiment provide significant guidance for future experiments desiring these types of data.

2. GCFR SHIELD DESIGN REQUIREMENTS

2.1 Shield Design and Exposure Limits

At the time that the Radial Blanket and Shield Experiment was designed and executed, the GCFR demonstration plant design incorporated a downward coolant flow through the grid-plate-suspended fuel and blanket assemblies. The core and blankets were surrounded radially by two rows of axially-segmented removable shields followed by a permanent outer radial shield. The complete shield design was designated "Conceptual Shielding Configuration I" (CSC-I)[6] and is pictured in Fig. 1. The composition and dimensions of the shield design at the axial level of the core midplane are given in Table 1. As shown in Table 1, the removable inner shield consisted of a row of steel-clad boronated graphite and a row of solid stainless steel. The laminated outer shield contained a large graphite layer surrounded by a thin boronated graphite layer and an outer layer of stainless steel.

Irradiation exposure limits, which largely determined the shield design, were based on an inadequate irradiation effects data base and with minimal guidance on how to apply existing data into structural design criteria.[2] As a consequence, criteria were generally based on exposure limits which were considered highly conservative. The

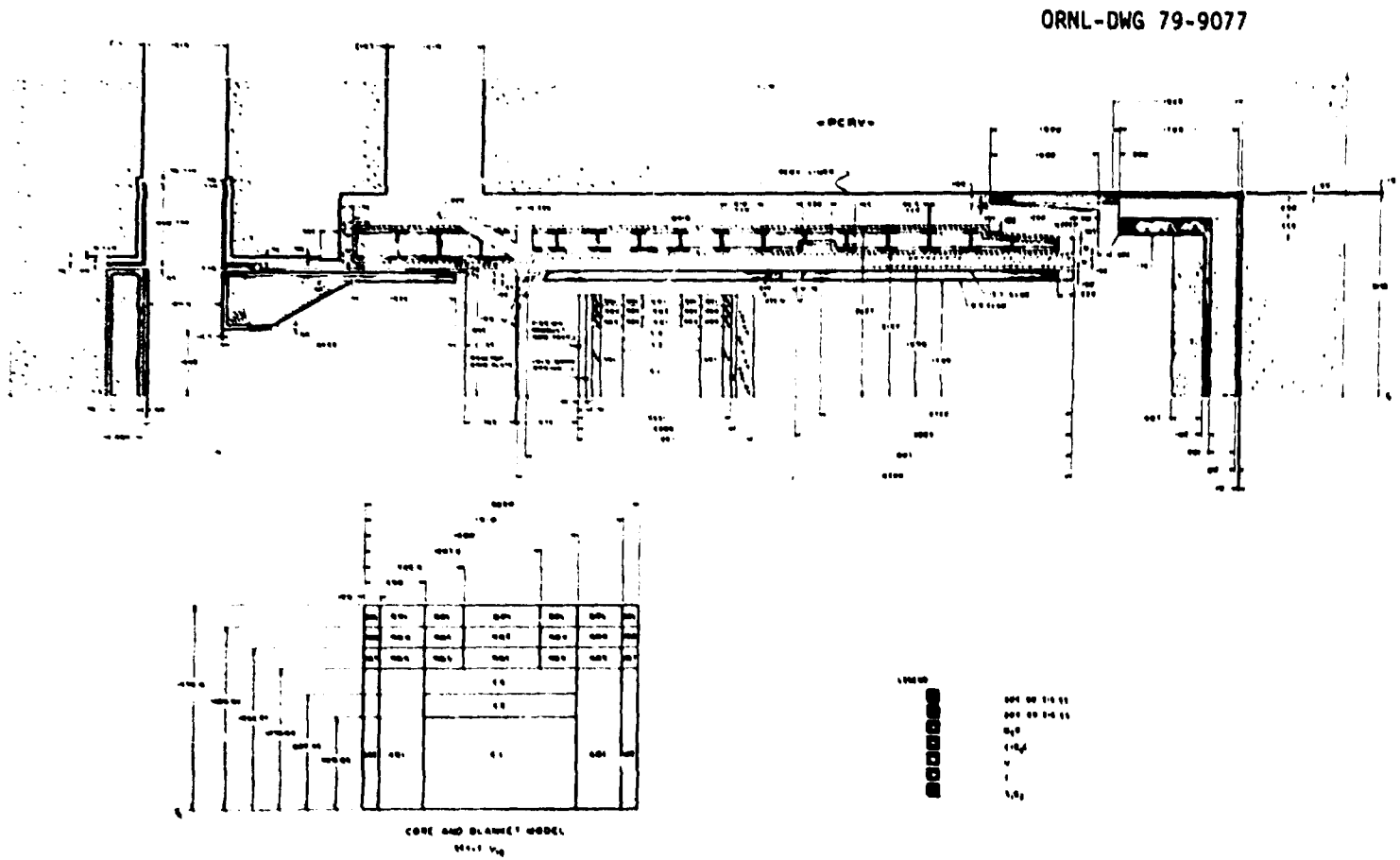

Fig. 1. Schematic of reference downflow GCFR shield design designated as "Conceptual Shielding Configuration 1."

Table 1. Geometry and Materials for Conceptual Shielding Configuration I at the Core Midplane Level

Region and Material		Inner Radius (cm)	Outer Radius (cm)	Thickness (cm)
Core:	Enrichment Zone 1	0.0	77.9	77.9
	Enrichment Zone 2	77.9	96.9	19.0
	Enrichment Zone 3	96.9	115.6	18.7
Radial Blanket:	Row 1	115.6	134.1	18.5
	Row 2	134.1	152.6	18.5
	Row 3	152.6	171.0	18.4
Helium Gap		171.0	194.0	23.0
Inner Shield 1:	SS-316	194.0	195.0	1.0
	C + B_4C*	195.0	207.7	12.7
	SS-316	207.7	209.0	1.3
Helium Gap		209.0	214.1	5.1
Inner Shield 2:	SS-316	214.1	229.1	15.0
Helium Gap		229.1	234.2	5.1
Outer Shield:	SS-316	234.2	239.3	5.1
	C + B_4C*	239.3	244.4	5.1
	Graphite	244.4	267.0	22.6
	C + B_4C*	267.0	272.1	5.1
	SS-316	272.1	277.2	5.1
Helium Gap		277.2	312.9	35.7
PCRV Liner:	Fe	312.9	314.7	1.8
PCRV		314.7		

*25 weight-% boron mixture of graphite and B_4C at 1.6 g/ml bulk density.

radial shields in the CSC-I design were cooled by outlet helium, and hence were subject to criteria for components which might exceed 550°C temperatures. These criteria were that the total lifetime fluence could not exceed 10^{21} cm^{-2} and the helium concentration in steel could not exceed 1 appm (atomic part per million). In addition, the total lifetime fluence at any point in the prestressed concrete reactor vessel (PCRV) or the PCRV liner could not exceed 10^{19} cm^{-2}.

Design calculations performed at ORNL and at GAC showed that the radial shields in CSC-I were adequate for satisfying the design criteria if the inner-most row of shield were replaced every three years and the second row of shield every six years. Besides the obvious cost of frequently replacing the large bulk of shield material, an enormously long reactor down time would be required to perform the shield replacement. Therefore, considerable economic motivation existed to verify the design calculations and to define relevant uncertainties which might subsequently help to reduce the design conservatisms.

2.2 Design Uncertainties

The most obvious uncertainty in the radial shield design was the design itself. Although the CSC-I design and corresponding reactor core and blanket configuration were specified in considerable detail, assessment studies were in

progress at the time of the experiment to determine the desirability of using ThO_2 rather than UO_2 blankets, and the implications of directing the helium coolant upward through the core rather than downward. Additionally, a lateral core restraint system was being considered which would require some radial shielding to be suspended from (or rested upon) the core support grid plate.

Other than design, the largest source of uncertainties was felt to be the nuclear data used in the design calculations. Extreme attenuations through iron, sodium, and stainless steel have been investigated in previous TSF experiments; however, the GCFR shields employed substantial amounts of graphite and boronated graphite laminated with stainless steel yielding overall attenuations on the order of 10^5. Uncertainties in the blanket data, especially for thorium were also of concern since the blanket determines the source term for the radial shield.

Therefore, the objectives of the Radial Blanket and Shield Experiment were to (a) verify the accuracy of nuclear data used in design calculations for the GCFR radial shield, (b) define experimental and analytic uncertainties in terms of their implications to design calculations and design criteria, and (c) provide experimental comparisons of the relative effectiveness of alternate shield concepts. All of the objectives were satisfied by the measurements and subsequent analysis.

3. EXPERIMENTAL CONFIGURATIONS AND MEASUREMENTS

The GCFR Radial Blanket and Shield Experiment was performed in 1979 at the ORNL Tower Shielding Facility (TSF). A complete description of the experiment and the measurements is given in ORNL/TM-7237;[5] however, a brief description will be given here for completeness. The detailed experiment program plan is given in App. A which specifies each configuration and measurement. This information is summarized in Table 2.

Typical configurations are shown schematically in Figs. 2-5. All configurations consisted of 1.5-m by 1.5-m slabs placed contiguously along the beam centerline of the TSF reactor source. The mockups were preceded by a spectrum modifier which was designed to produce a source spectrum typical of a fast reactor core. The slabs were all surrounded by a concrete shield which was required to reduce background radiation at the detector locations. A layer of lithiated paraffin between the slabs and the concrete minimized the contribution of neutrons which were reflected from the concrete back into the test assemblies. Figure 2 shows a three-row ThO_2 blanket mockup, while Fig. 3 shows the addition of the reference inner shield mockup (corresponds to CSC-1). Figure 4 shows a UO_2 blanket plus an alternate inner shield mockup. Finally, Fig. 5 shows the largest configuration investigated - a ThO_2 blanket plus the

Table 2. Summary of Configurations and Measurements for GCFR Radial Blanket and Shield Experiment

Configuration	Description[a]	Measurements[b]
I.A	Spectrum modifier only	BB,S
I.B	1/2 ThO_2 blanket row	BB
I.C	1 ThO_2 blanket row	BB
I.D	2 ThO_2 blanket rows	BB,S,TLD
I.E	3 ThO_2 blanket rows	BB,S,TLD
I.F	Conf. I.E + Fe reflector	TLD
II.A	3 UO_2 blanket rows	BB,S,TLD
II.B	Conf. II.A + reference inner shield	BB,S
III.A	Conf. I.E + boronated graphite	BB,S
III.B	Conf. III.A + stainless steel	BB,S
IV.A	Conf. III.B + 1/3 reference outer shield	BB
IV.B	Conf. III.B + 2/3 reference outer shield	BB
IV.C	Conf. III.B + reference outer shield	BB,S
IV.D	Conf. IV.C + Fe + concrete	BB,TLD
IV.E	Reference inner and outer shields	BB,S
V.A	Conf. II.A (repeat)	BB
V.B	Conf. V.A + graphite	BB,S
V.C	Conf. V.B + boronated graphite + steel	BB,S,TLD
V.D	Conf. V.C + steel	BB,TLD
V.E	Conf. V.A + boronated graphite + steel	BB,TLD
VI.A	Lead only	S
VI.B	Lead + spectrum modifier	S
VI.C	UO_2 only	S
VI.D	UO_2 + spectrum modifier	BB,S

[a] Reference shields refer to "Conceptual Shielding Configuration I."

[b] BB = Bonner ball; S = spectrometers; TLD = thermoluminescent dosimeter.

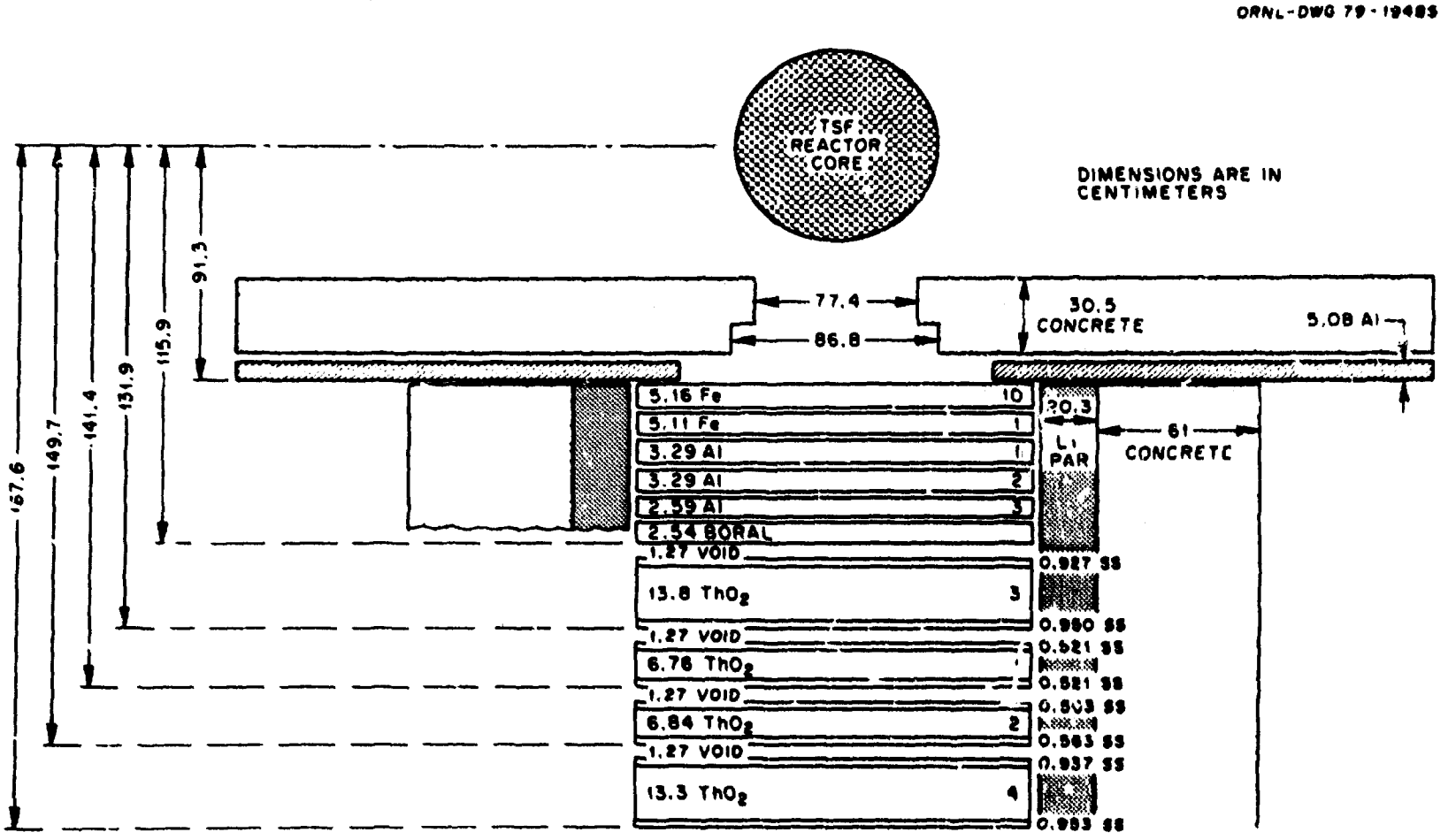

Fig. 2. Mockup of spectrum modifier and full thickness ThO_2 radial blanket slabs surrounded by lithiated paraffin and concrete (*Item I-K*).

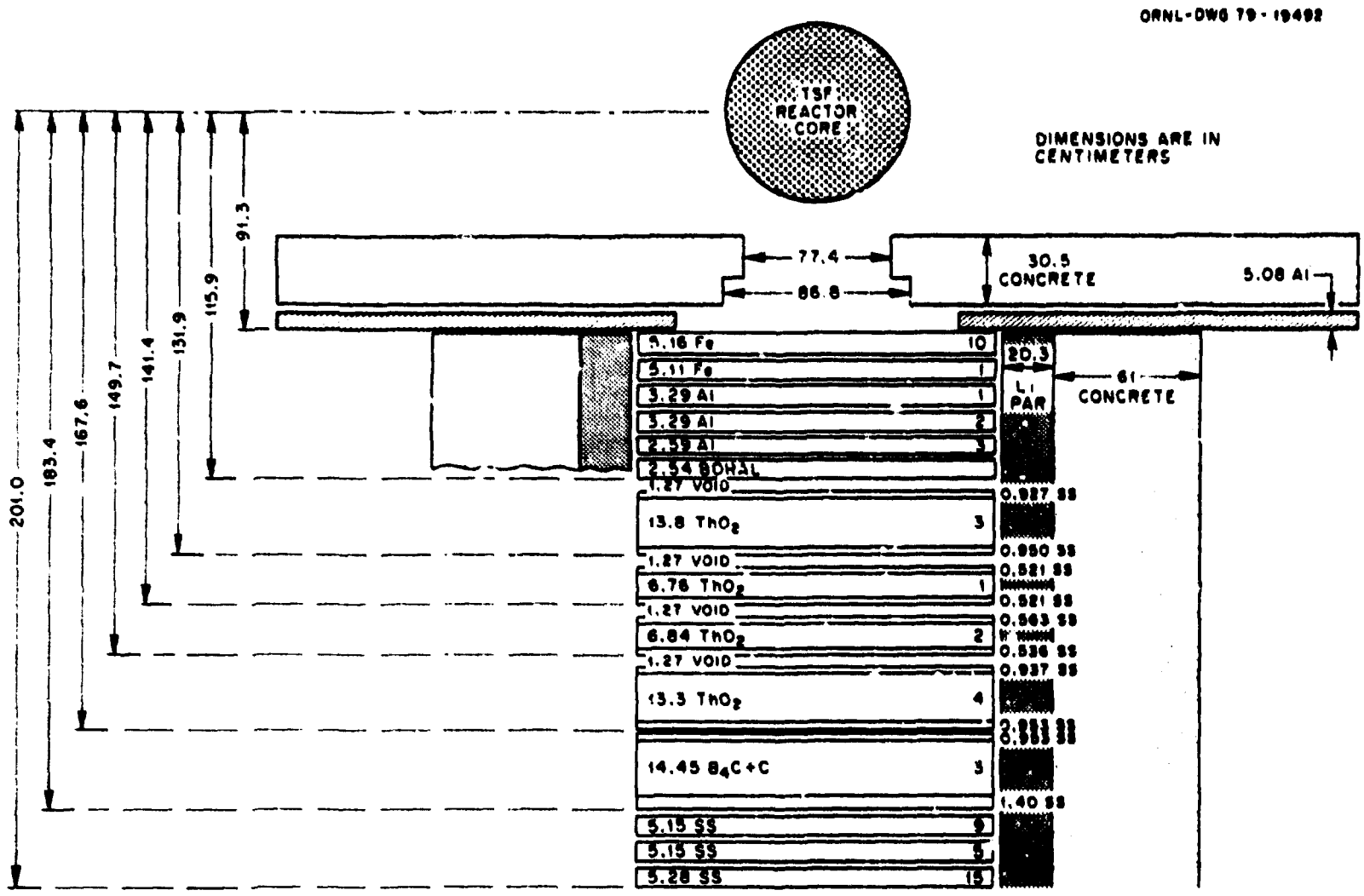

Fig. 3. Mockup of spectrum modifier, ThO_2 radial blanket, and reference inner radial shield surrounded by lithiated-paraffin and concrete (*Items III-A, III-B*).

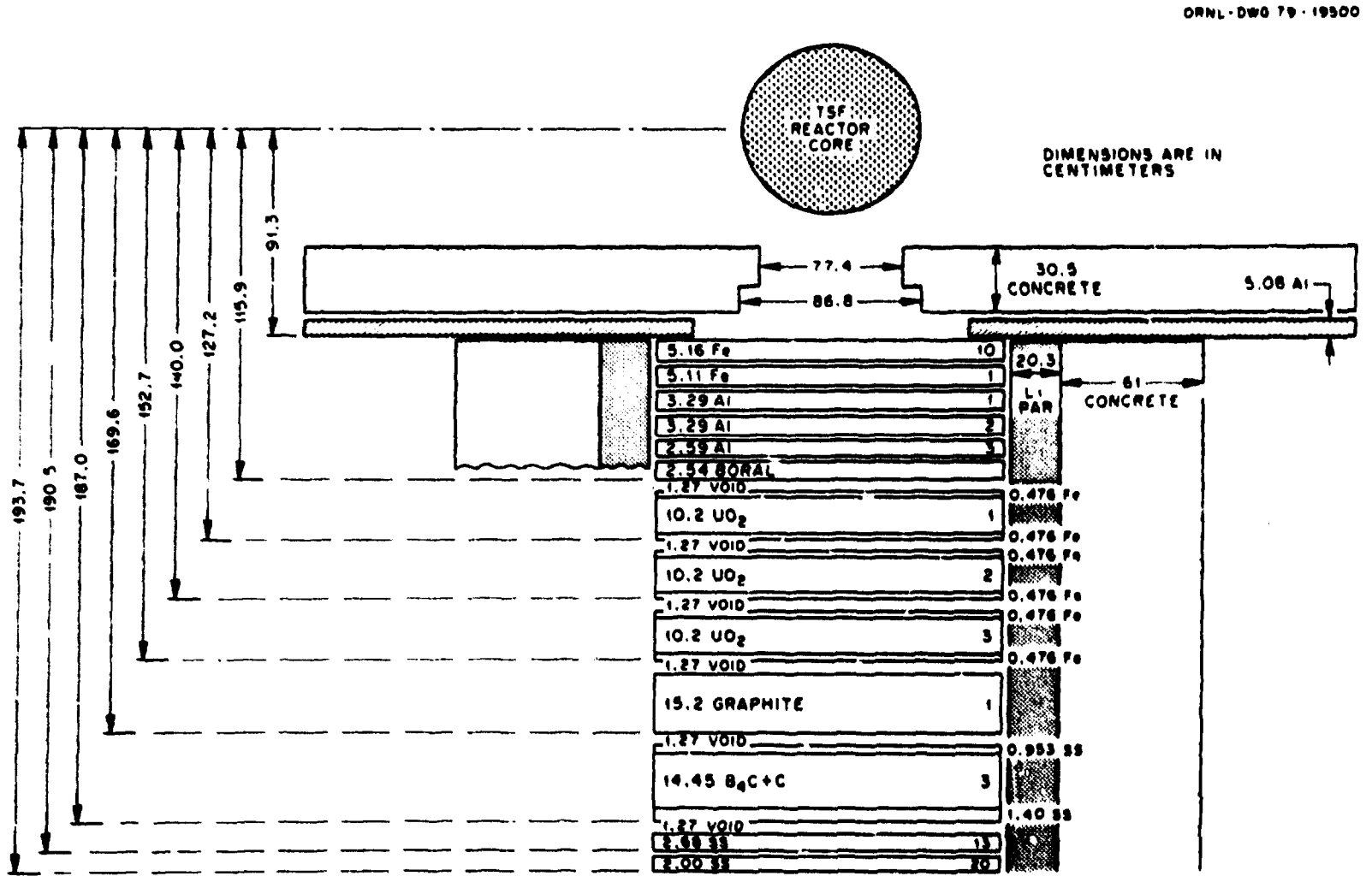

Fig. 4. Mockup of spectrum modifier, UO_2 radial blanket, and an alternate inner radial shield surrounded by lithiated-paraffin and concrete (*Items V-A, V-B, V-C*).

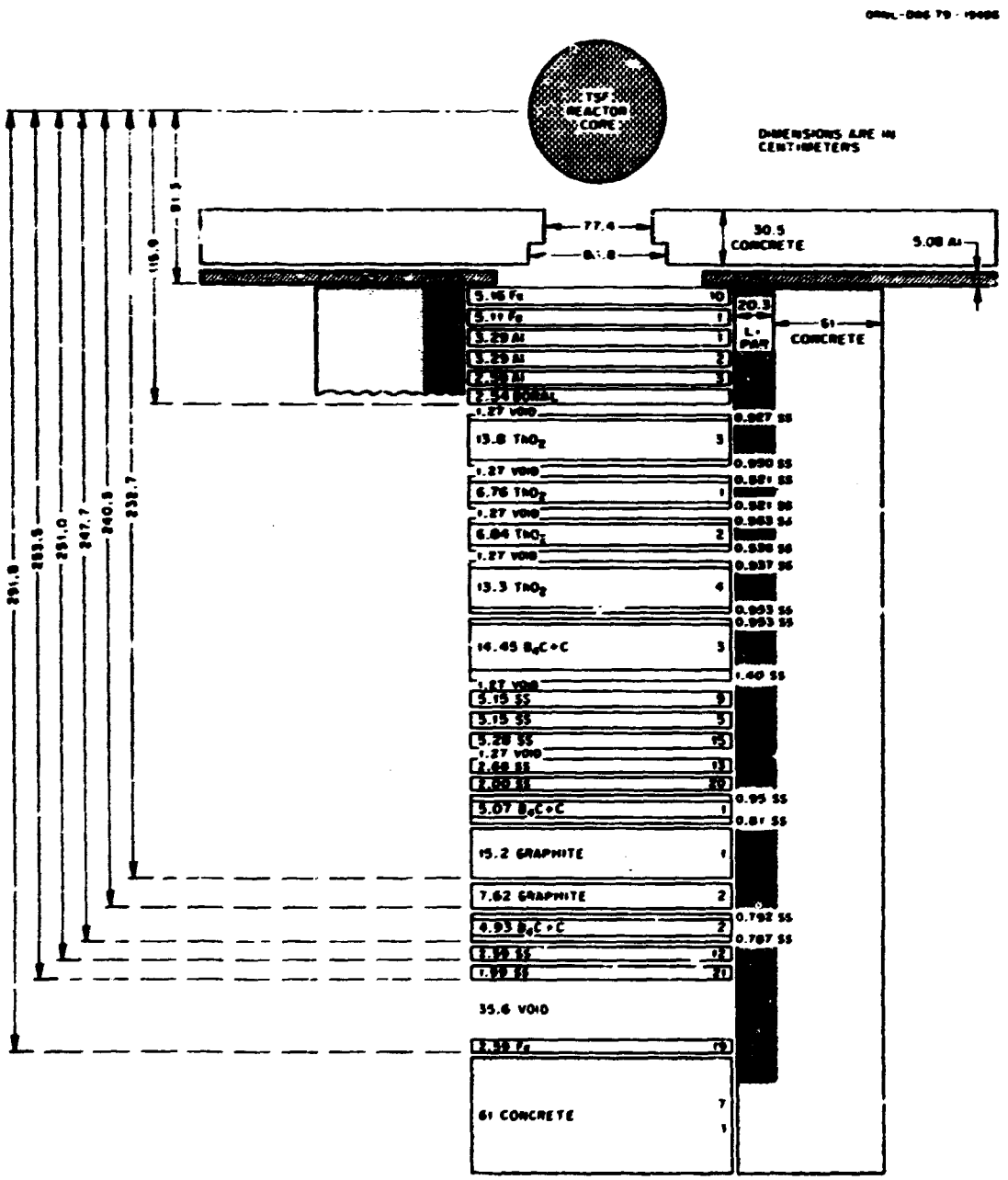

Fig. 5. Mockup of spectrum modifier, ThO_2 radial blanket, inner radial shield, full outer radial shield (*Items IV-B, IV-C*), and PCRV (*Item IV-D*) surrounded by lithiated paraffin and concrete.

reference inner and outer radial shields. A mockup of the PCRV and liner was also included in the configuration.

Both integral and spectral data for neutrons and gamma rays were measured. Integral neutron data were obtained using Bonner ball detectors with nominal outside diameters of 3, 6, and 10 inches. Neutron energy spectra were measured above 40 keV using a 5-cm cylindrical NE-213 scintillator (from 1 to 20 MeV) and 5-cm spherical hydrogen proportional counters (from 40 to 1500 keV). The NE-213 detector was also used to measure gamma-ray spectra above 1 MeV. The NE-213 data were unfolded using the FERD code[7] while the hydrogen data were unfolded using SPEC-4.[8] The Bonner ball and spectra measurements were always located on the reactor beam centerline "behind" the test configuration, i.e., on the side opposite the TSF reactor. In addition, gamma-ray heating data were obtained from thermoluminescent dosimeters (TLDs) located between the test slabs but always on the beam centerline.

4. ANALYSIS PROCEDURES

4.1 Analytic Methods and Models

Analysis of the Radial Blanket and Shield Experiment was based solely upon discrete-ordinates transport methods. Neutron and gamma-ray transport through the configurations was calculated using primarily the DOT-IV two-dimensional code[9] (version 4.3) which provided an absolute comparison with the measured data. Also, some one-dimensional calculations were performed using the ANiSN code[10] which provided an inexpensive way to investigate small variations in the computational parameters. Other codes utilized for the analysis include AMPX[11] and AXMIX[12] for preparing macroscopic cross sections, FALSTF[13] for computing the flux at detector locations outside the configurations, and several of the DOGS codes[14] for calculating detector activities and graphical output of the data. Table 3 lists all the codes used in this analysis.

The bulk of the computational effort was expended in calculating the radiation transport through two-dimensional (2D) models of the blanket and shield mockups. The calculations were run in R-Z cylindrical geometry and used an external boundary angular flux (always at the top boundary) as the fixed source. The blanket calculations included multiple source iterations to account for fissions within the blanket slabs, and the larger shield

Table 3. Computer Codes Used in Analysis of Radial Blanket and Shield Experiment

Code	Function
ACTUAL	- DOG. code to calculate activities from DOT fluxes
ANISN	- Perfo.n 1D radiation transport calculations
ASPECT	- DOGS cod. to plot 1D or 2D energy spectra
AXMIX	- Mix ANISN-formatted cross sections
BONAMI	- AMPX code to perform energy self-shielding of cross sections
CHOX	- AMPX code to couple neutron and gamma-ray libraries
DOT 4.3	- Perform 2D radiation transport calculations
EGAD	- DOGS code to plot 2D geometries
FACT	- Change spatial mesh on boundary angular source
FALSTF	- Calculate detector responses outside 2D geometries
ISOPLOT4	- DOGS code to plot 2D isoflux contours
MALOCS	- AMPX code to collapse cross sections
NITAWL	- AMPX code to reformat cross sections
ROSIE	- Interpolate 76-group scale factors to 207 groups
XSPECT	- Extended version of ASPECT to plot measured spectra

configurations were "bootstrapped" using internal boundary angular fluxes. All calculations used an S_{10} symmetric angular quadrature (70 angles). A listing of the quadrature angles and weights is given in App. B along with an edit of the input parameters for a typical DOT-IV case. A few significant parameters for all of the 2D calculations are summarized in Table 4.

As seen in Table 4, the spatial meshes for the computational models ranged from 2600 to 5800 intervals.

Table 4. Summary of DOT-IV Calculations

Case	Configuration	Mesh Size (R,Z)	Source Iterations	Total Flux Iterations	Time (min/cpu)[a]	Boundary Source Location
1[b]	I.A	59,62	1	76	45/91	TSF Collimator
2[c]	I.D	50,54	3 3	713 522	143/91 112/91	Spectrum Modifier
3[c]	I.E	50,69	3 2	741 473	186/91 118/91	Spectrum Modifier
4	II.A	59,52	3	1030	220/91	Spectrum Modifier
5	II.B	48,69	3	986	219/91	Second UO_2 Slab
6[c]	III.A	50,90	3 2	744 473	247/91 156/91	Spectrum Modifier
7	III.B	50,62	2	627	134/91	Third ThO_2 Slab
8	IV.C	50,97	1	581	174/91	Blanket/Shield Interface
9	IV.E	50,115	1	588	208/33	Spectrum Modifier
10[d]	V.B	48,65	2 1	708 202	171/91 63/91	Spectrum Modifier
11	V.C	48,66	3	999	210/91	Second UO_2 Slab

[a]Machine execution time on either an IBM 360/91 (/91) or an IBM 370/3033 (/33).

[b]Case originally run at Argonne National Laboratory; restarted at ORNL.

[c]Case restarted to correct mistake in macroscopic cross sections.

[d]Case restarted to correct premature termination.

Because of the simple design of the experiment, the configurations were modeled almost exactly; the only significant approximation was due to the cylindrical representation of the square slabs. It is felt, however, that the large lateral dimensions of the slabs permit such an approximation without significantly affecting results on the beam centerline. Axial dimensions were taken directly from Ref. 5. Two representative models are given in Figs. 6 and 7 which show the ThO_2 blanket mockup (Fig. 6) and the UO_2 blanket with an alternate inner shield mockup (Fig. 7). The boundary source at the top of the geometry in Fig. 7 had been determined from a previous calculation which spanned the region from the spectrum modifier through the 15-cm graphite section.

After performing the DOT calculation within the boundaries of the configuration, a FALSTF calculation was then performed which used the space-energy scattering source calculated by DOT to determine the neutron and gamma-ray flux at external detector locations. The last-flight flux estimation also included the space-dependent fission source, and employed a collimator option which defined a detector solid angle corresponding to the experimental arrangement. Appendix B includes an edit of the input parameters for a typical FALSTF case.

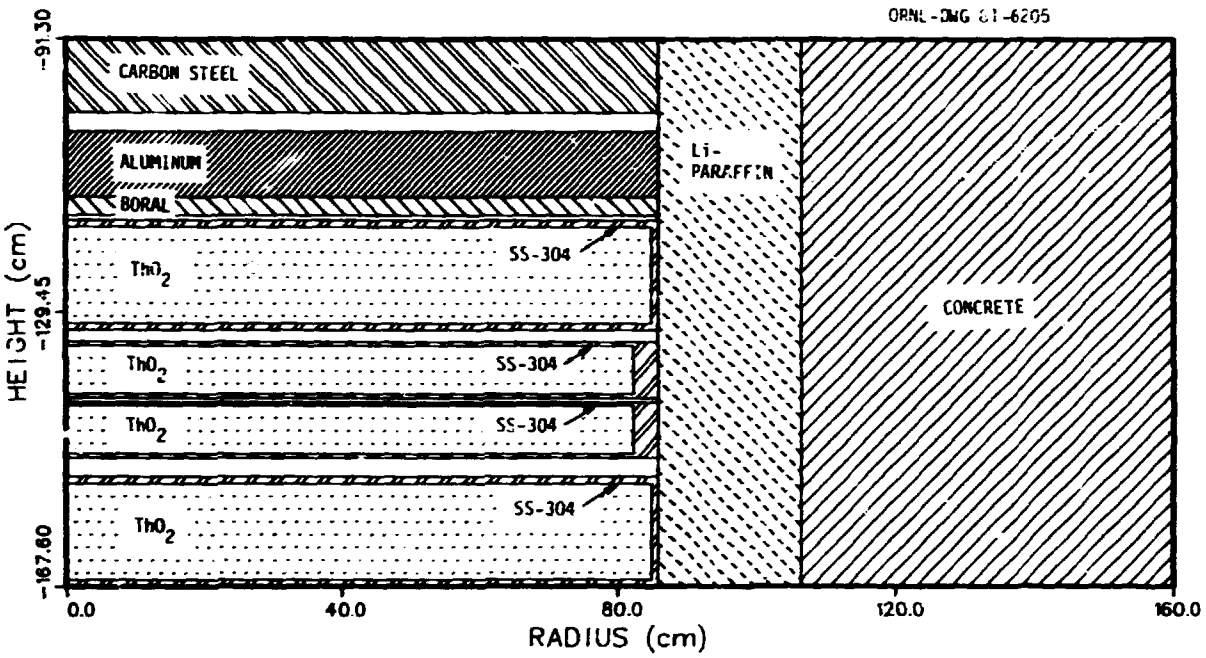

Fig. 6. Two-dimensional R-Z model for ThO_2 blanket mockup (Configuration I.E).

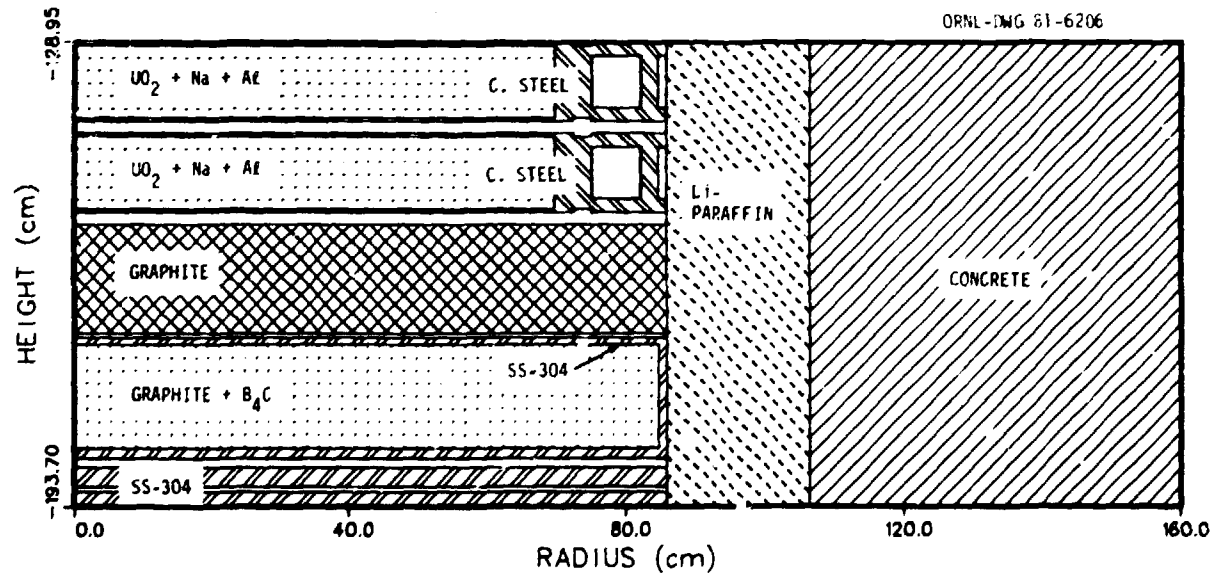

Fig. 7. Two-dimensional R-Z model for UO_2 blanket with an alternate shield mockup (Configuration V.C).

Before comparing the FALSTF fluxes to the unfolded neutron and gamma-ray energy spectra, the calculated spectra were smoothed with a Gaussian function to simulate the energy resolution inherent in the detector system. The fluxes were also folded with energy-dependent response functions for comparison with the measured Bonner ball data. Similarly, the calculated DOT fluxes were folded with energy-dependent response functions for comparison with the *in situ* TLD data. The Bonner ball and TLD response functions are given in Sec. 4.3.

The full analytic approach is diagrammed in Fig. 8. In addition to the normal DOT/FALSTF sequence, ANISN was used to perform 1D calculations for the purpose of comparing different cross-section data. The 1D slab geometries used in the ANISN calculations represented the axial dimension in the corresponding 2D calculations and used the same TSF source spectrum as a left boundary condition. Unfortunately, the economic advantage of using 1D calculations is balanced by the loss of an absolute flux normalization due to the inability of a 1D slab geometry to account for geometric attenuation of the TSF source. This limitation was circumvented through the use of 2D scaling.

The concept of scaling[15] assumes that

$$DOT(B) = DOT(A) \times \frac{ANISN(B)}{ANISN(A)} = SF(A) \times ANISN(B)$$

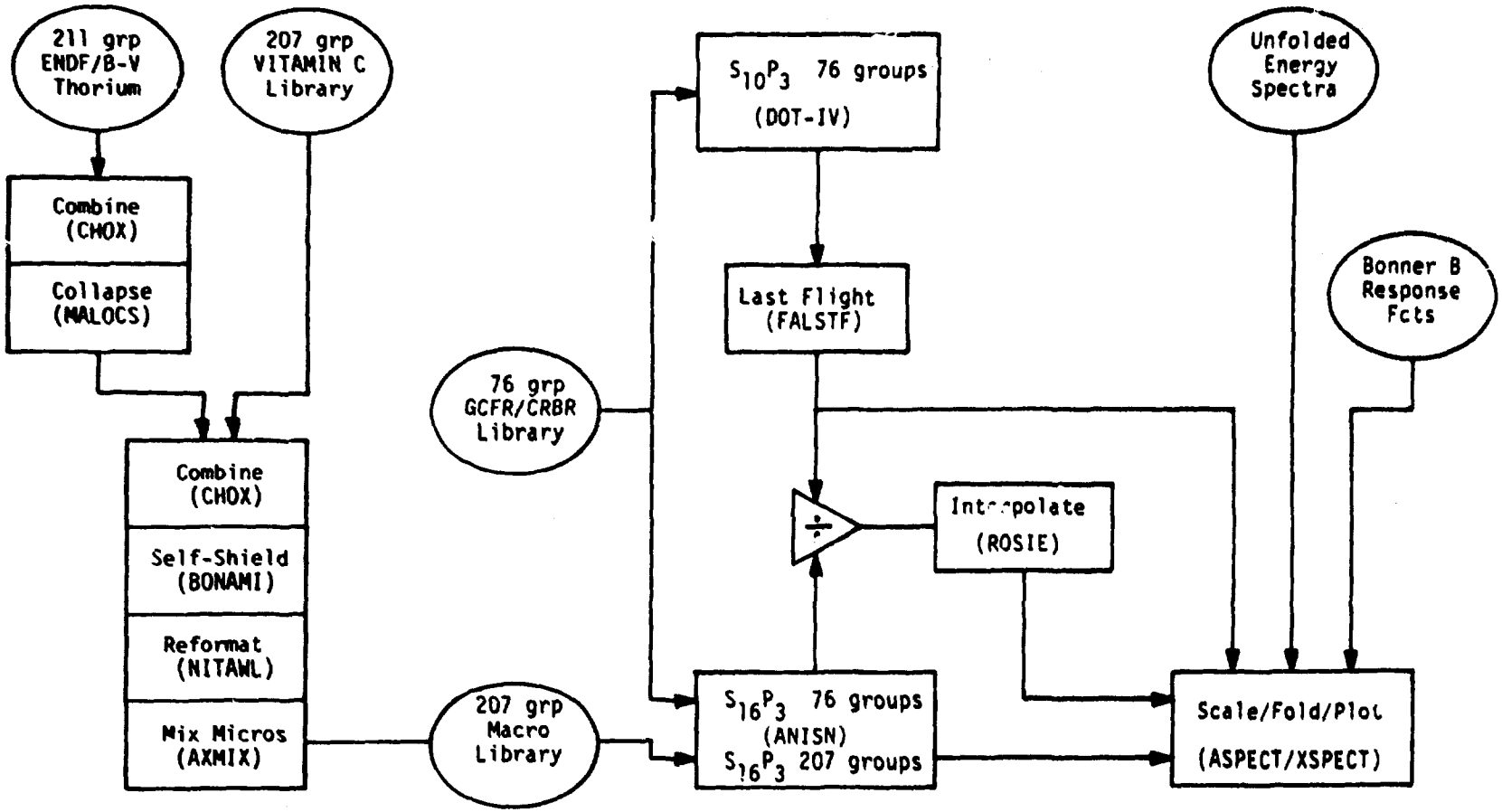

Fig. 8. Diagram of procedure used to analyze Radial Blanket and Shield Experiment.

where A and B represent variations of the computational parameters. Therefore, the 2D result for parameter set B can be approximated by a properly scaled 1D result. Specifically, ENDF/B-IV and -V data for thorium were compared at a fine-group level (207 energy groups) using scale factors that were determined from 76-group DOT and ANISN calculations. As indicated in Fig. 8, the 76-group 2D fluxes were divided by the corresponding 1D fluxes to yield 76-group scaling factors which were then interpolated to the 207-group structure. The fine-group scaling factors were then folded with the different 1D results and compared on an absolute basis with the measured data.

4.2 Cross Section Data

The 2D transport calculations were all performed using a coupled multigroup cross-section set containing 51 neutron groups and 25 gamma-ray groups. The P_3 microscopic cross-section library was derived primarily from ENDF/B-IV data, and has been used extensively at ORNL for fast reactor analyses.[16] Because ENDF/B-IV does not contain secondary gamma-ray production data for thorium, a special ^{232}Th cross section set was generated which contains gamma-ray production data that was estimated from the corresponding ^{238}U data. Macroscopic cross sections were prepared from the microscopic library using the AXMIX code and the material number densities given in Table 5. The number

Table 5. Composition of Materials (Atoms·barn^{-1}·cm^{-1})

	Concrete	[illegible]304	Aluminum	Boral	C. Steel	Li-Paraffin	Li-Hydride	Graphite	Bor'd Graph (15 cm)	Bor'd Graph (5 cm)	UO_2 Slabs	ThO_2 Slabs[a]
H-1	7.30(-3)[b]	--	--	--	--	5.930(-2)	5.610(-2)	--	--	--	--	--
Li-6	--	--	--	--	--	5.565(-4)	4.163(-3)	--	--	--	--	--
Li-7	--	--	--	--	--	6.940(-3)	5.194(-2)	--	--	--	--	--
B-10	--	--	--	5.128(-3)	--	--	--	--	4.017(-3)	4.237(-3)	--	--
B-11	--	--	--	2.077(-2)	--	--	--	--	1.627(-2)	1.716(-2)	--	--
C	1.07(-2)	--	--	6.45(-3)	9.185(-4)	3.420(-2)	--	8.675(-2)	5.151(-2)	5.021(-2)	--	--
O	4.47(-2)	--	--	--	--	1.125(-2)	--	--	--	--	2.95(-2)	3.30(-2)
Na	--	--	--	--	--	--	--	--	--	--	5.19(-3)	--
Al	--	--	6.05(-2)	3.65(-2)	--	--	--	--	--	--	7.05(-3)	--
Si	3.80(-3)	--	--	--	--	--	--	--	--	--	--	--
Ca	1.22(-2)	--	--	--	--	-	--	--	--	--	--	--
Cr	--	1.69(-2)	--	--	--	--	--	--	--	--	--	--
Mn	--	1.20(-3)	--	--	5.150(-4)	--	--	--	--	--	--	--
Fe	--	5.94(-2)	6.00(-4)	7.70(-4)	8.372(-2)	--	--	--	--	--	--	--
Ni	--	7.90(-3)	--	--	--	--	--	--	--	--	--	--
Th-232	--	--	--	--	--	--	--	--	--	--	--	1.65(-2)
U-235	--	--	--	--	--	--	--	--	--	--	1.08(-4)	--
U-383	--	--	--	--	--	--	--	--	--	--	1.469(-2)	--

[a]Composition is for an average slab density of 7.24 g/cm^3. Actual densities of 7.10, 7.33, 7.37, and 7.14 g/cm^3 were used in the calculations.

[b]Read as 7.3×10^{-3}.

densities were calculated based on information reported in Ref. 5.

In addition to the 51-25-group calculations, some 1D calculations were performed using the 171-neutron, 36-gamma-ray group Vitamin C cross-section library.[17] These cross sections were processed using the AMPX code system[11] to generate a coupled macroscopic library in the required ANISN format. Also, a separate fine-group cross-section set was prepared for thorium using data derived from ENDF/B-V. The procedure for processing the Vitamin C cross sections and the ENDF/B-V-based thorium data is outlined in the left-hand portion of Fig. 8.

4.3 ISE Source and Detector Response Functions

The neutron source for the experiment was provided by the TSF reactor and large beam collimator. The angle and energy distribution from the surface of the reactor has been previously determined,[18] and a computer code was developed to convert the spherical leakage source to a disk boundary source suitable for use with R-Z geometries.[19] It was necessary, however, to perform a 2D calculation which included the disk source and a mockup of the reactor and beam collimator in order to generate a boundary source at the surface of the spectrum modifier. The geometry for the DOT-IV calculation is shown in Fig. 9. The spectrum

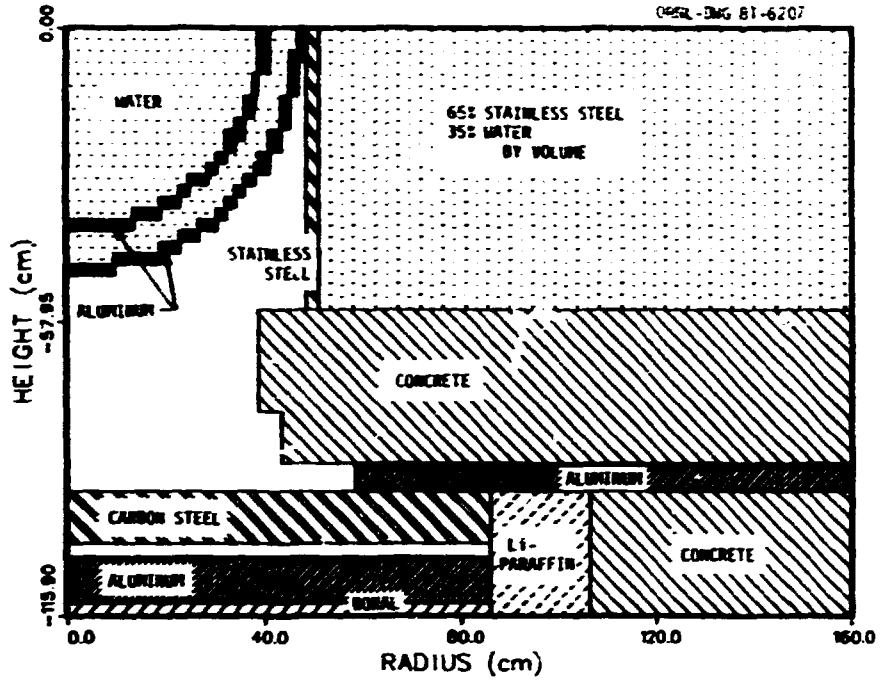

Fig. 9. Two-dimensional R-Z model of TSF reactor, beam collimator, and spectrum modifier (Configuration I.A.).

modifier and peripheral shielding were included in the calculation so that the resulting boundary source could be used as an external source for subsequent calculations.

As mentioned in Sec 4.1, the calculated neutron and gamma-ray fluxes were folded with energy-dependent response functions for comparison with measured Bonner ball and TLD data. Three Bonner balls were used: the 3" ball which measures primarily low energy neutron flux, the 6" ball which represents a total flux detector, and the 10" ball which measures primarily the fast neutron flux. The Bonner

ball response functions which were originally calculated several years ago[20] have been used extensively for TSF analyses with only minor corrections.[15] For completeness, these responses in the 51-group energy structure are listed in Table 6 and plotted in Fig. 10.

The CaF_2:Mn TLD gamma-ray heating response and corresponding neutron sensitivity have also been used in previous analyses.[15] Table 7 lists the TLD response while Fig. 11 compares the response to the gamma-ray heating response for type-316 stainless steel. Although type-304L steel was used in the experiment, its heating response should be quite similar to that of type-316 steel. The neutron sensitivity of the CaF_2 TLD is listed in Table 8. The total TLD response was calculated as merely the sum of the gamma-ray response and the neutron sensitivity, and then compared to the measured TLD data. For most configurations, the neutron sensitivity was approximately 10% of the total response.

Table 6. Response Functions for the Bonner Balls in Counts per Neutron/cm^2

Group	3-in. BB	6-in. BB	10-in. BB
1	3.44(-3)*	2.29(-1)	5.75(-1)
2	4.37(-3)	2.93(-1)	7.01(-1)
3	5.51(-3)	3.71(-1)	8.40(-1)
4	6.86(-3)	4.55(-1)	9.47(-1)
5	9.25(-3)	5.51(-1)	1.05(0)
6	1.10(-2)	6.16(-1)	1.11(0)
7	1.35(-2)	7.03(-1)	1.12(0)
8	1.69(-2)	7.96(-1)	1.14(0)
9	2.11(-2)	9.04(-1)	1.19(0)
10	2.61(-2)	1.01(0)	1.21(0)
11	3.20(-2)	1.11(0)	1.19(0)
12	3.88(-2)	1.19(0)	1.13(0)
13	4.67(-2)	1.26(0)	1.06(0)
14	5.58(-2)	1.32(0)	9.77(-1)
15	6.60(-2)	1.36(0)	8.90(-1)
16	7.72(-2)	1.39(0)	8.04(-1)
17	8.94(-2)	1.40(0)	7.22(-1)
18	1.03(-1)	1.40(0)	6.47(-1)
19	1.16(-1)	1.40(0)	5.80(-1)
20	1.30(-1)	1.38(0)	5.23(-1)
21	1.45(-1)	1.37(0)	4.72(-1)
22	1.59(-1)	1.34(0)	4.30(-1)
23	1.73(-1)	1.32(0)	3.94(-1)
24	1.88(-1)	1.29(0)	3.64(-1)
25	2.05(-1)	1.27(0)	3.35(-1)
26	2.36(-1)	1.22(0)	2.94(-1)
27	2.60(-1)	1.18(0)	2.69(-1)
28	2.77(-1)	1.17(0)	2.57(-1)
29	2.93(-1)	1.15(0)	2.47(-1)
30	3.10(-1)	1.14(0)	2.38(-1)
31	3.26(-1)	1.13(0)	2.30(-1)
32	3.61(-1)	1.11(0)	2.18(-1)
33	4.07(-1)	1.09(0)	2.05(-1)
34	4.37(-1)	1.08(0)	1.98(-1)
35	4.59(-1)	1.08(0)	1.94(-1)
36	4.81(-1)	1.07(0)	1.90(-1)
37	5.05(-1)	1.07(0)	1.86(-1)
38	5.30(-1)	1.06(0)	1.83(-1)
39	5.55(-1)	1.05(0)	1.79(-1)
40	6.07(-1)	1.03(0)	1.70(-1)
41	6.98(-1)	1.00(0)	1.60(-1)
42	7.76(-1)	9.44(-1)	1.45(-1)
43	7.03(-1)	8.96(-1)	1.54(-1)
44	8.19(-1)	8.77(-1)	1.47(-1)
45	9.40(-1)	8.38(-1)	1.38(-1)
46	1.04(0)	7.74(-1)	1.25(-1)
47	1.14(0)	6.97(-1)	1.12(-1)
48	1.18(0)	5.97(-1)	9.49(-2)
49	8.67(-1)	3.53(-1)	5.58(-2)
50	0	0	0
51	0	0	0

*Read as 3.44×10^{-3}.

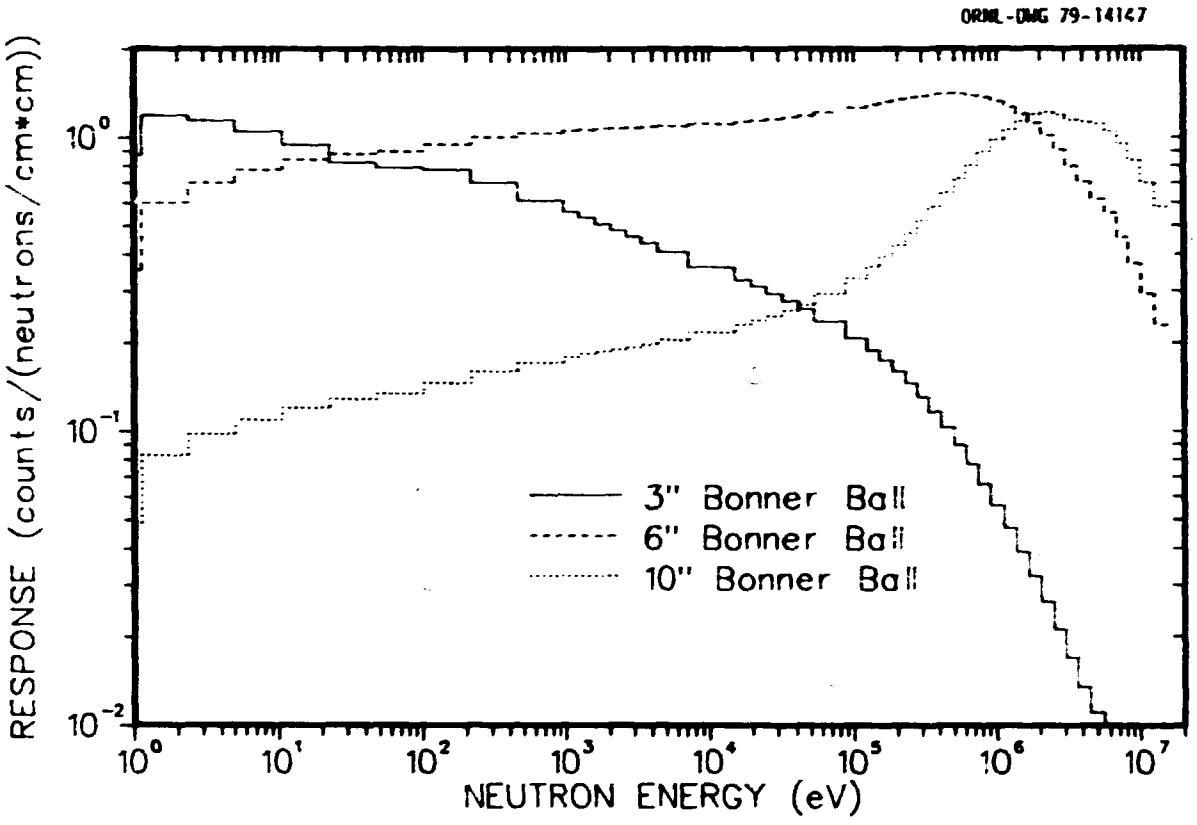

Fig. 10. Response functions for 3", 6", and 10" Bonner balls.

Table 7. Gamma-Ray Heating Response Function for CaF_2:Mn TLD in Units of MeV·Gram per Photon/cm^2

Group	Upper Energy	Response
52	13.0 MeV	0.270
53	10.197	0.202
54	7.998	0.153
55	6.274	0.118
56	4.921	0.0924
57	3.860	0.0737
58	3.028	0.0599
59	2.375	0.0492
60	1.863	0.0408
61	1.461	0.0339
62	1.146	0.0281
63	0.8990	0.0229
64	0.7051	0.0184
65	0.5531	0.0148
66	0.4338	0.0117
67	0.3403	0.00896
68	0.2669	0.00712
69	0.2094	0.00606
70	0.1642	0.00593
71	0.1288	0.00630
72	0.1010	0.00797
73	0.07925	0.0118
74	0.06216	0.0181
75	0.04876	0.0296
76	0.03825	0.0468
	0.030	

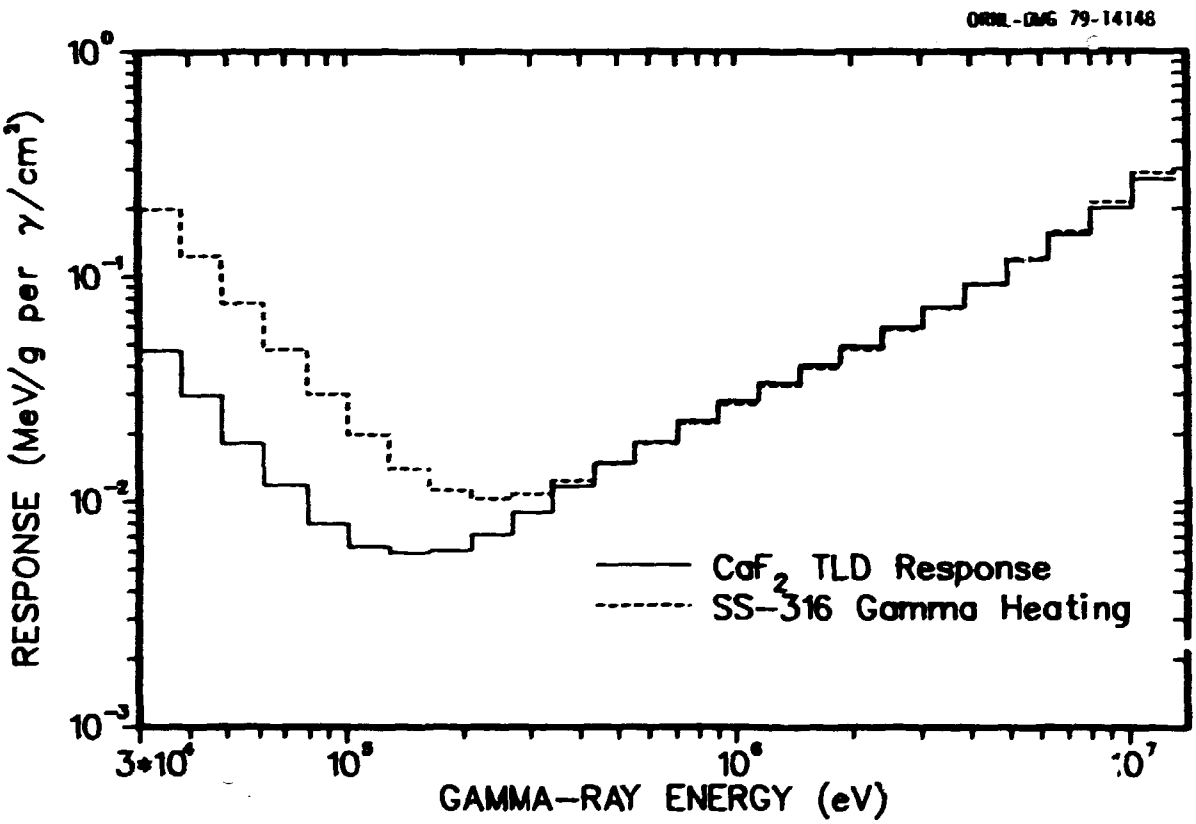

Fig. 11. Response function for CaF_2 TLD compared to gamma-ray heating response of stainless steel-316.

Table 8. TLD Neutron Sensitivity Function in Units of MeV/Gram Per Neutron/cm^2 for CaF_2:Mn

Group	Upper Energy	Response	Group	Upper Energy	Response
1	14.92 MeV	5.95(-2)†	26	86.52 keV	1.04(-4)
2	12.21	6.18(-2)	27	52.48	2.13(-4)
3	10.00	5.84(-2)	28	40.87	6.74(-5)
4	8.187	5.23(-2)	29	31.83	2.50(-4)
5	6.703	4.26(-2)	30	24.79	7.58(-5)
6	5.488	2.66(-2)	31	19.31	5.17(-4)
7	4.493	1.61(-2)	32	15.03	6.01(-5)
8	3.679	8.87(-3)	33	7.102	2.13(-5)
9	3.012	4.03(-3)	34	4.307	1.88(-5)
10	2.466	1.93(-3)	35	3.355	4.29(-5)
11	2.019	1.22(-3)	36	2.613	1.57(-4)
12	1.653	9.21(-4)	37	1.035	5.52(-5)
13	1.353	8.26(-4)	38	1.585	4.33(-5)
14	1.108	6.57(-4)	39	1.234	5.06(-4)
15	0.9072	5.56(-4)	40	961.1 eV	6.07(-5)
16	0.7427	4.38(-4)	41	454.0	8.43(-4)
17	0.6081	4.66(-4)	42	214.5	1.70(-4)
18	0.4979	4.89(-4)	43	101.3	1.25(-4)
19	0.4076	5.17(-4)	44	47.85	1.43(-4)
20	0.3337	4.83(-4)	45	22.60	1.87(-4)
21	0.2732	3.60(-4)	46	10.68	2.58(-4)
22	0.2237	2.36(-4)	47	5.043	3.61(-4)
23	0.1832	1.89(-4)	48	2.382	5.23(-4)
24	0.1500	1.64(-4)	49	1.125	7.92(-4)
25	0.1228	3.15(-4)	50	0.4140	1.40(-3)
			51	0.1000	2.90(-3)

†Read as 5.95×10^{-2}.

5. COMPARISON OF CALCULATIONS AND MEASUREMENTS

This section is devoted to the presentation of comparisons between analytic calculations and the corresponding measurements. Conclusions regarding individual configurations and specific discrepancies are discussed; however, general comments and conclusions are presented in Sec. 6. The Bonner ball, spectral, and TLD data are compared in the first three subsections for the spectrum modifier, the blanket configurations, and the shield configurations, respectively. The fourth subsection describes the results from an investigation of the substantial disagreement observed between the measured and calculated gamma-ray spectra. Unless otherwise noted, all of the calculated results were determined using the procedures described in Sec. 4.

5.1 Spectrum Modifier

As mentioned earlier, a spectrum modifier (SM) was placed in the TSF neutron beam to provide a source spectrum that was more typical of the leakage spectrum from a fast reactor core than was the bare TSF reactor (TSR-II). Measurements and calculations were made for the SM configuration in order to confirm our knowledge of the modified source spectrum. The resulting comparisons for the three Bonner balls located at several distances behind the SM are given in Table 9.

Table 9. Calculation-To-Experiment Ratios for Bonner Ball Detectors Behind Spectrum Modifier Configuration (I.A)

Distance (cm)	C/E			Uncollided Flux[a]
	3" BB	6" BB	10" BB	
30.5	1.06	1.07	1.01	FALSTF
304.8	0.94	0.93	0.93	FALSTF
396.9	1.00	0.95	0.93	FALSTF
396.9	1.06	1.04	1.07	Point TSF Source
396.9	1.02	0.99	1.01	Shell TSF Source

[a]All calculations included the last-flight flux calculated by FALSTF.

Unlike all other configurations investigated, the SM assembly was sufficiently thin to allow a significant portion of the TSF reactor beam to be transmitted through the assembly without a single collision. Therefore, a determination of the neutron flux at detector positions behind the SM had to account for the uncollided flux from the source as well as the scattering source from within the configuration. FALSTF was used to perform the uncollided flux calculation; however, the moderately coarse angular quadrature resulted in a severe underprediction of the uncollided flux on the axial centerline at large distances. This effect is apparently demonstrated in the 10" Bonner ball results given in Table 9. Hence, an alternate approach was used to calculate the uncollided flux at the most distant detector location.

Actually, two similar approaches were tried. The first method approximated the TSR-II as a point source and used the simple relation:

$$\phi_u = \frac{S}{4\pi R^2} \cdot \exp\left[-(\Sigma_T X)_{Fe} - (\Sigma_T X)_{Al} - (\Sigma_T X)_{Boral}\right]$$

where ϕ_u is the uncollided flux,
S is the TSR-II source strength,
R is the distance from the TSR-II to the detector,
Σ_T is the total macroscopic cross section,
X is the slab thickness.

The uncollided flux was calculated by group and added to the FALSTF calculation of the last-flight flux. As shown in Table 9, this approach yielded a small overprediction of the measured count rates. The second approach used the same equation given above to calculate the uncollided flux, but treated the TSF reactor as a shell source which required an integration over the surface of the reactor. This more sophisticated method yielded the best results as indicated in Table 9.

Figure 12 compares the neutron spectrum measured behind the SM with three calculated spectra. The calculated spectrum labeled "Last Flight Only" was calculated using FALSTF, while the other two calculations included the addition of the uncollided flux using the two methods described above. Although supplying more detailed information than the Bonner ball data, the conclusion is the same: the shell source approximation for the uncollided flux appears to give the best overall comparison with the measurement.

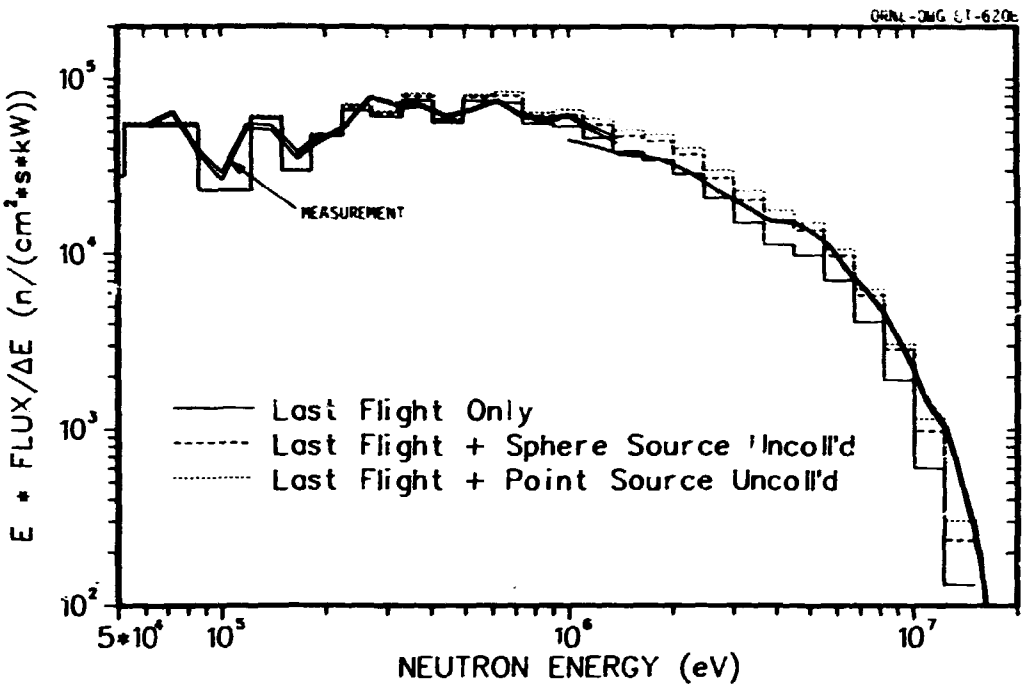

Fig. 12. Measured neutron spectrum behind spectrum modifier compared with spectra calculated using different approximations for the uncollided flux.

5.2 Blanket Configurations

5.2.1 Two-dimensional analysis

Both UO_2 and ThO_2 blanket mockups were investigated in the experiment. Emphasis was placed on the ThO_2 measurements because of particular interest in alternate fuel cycles and because the uncertainties in thorium cross sections were expected to be greater than for uranium. Also, due to budget constraints, the UO_2 blanket mockup was assembled from slabs which had been fabricated for previous LMFBR experiments. Therefore, while the ThO_2 slabs were

designed relatively clean, the UO_2 slabs were more complex, containing significant amounts of aluminum and sodium. As a consequence, a rigorous comparison of the UO_2 and ThO_2 results cannot be made; however, some comparative information can be concluded from the data.

Calculation-to-experiment (C/E) ratios for the three Bonner balls located behind the 30-cm UO_2 blanket and the 30-cm and 45-cm ThO_2 blankets are given in Table 10. A few systematic trends are apparent in the data: (a) the calculations underpredict neutron transmission through the UO_2, (b) the degree of underprediction increases with energy, and (c) calculated values at the most distant detector location behind the ThO_2 are somewhat overpredicted. In light of the combined experimental and analytical uncertainties, which are estimated to be 7-10% for the 3" Bonner ball, 12-15% for the 6" ball, and 15-20% for the 10" ball, the C/E values are all very good. Exceptions to this are the 10" ball behind the UO_2 and the 13-in location behind the ThO_2.

Figure 13 shows the neutron and gamma-ray spectra measured behind the 30-cm UO_2 blanket assembly compared with the analytic predictions. The neutron spectra compare well with only a 20-30% underprediction appearing below about 2 MeV. The gamma-ray spectra show a much greater discrepancy ranging from 50% at 1 MeV to a factor of 5 at 7 MeV. Also,

Table 10. Calculation-To-Experiment Ratios for Bonner Ball Detectors Behind UO_2 and ThO_2 Blanket Configurations

Configuration	Description[a]	Distance[b] (cm)	C/E		
			3" BB	6" BB	10" BB
II.A	30-cm UO_2	30.5	0.98	0.91	0.83
		285.4	0.88	0.86	0.77
		304.8	0.88	0.84	0.77
I.D	30-cm ThO_2	30.5	0.99	0.95	0.91
		304.8	1.03	1.05	0.96
		1314.1	1.28	1.26	1.12
I.E	45-cm ThO_2	30.5	1.02	1.03	0.99
		304.8	1.01	1.09	0.88
		1296.4	1.27	1.36	1.20

[a]Each configuration was preceded by spectrum modifier. Dimensions represent nominal thickness of slabs.

[b]Distance between detector and final surface in configuration.

the energy group structure of the calculated gamma-ray spectrum is too broad above 4 MeV to represent the structure observed in the measured spectrum.

Figures 14 and 15 show similar comparisons for the neutron and gamma-ray spectra behind the 30-cm ThO_2 and 45-cm ThO_2 blankets, respectively. The overprediction of the neutron spectrum below 2 MeV is apparent in both configurations, although it is worse for the thicker blanket assembly. The gamma-ray spectra show fair agreement below 4 MeV, but enormous discrepancies above 4 MeV. It should be noted that the cross sections used in the calculations shown in Figs. 14 and 15 are based on ENDF/B-IV data, and the gamma-ray production data for thorium was merely estimated

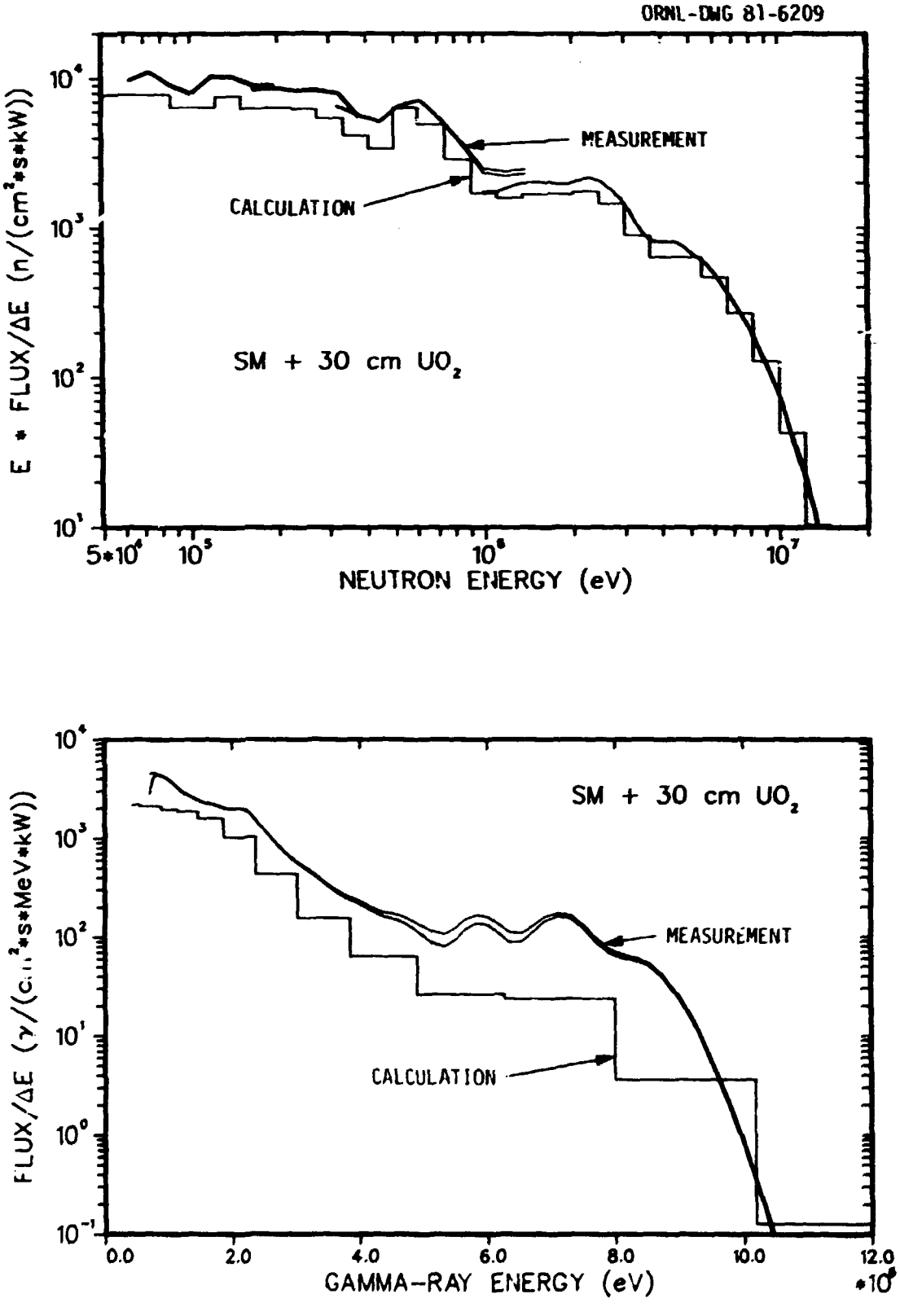

Fig. 13. Comparison of measured and calculated spectra for neutrons (above) and gamma rays (below) behind UO_2 blanket mockup (Configuration II.A).

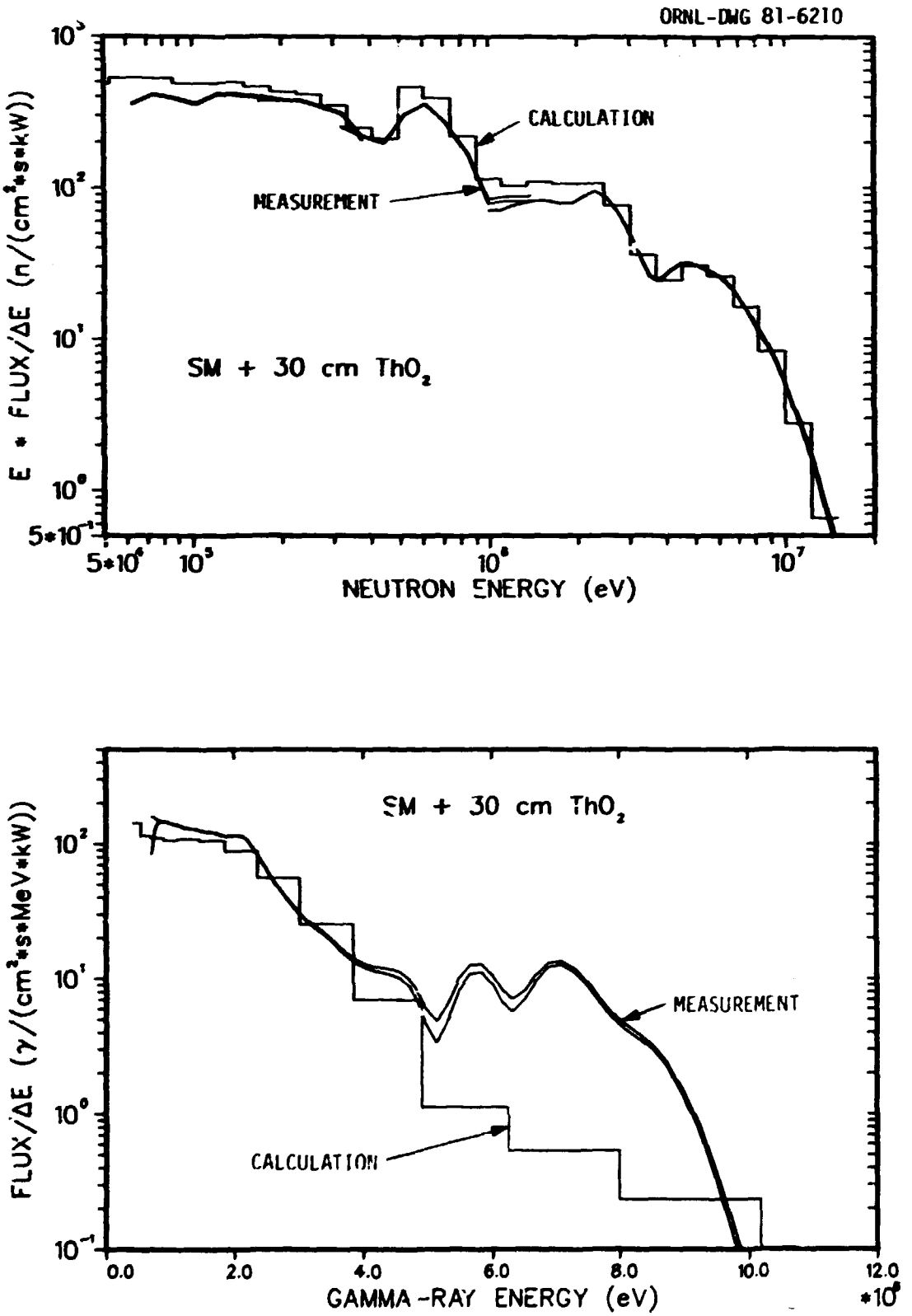

Fig. 14. Comparison of measured and calculated spectra for neutrons (above) and gamma rays (below) behind 30-cm ThO_2 blanket mockup (Configuration I.D).

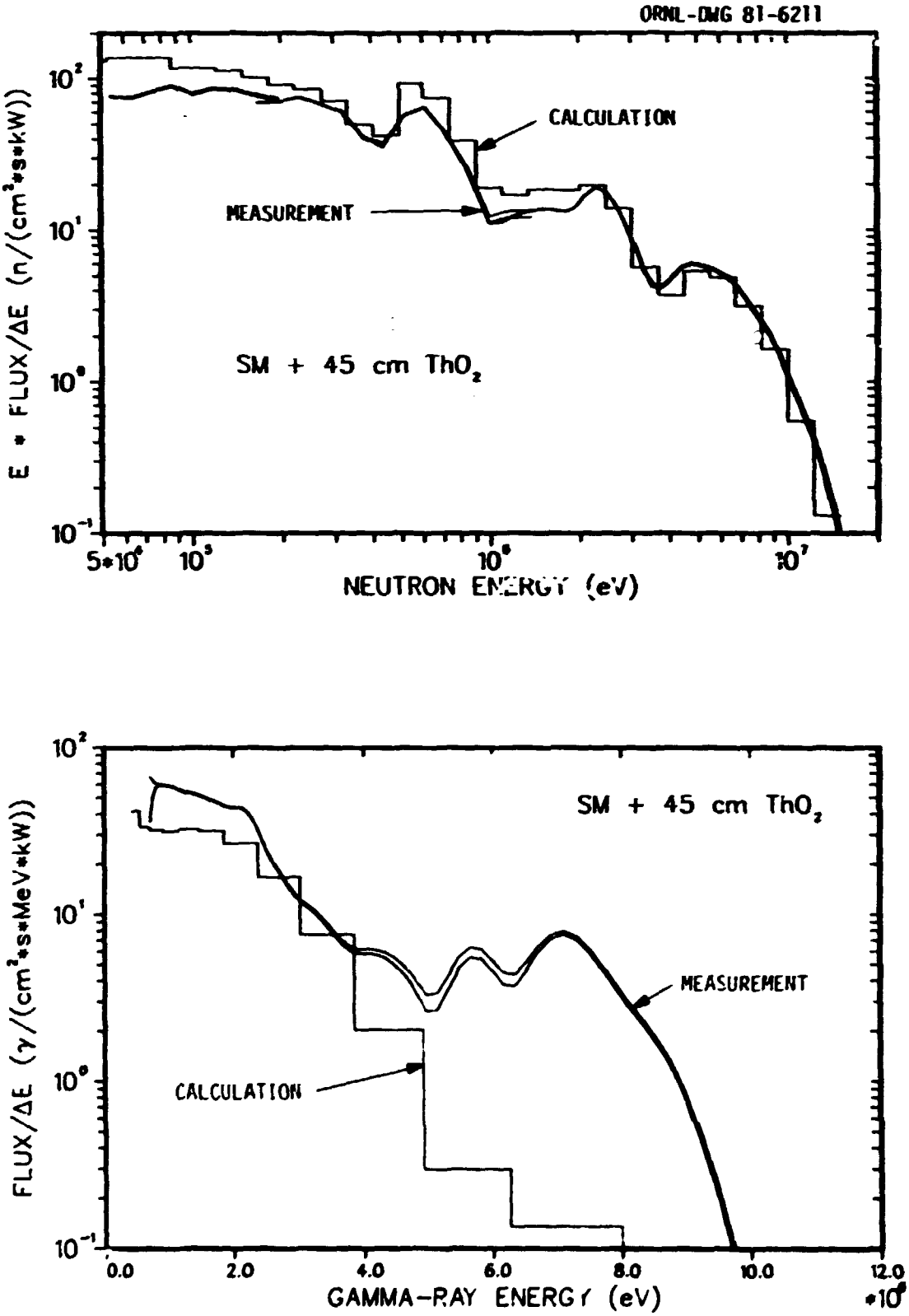

Fig. 15. Comparison of measured and calculated spectra for neutrons (above) and gamma rays (below) behind 45-cm ThO_2 blanket mockup (Configuration I.E).

(see Sec. 4.2). The resulting gamma-ray spectra behind the ThO_2 blankets should be viewed accordingly.

Comparisons of measured and calculated TLD data are given in Table 11. The calculations significantly underpredict the measured TLD response directly behind the spectrum modifier, but this is due to the absence of a gamma-ray component in the TSR-II source spectrum. Beyond the first blanket slab, the dominant source of gamma rays is from secondary production, so that the absence of the TSR gamma-ray source is no longer significant. The TLD data comparison for the UO_2 case shows the calculations to be within the 7-10% uncertainties of the experiment while the ThO_2 case shows much larger discrepancies. As mentioned above, however, this is likely due to the nature of the gamma-ray production data for the particular thorium cross-section set used in the calculation.

5.2.2 Comparison of ENDF/B-IV and -V thorium data

It was originally intended to investigate the impact of the recently released ENDF/B-V data on several of the blanket and shield configurations, but changes in the GCFR program emphasis did not permit such a study. However, one configuration - the 45-cm ThO_2 blanket - was analyzed using ENDF/B-V-derived data. This was accomplished by performing a 76-group ANISN calculation which used the same cross sections and geometry (along the axial centerline) as the

Table 11. TLD Results for UO_2 and ThO_2 Blanket Configurations

Configuration	Description[a]	Response [MeV/(g·sec·kW)] Meas.	Calc-(γ)	Calc-(n)	C/E
II.B	Spectrum Modifier				
	V_1 10-cm UO_2	9.60(5)[b]	5.05(5)	4.48(4)	0.57
	V_2 10-cm UO_2	1.26(5)	1.02(5)	1.59(4)	0.93
	V_3 10-cm UO_2	4.52(4)	4.17(4)	5.38(3)	1.04
I.E	Spectrum Modifier				
	V_1 15-cm ThO_2	9.72(5)	5.00(5)	4.10(4)	0.56
	V_2 7.5-cm ThO_2	7.77(4)	8.92(4)	8.25(3)	1.25
	V_3 7.5-cm ThO_2	4.00(4)	5.08(4)	3.80(3)	1.37
	V_4 15-cm ThO_2	1.88(4)	2.37(4)	1.61(3)	1.34

[a]Nominal thickness of slabs.
[b]Read as 9.60×10^5.

corresponding DOT case, and then calculating scale factors as described in Sec. 4.1. These scale factors which are shown in Fig. 16 were then used to multiply similar 1D calculations which used 207-group cross sections from both ENDF/B-IV and ENDF/B-V.

The scaled 1D calculations are compared with the measured neutron spectrum in Fig. 17. The two calculations are 20 to 40% different in the energy range of 0.1 to 3 MeV with ENDF/B-V-based data showing the better agreement with the measurement. The differences are essentially a direct

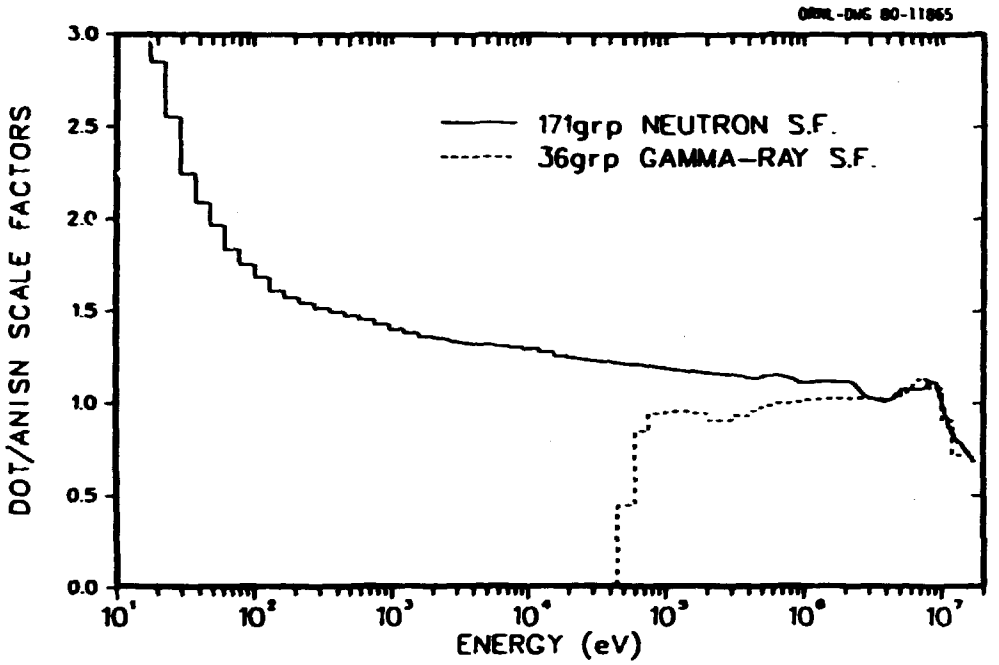

Fig. 16. Scale factors (S.F.) calculated for 45-cm ThO_2 blanket mock-up (Configuration I.E) at NE-213 detector location.

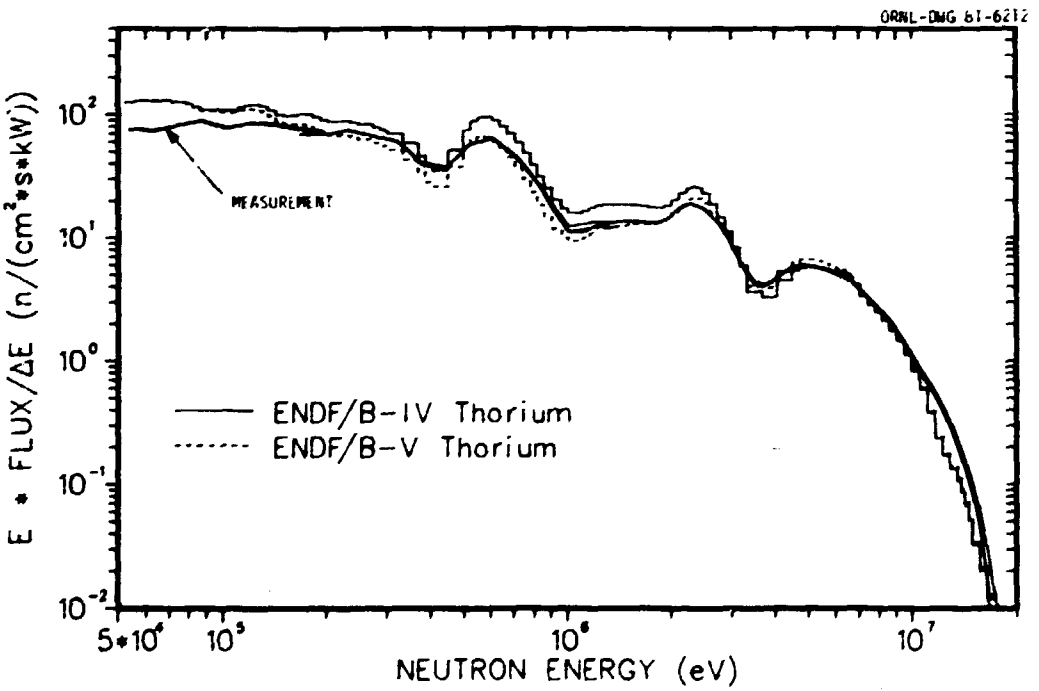

Fig. 17. Measured neutron spectrum for 45-cm ThO_2 blanket compared with calculations which used ENDF/B-IV and -V data for thorium.

reflection of the differences in the total cross section for thorium as demonstrated in Fig. 18.

The gamma-ray spectra behind the ThO_2 are compared in Fig. 19. The spectrum calculated using ENDF/B-IV thorium data is not too surprising since no gamma-ray production data was included in the fine-group thorium data set. The newer ENDF/B-V thorium data does include gamma-ray production which significantly improves the agreement with the measurement below 4.5 MeV, although the calculation is still a factor of 2 to 3 too low. Above 4.5 MeV, both cross section sets give nearly the same result which is about a factor of 50 too low. In addition, the peak in the calculated spectra appear at a different energy than does the measurement. The latter problem is not presently understood; however, the former problem associated with the magnitude of the calculated spectra is addressed in Sec. 5.4.

To further investigate the differences in the cross section data, the scaled 1D fluxes presented above were folded with the TLD gamma-ray heating response and neutron sensitivity and compared to the measured TLD data. The results are presented in Table 12 along with the 2D results which were given in Table 11. Whereas the ENDF/B-IV data understandably yielded very low C/E values, the newer ENDF/B-V data yielded excellent agreement with the

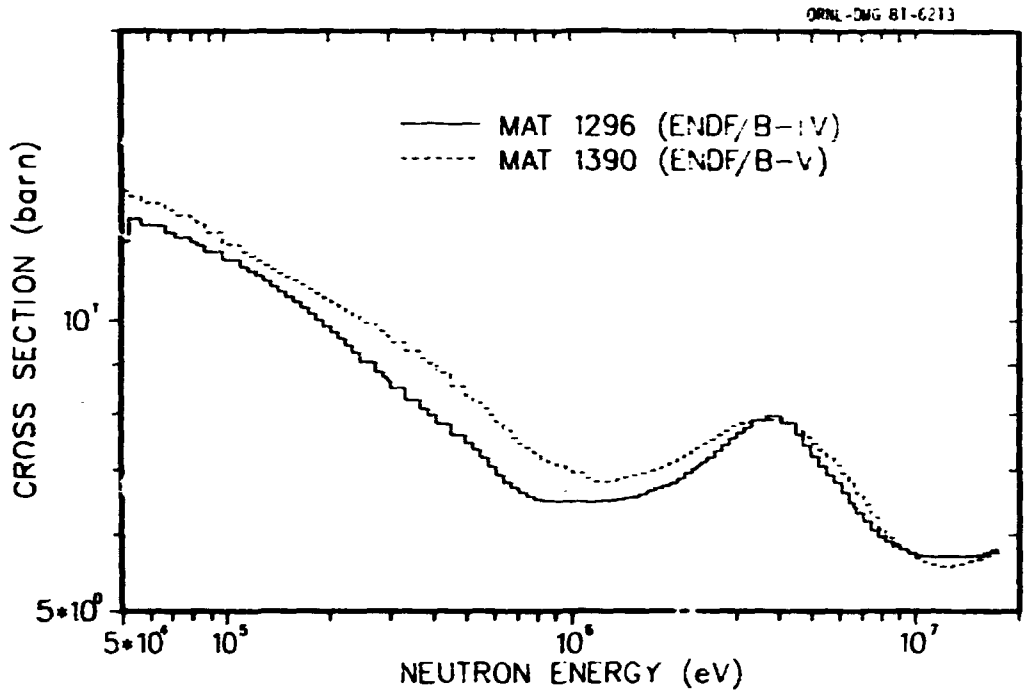

Fig. 18. Comparison of ENDF/B-IV and ENDF/B-V ^{232}Th total neutron cross section in 171 group structure.

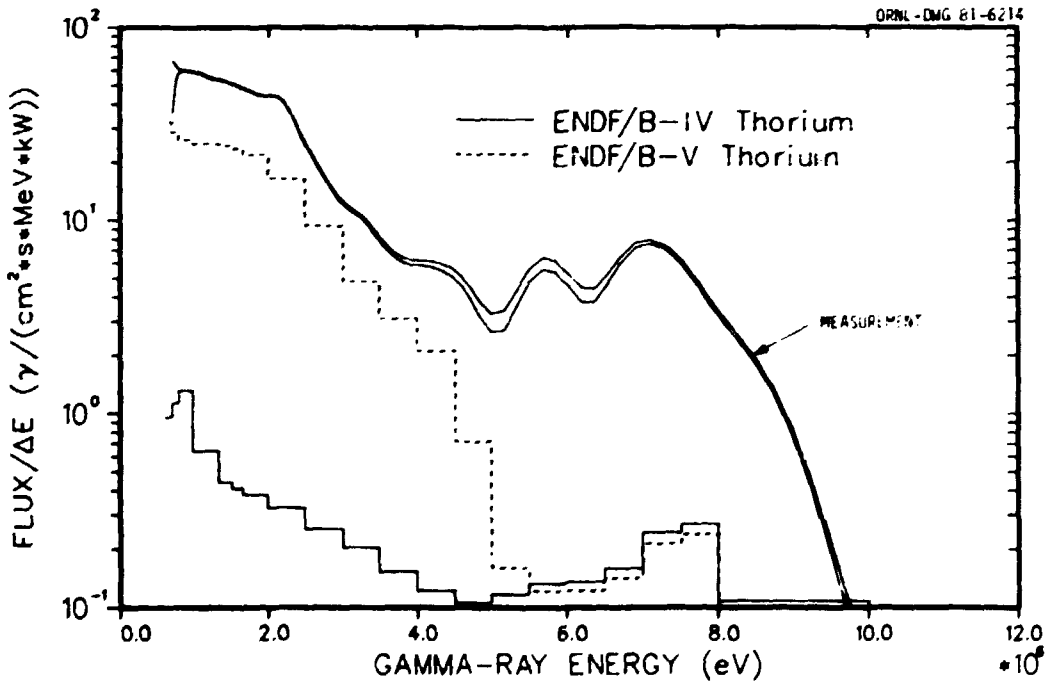

Fig. 19. Measured gamma-ray spectrum for 45-cm ThO_2 blanket compared with calculations which used ENDF/B-IV and -V data for thorium.

Table 12. Comparison of ENDF/B-IV and ENDF/B-V Calculation-To-Experiment Ratios for TLD Results in ThO_2 Blanket Mockup

Configuration[a]	C/E		
	ENDF/B-IV[b]	ENDF/B-IV[c]	ENDF/B-V[c,d]
Spectrum Modifier			
V_1	0.56	0.48	0.54
15-cm ThO_2			
V_2	1.25	0.36	1.01
7.5-cm ThO_2			
V_3	1.37	0.31	1.08
7.5-cm ThO_2			
V_4	1.34	0.37	1.08
15-cm ThO_2			

[a]Nominal thickness of slabs.

[b]Two-dimensional 76-group calculation using special ORNL thorium data set containing "estimated" gamma-ray production cross sections.

[c]One-dimensional scaled 207-group calculations.

[d]Only thorium data was from ENDF/B-V - all other materials were ENDF/B-IV.

measurements. The energy dependence of the TLD response is such that, for typical locations within the ThO_2 blanket, approximately 65% of the total TLD response is due to gamma rays above 1.5 MeV and 15% of the response is due to gamma rays above 4 MeV. Therefore, the good agreement between measured and calculated TLD results is inconsistent with the bad agreement observed in the spectral comparisons. This suggests that either there was a problem in measuring the gamma-ray spectrum, or that there was a problem in projecting the calculated gamma-ray fluxes to the distant location of the NE-213 spectrometer. The latter case is discussed more fully in Sec. 5.4.

5.3 Shield Configurations

5.3.1 Inner shield configurations

Table 13 presents Bonner ball C/E ratios for several inner shield mockups. Configurations II.B and III.B represent the reference inner shield (CSC-I shield design) preceded by a UO_2 blanket and a ThO_2 blanket, respectively. The results are similar to the corresponding blanket-only configurations, i.e., the UO_2 case is always underpredicted while the ThO_2 case is generally overpredicted. The partial shield mockup in configuration III.A shows unusually large overpredictions of the Bonner ball data, especially at lower energies. Configurations V.B and V.C, which consisted of a UO_2 blanket followed by a partial or a full alternate inner shield mockup, again yield results typical of UO_2 cases. Hence, it is difficult to discern from Table 13 exactly how well the individual shield assemblies were calculated because of discrepancies introduced by the preceding blanket slabs. This difficulty is largely eliminated in Sec. 5.3.3 which compares measured and calculated attenuation factors for the various shield mockups.

Comparisons of measured and calculated neutron and gamma-ray spectra are given in Fig. 20 for a ThO_2 blanket followed by the first row (15-cm boronated graphite) of the reference inner shield, and in Fig. 21 for the addition of the second row (15-cm stainless steel). The calculated

Table 13. Calculation-To-Experiment Ratios for Bonner Ball Detectors Behind Inner Shield Configurations

Conf.	Description[a]	Distance[b] (cm)	C/E		
			3" BB	6" BB	10" BB
III.A	45-cm ThO_2 +	30.5	1.57	1.43	1.29
	15-cm ($C+B_4C$)	304.8	1.53	1.39	1.25
		1280.6	1.83	1.70	1.52
III.B	45-cm ThO_2 +	30.5		1.09	1.00
	15-cm ($C+B_4C$) +	304.8	1.19	1.03	0.97
	15-cm Stainless Steel	1263.0	1.36	1.22	1.10
II.B	30-cm UO_2 +	30.5	0.89	0.79	0.71
	15-cm ($C+B_4C$) +	304.8	0.82	0.69	0.64
	15-cm Stainless Steel	1277.2	0.97	0.83	0.73
V.B	30-cm UO_2 +	30.5	0.97	0.87	0.73
	15-cm Graphite	304.8	0.94	0.84	0.72
		1294.4	1.30	1.15	0.95
V.C	30-cm UO_2 +	30.5	0.91	0.81	0.72
	15-cm Graphite +	304.8	0.82	0.75	0.69
	15-cm ($C+B_4C$) +	1270.0	0.91	0.84	0.73
	4.5-cm Stainless Steel				

[a]Each configuration was preceded by spectrum modifier. Dimensions represent nominal thickness of slabs.

[b]Distance between detector and final surface in configuration.

neutron spectrum behind the first row shows that the significant overprediction observed in the Bonner ball data for this configuration is apparently due to a uniform overprediction of the measured spectrum below about 2 MeV. This discrepancy is mostly removed when the 15-cm stainless steel row was added; however, an underprediction above 4 MeV is observed. The relatively broad structure in the spectra appear to be well calculated in both cases. As with the blanket mockups, substantial discrepancies are observed in

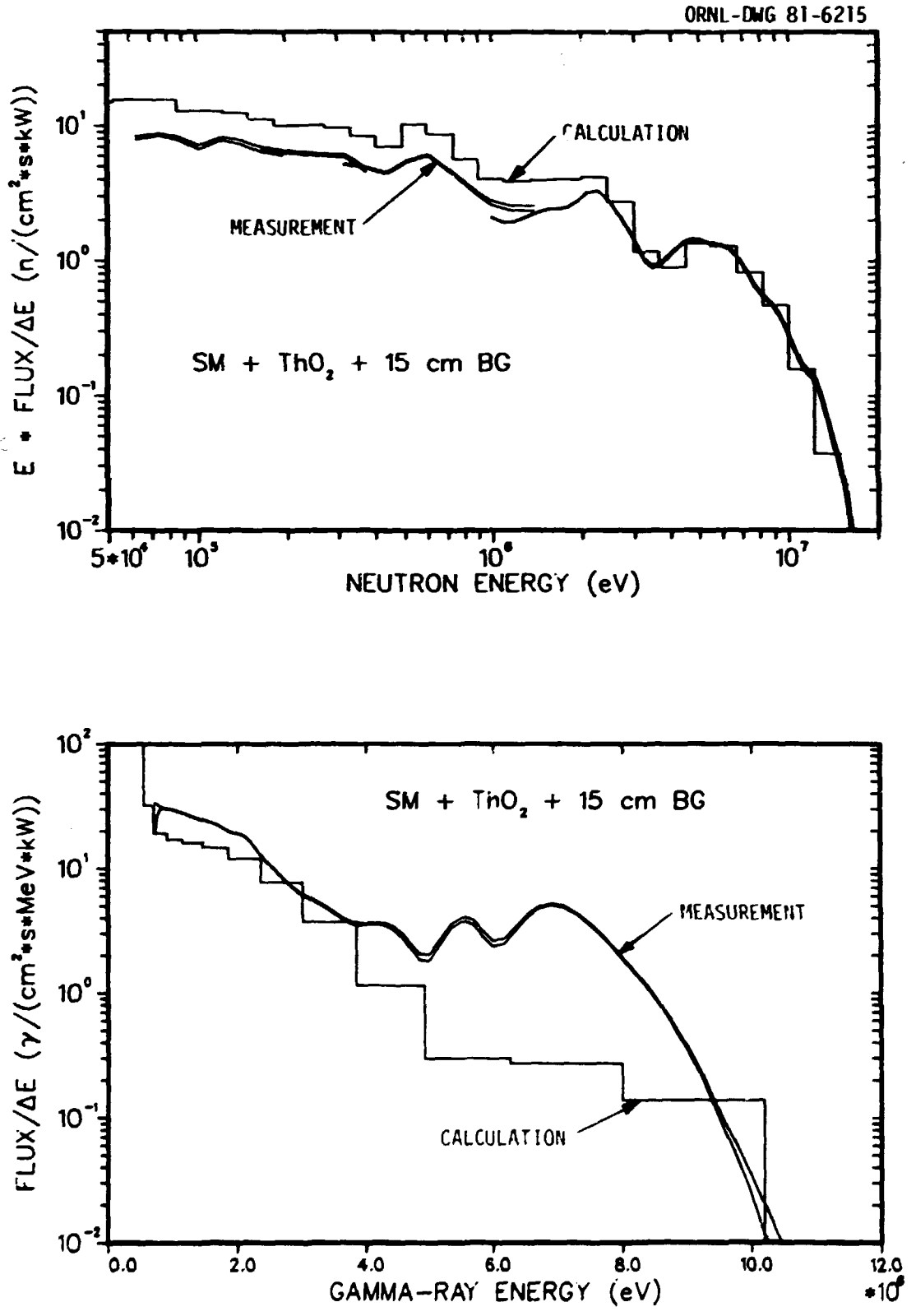

Fig. 20. Comparison of measured and calculated spectra for neutrons (above) and gamma rays (below) behind the first row of the inner shield modules (Configuration III.A).

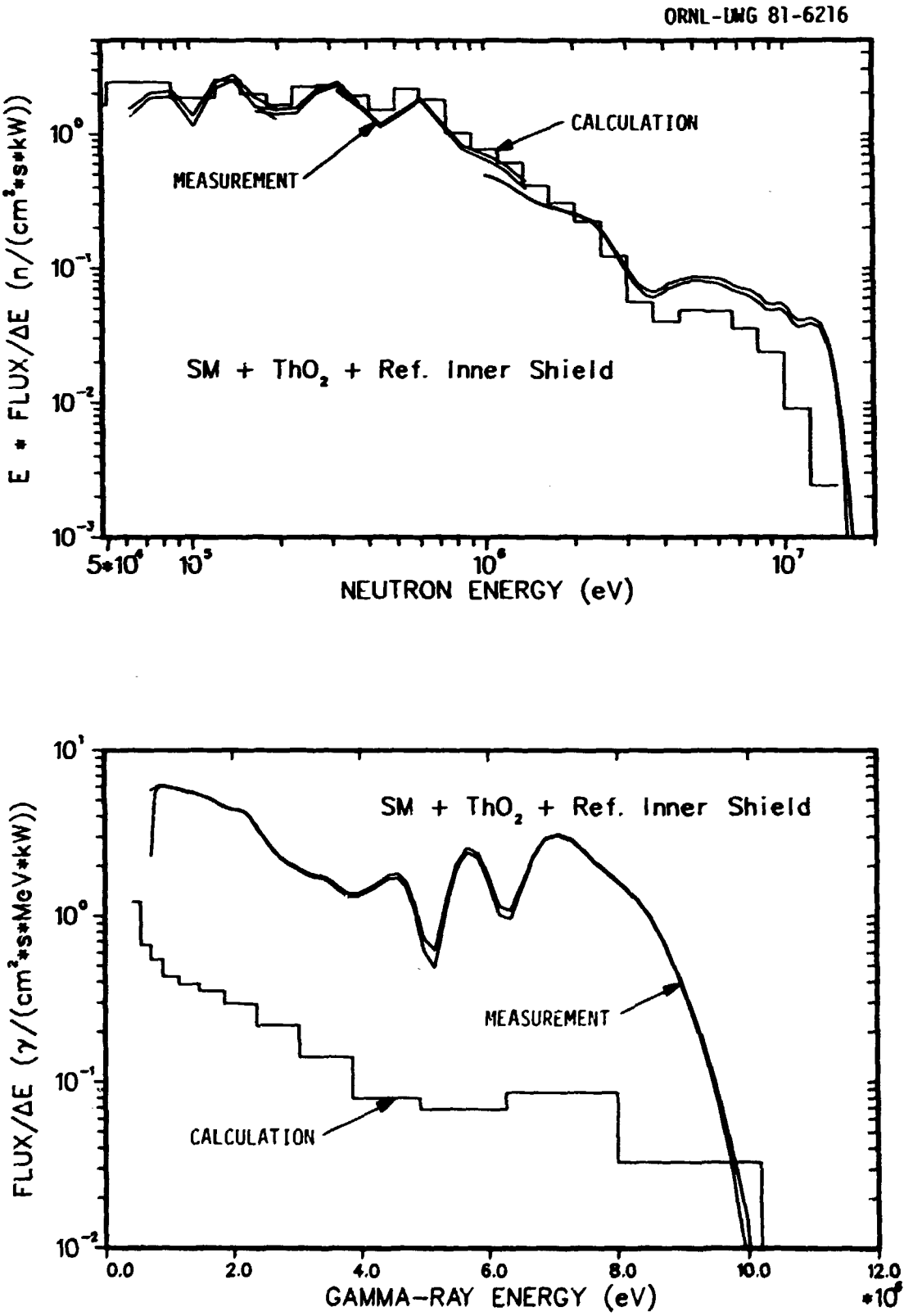

Fig. 21. Comparison of measured and calculated spectra for neutrons (above) and gamma rays (below) behind the reference inner shield mockup (Configuration III.B).

the comparison of gamma-ray spectra, and comments on these discrepancies are deferred to Sec. 5.4.

Figure 22 shows comparisons of measured and calculated spectra behind the UO_2 blanket followed by the reference inner shield. Both the neutron and gamma-ray results are similar to those given in Fig. 21, except that the neutron spectrum is more uniformly underpredicted (although to a lesser extent) than in the previous case.

Neutron and gamma-ray spectra are compared in Fig. 23 for the case of a UO_2 blanket followed by a 15-cm graphite shield, and in Fig. 24 for the same configuration with an additional 15-cm boronated graphite shield and a 4.5-cm stainless steel slab. The steel slab was added to simulate the lateral core restraint system (core barrel). Both cases show a slight underprediction of the neutron spectra, especially near the broad peak at 5 MeV. In general, however, the agreement is quite satisfactory. The gamma-ray spectra show considerably better agreement than with the reference shield cases, although discrepancies on the order of 200 to 400% are still present.

Data for the TLD measurements made within the shield configuations are compared to calculated values in Table 14. The first two cases listed in Table 14 do not represent "clean" comparisons since in both cases, somewhat different materials were present behind the last detector position for

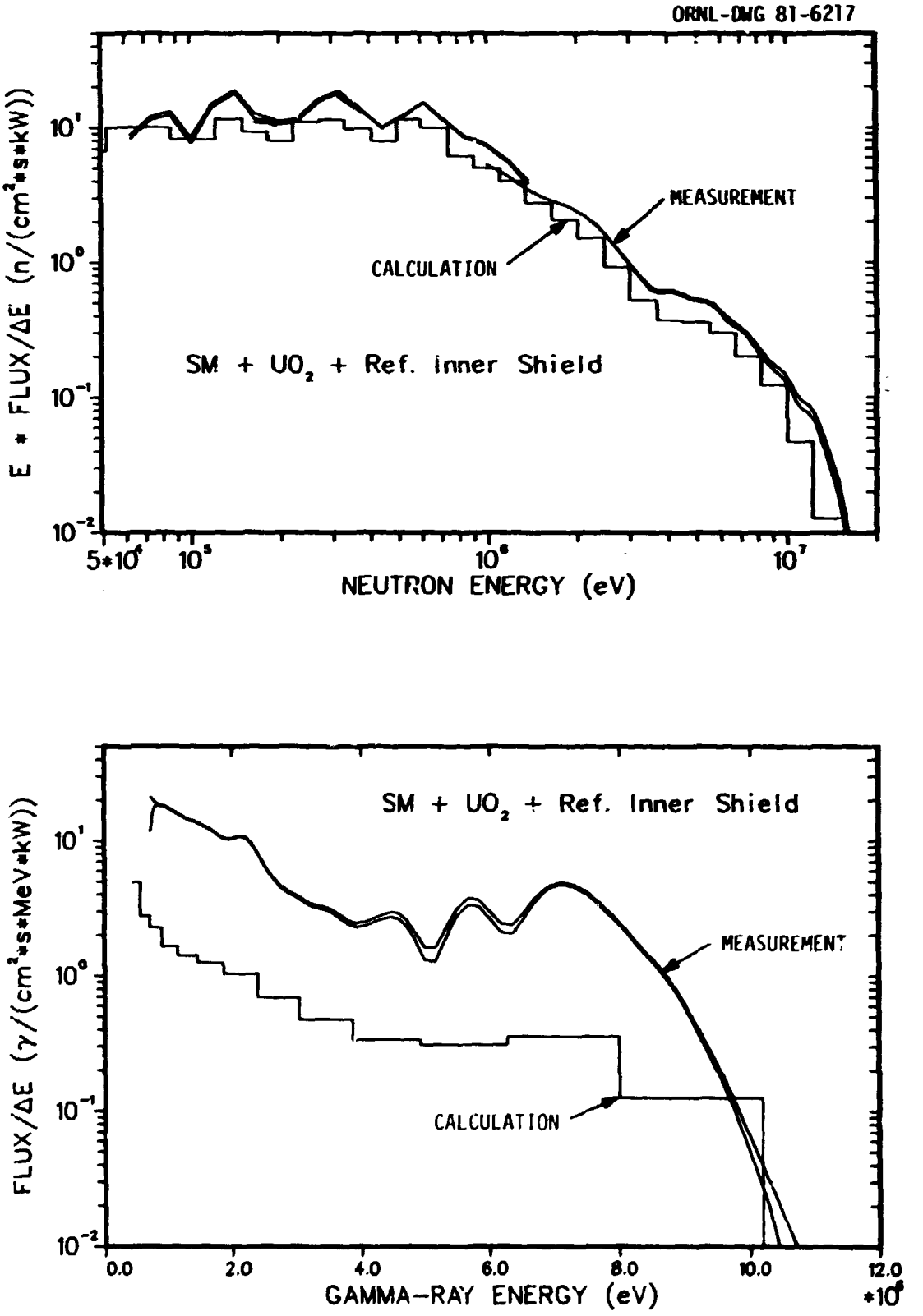

Fig. 22. Comparison of measured and calculated spectra for neutrons (above) and gamma rays (below) behind the reference inner shield mockup (Configuration II.B).

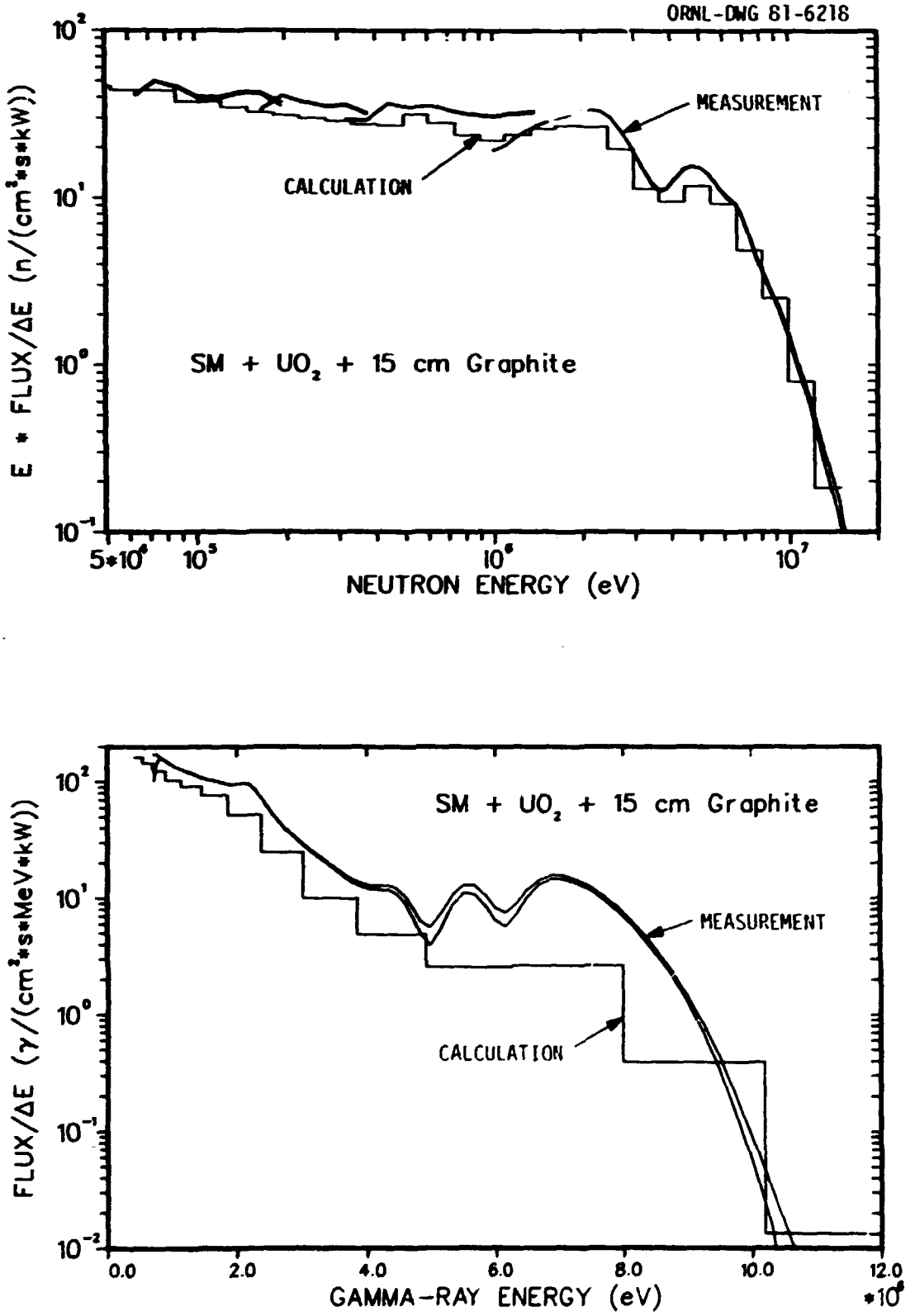

Fig. 23. Comparison of measured and calculated spectra for neutrons (above) and gamma rays (below) behind the 15-cm graphite shield mockup (Configuration V.B).

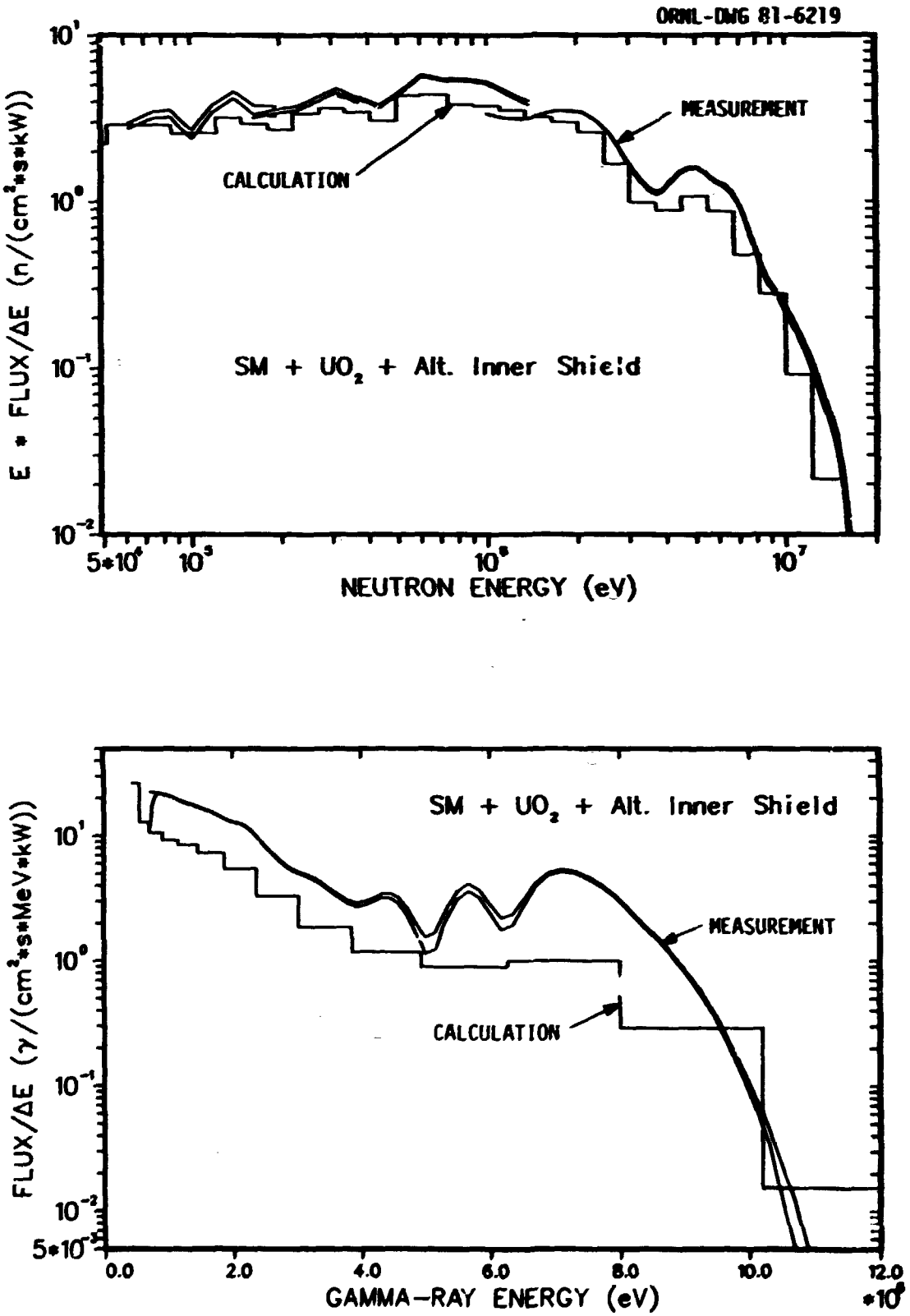

Fig. 24. Comparison of measured and calculated spectra for neutrons (above) and gamma rays (below) behind an alternate inner shield mockup (Configuration V.C).

Table 14. Comparison of Measured and Calculated TLD Results for Inner Shield Configurations

Conf.	Description	Response [MeV/(g·s·kW)] Meas.	Calc(γ)	Calc(n)	C/E
II.B (V.E)	Spectrum Modifier				
	30-cm UO_2				
	V_1	1.03(6)[a]	9.81(5)	1.06(5)	1.06
	15-cm (C+B_4C)				
	V_2	2.08(5)	2.64(5)	1.47(4)	1.34
	Stainless Steel[b]				
III.B (IV.D)	Spectrum Modifier				
	45-cm ThO_2				
	V_1	5.60(4)	8.01(4)	2.72(3)	1.48
	15-cm (C+B_4C)				
	V_2	8.50(3)	9.77(3)	5.66(2)	1.22
	15-cm Stainless Steel				
	Reference Outer Shield[c]				
V.C	Spectrum Modifier				
	30-cm UO_2				
	V_1	1.98(6)	1.77(6)	1.94(5)	0.99
	15-cm Graphite				
	V_2	1.02(6)	9.86(5)	6.6(4)	1.03
	15-cm (C+B_4C)				
	V_3	1.35(5)	1.43(5)	2.72(3)	1.08
	4.5-cm Stainless Steel				

[a] Read as 1.03×10^6.

[b] Calculation had 15.2-cm stainless steel (Conf. II.B) while measurement had only 4.5-cm steel (Conf. V.E).

[c] Calculation had nothing beyond 15-cm steel (Conf. III.B) while measurement had outer shield and PCRV (Conf. IV.D).

the measurement than for the calculation. This occurred since not all configurations were calculated, but it was felt that similar cases could be substituted. Unfortunately, the differences did appear to have some effect on the C/E ratios for the last TLD position, so that the data should be viewed accordingly. The third case

listed in Table 14 (Configuration V.C) was a clean comparison, and the agreement between the measurement and calculation is excellent.

5.3.2 Inner plus outer shield configurations

Bonner ball results for the reference inner plus outer shield configuration are given in Table 15. Two separate mockups were analyzed - one with a 45-cm ThO_2 blanket preceding the shield and one with no blanket. The no-blanket case was included since the presence of the blanket introduced an additional uncertainty in the total transmission data, and because the overall attenuation of the blanket and shield assembly resulted in an unacceptably low detector counting rate for the spectrum measurements. Both cases yield very good agreement between the measurements and calculations, except for the 3" and 6" balls at the most distant detector location.

Table 15. Calculation-To-Experiment Ratios for Bonner Ball Detectors Behind Reference Inner-Outer Shield Configurations

Conf.	Description[a]	Distance[b] (cm)	C/E		
			3" BB	6" BB	10" BB
IV.C	45-cm ThO_2 +	30.5	1.08	1.06	0.98
	Ref. Inner Shield +	304.8	1.04	1.13	1.01
	Ref. Outer Shield	1210.5	1.38	1.23	1.00
IV.E	Ref. Inner Shield +	30.5	1.15	1.01	0.93
	Ref. Outer Shield	304.8	1.18	1.04	0.97
		1264.9	1.46	1.29	1.10

[a] Each configuration was preceded by a spectrum modifier. The "reference" shields refer to CSC-I design.

[b] Distance between detector and final surface in configuration.

The measured and calculated neutron and gamma-ray spectra behind the reference inner and outer shield mockup (with no blanket) are compared in Fig. 25. An obvious error in a segment of the measured neutron spectrum corresponding to one of the three hydrogen counters was likely due to the very low counting rates observed behind the full shield assembly. Discounting this problem, the comparison is reasonably good, except for the underprediction above about 4 MeV. As before, the gamma-ray spectra show significant discrepancies, although the agreement is better than that with only the inner shield mockup.

5.3.3 Shield attenuation factors

The Bonner ball data presented thus far have represented neutron transmission though entire configurations consisting of a spectrum modifier, a blanket mockup, and/or a shield mockup. Although providing useful information, data for the larger configurations are subject to uncertainties in the transmission through the initial sections of the configuration which can often dominate the total uncertainty for the full assembly. This was seen to be the case in many of the inner shield configurations where the magnitude of the C/E values seemed to depend more on the type of blanket than on the particular shield. To circumvent this difficulty, another approach was used which focused on the attenuation properties of the individual shield assemblies.

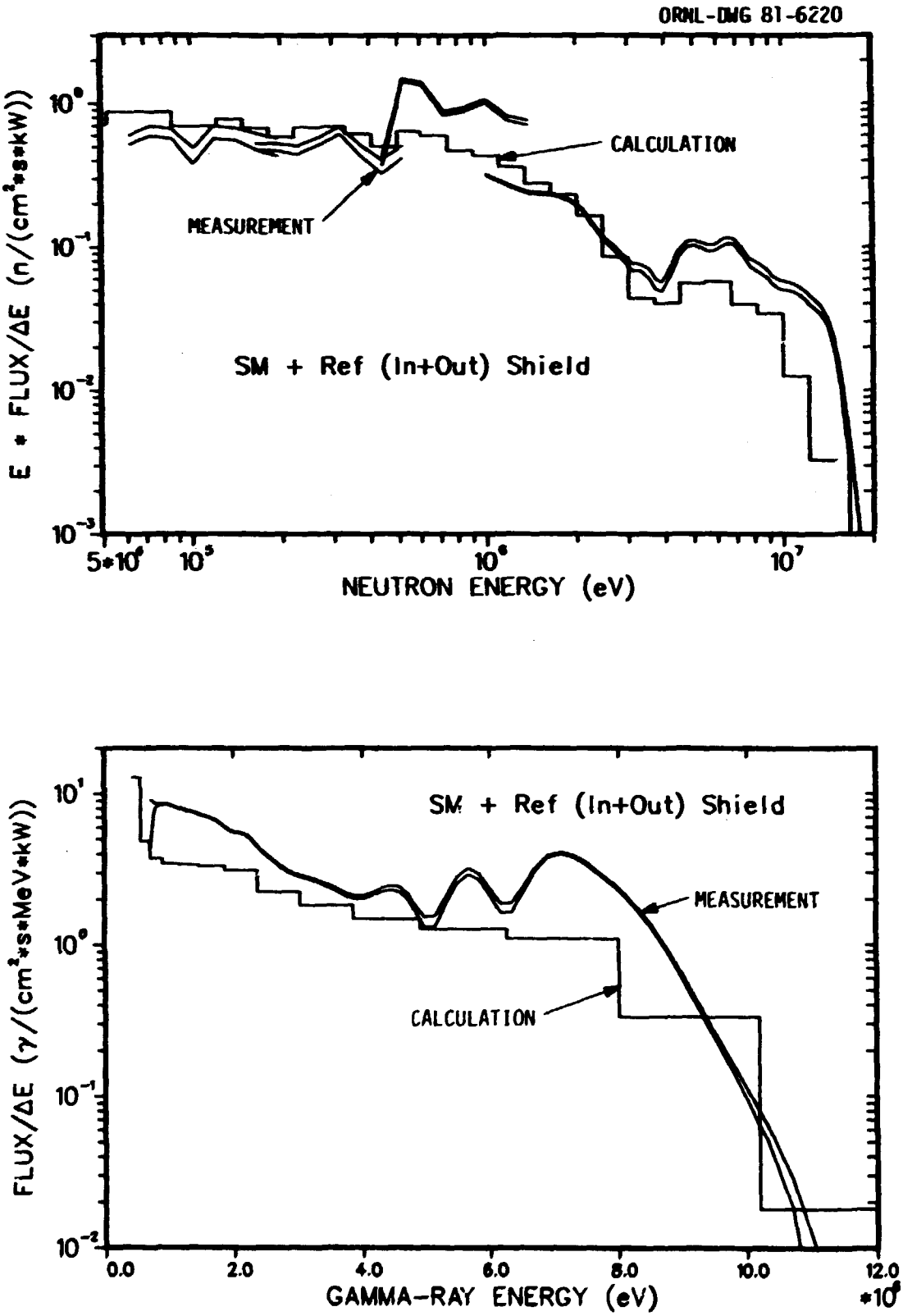

Fig. 25. Comparison of measured and calculated spectra for neutrons (above) and gamma rays (below) behind the full reference inner and outer shield mockup (Configuration IV.E).

The preferred approach to determine individual attenuation factors is to perform measurements at a fixed (and distant) location for each of the intermediate stages of the configuration assembly, and then ratio the data for consecutive stages. This was done for some configurations; however, difficulties in calculating fluxes at distant detector positions overshadowed any conclusions regarding shield attenuations. Therefore, an alternate approach was used whereby the Bonner ball data at the 30-cm position for consecutive configurations were ratioed. Since the detectors had to be moved away from the TSF as the next shield section was added in order to maintain the 30-cm separation between the shield and the detector, the attenuation factors determined in this manner include both geometric attenuation of the TSF source as well as material attenuation. Nevertheless, this type of analysis does provide useful insight into our ability to calculate neutron transport through the shield assemblies.

The resulting measured and calculated attenuation factors are given in Table 16 for several shield assemblies. One should note that although calculations underpredict attenuation in the 15-cm boronated graphite slab, attenuation in the adjacent stainless steel slab is overpredicted so that the combined assembly shows reasonably good agreement between calculations and measurements. Good agreement is observed in Case 4 which is also for the

Table 16. Bonner Ball Attenuation Factors for the Inner and Outer Shield Assemblies

Case	Shield Configuration[b]	Attenuation Factors and C/E Values[a]					
		3" BB		6" BB		10" BB	
		Meas.	Calc.	Meas.	Calc.	Meas.	Calc.
1.	15-cm Boronated Graphite (I.E/III.A)	11.7	7.6 (0.65)	11.1	8.0 (0.72)	10.2	7.8 (0.77)
2.	15-cm Stainless Steel (III.A/III.B)	4.3	5.4 (1.27)[c]	4.7	6.1 (1.31)	4.7	6.1 (1.29)
3.	Reference Inner Shield (I.E/III.B)	47.8	40.9 (0.86)[c]	51.8	48.8 (0.94)	48.3	47.9 (0.99)
4.	Reference Inner Shield (II.A/II.B)	35.2	38.7 (1.10)	37.9	43.8 (1.16)	34.8	41.0 (1.18)
5.	15-cm Graphite (V.A/V.B)	1.3	1.3 (1.01)	3.1	3.3 (1.06)	3.8	4.4 (1.13)
6.	15-cm Boronated Graphite + 4.5-cm Stainless Steel (V.B/V.C)	99.5	106 (1.06)	34.4	36.7 (1.07)	20.1	20.4 (1.02)
7.	Reference Outer Shield (III.B/IV.C)	328	373 (1.14)[c]	477	491 (1.03)	539	549 (1.02)
8.	Inner + Outer Shield (I.A/IV.E)	2.68(+3)[d]	2.46(+3) (0.92)	5.19(+3)	5.51(+3) (1.06)	8.36(+3)	9.09(+3) (1.09)
9.	Inner + Outer Shield (I.E/IV.C)	1.63(+4)	1.54(+4) (0.95)	2.48(+4)	2.41(+4) (0.97)	2.60(+4)	2.63(+4) (1.01)

[a] Attenuation factors determined by dividing Bonner ball data 30 cm behind configuration without shield assembly by the corresponding data with shield assembly. C/E ratios are given in ()'s.

[b] Items in ()'s indicate which two configurations were used to determine attenuation factors.

[c] Due to an error in the 3" Bonner ball data at 30 cm behind configuration III.B, the 305-cm data was used to calculate attenuation factors for both calculations and measurements.

[d] Read as 2.68×10^3.

boronated graphite-stainless steel assembly but with a preceding UO_2 blanket. Case 6, which again consisted of the 15-cm boronated graphite slab followed by only 4.5-cm stainless steel, shows excellent agreement between calculations and measurements. These combined results suggest that the measurements and/or calculations behind only the boronated graphite slab (Config. III.A) may have been in error.

Another observation from Table 16 is that the relatively thick outer shield and the combined inner and outer shield cases yield very good agreement between calculations and measurements. Also, Cases 8 and 9, which represent the same shield assembly but preceded by only the spectrum modifier in one case and by the spectrum modifier plus a ThO_2 blanket in the other case, yield considerably different attenuation factors. The differences are even more significant since geometric attenuation of the neutron source would, by itself, cause a larger total attenuation for Case 8. Therefore, the much larger attenuation determined for the shield in Case 9 must be due to spectral differences in the incident source. For completeness, the neutron spectra calculated behind the spectrum modifier and the ThO_2 blanket are compared in Fig. 26. Although the blanket spectrum appears only moderately softer, the presence of the boronated graphite in the initial section of the shield yields a significantly higher shield effectiveness for the softer spectrum.

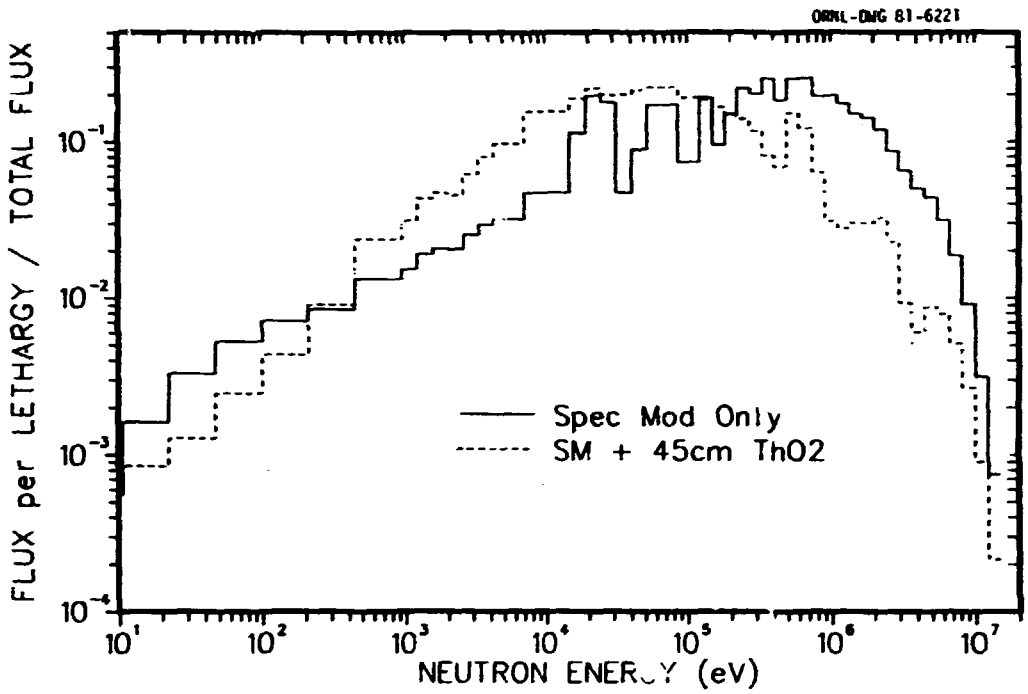

Fig. 26. Comparison of spectra incident on the full inner and outer shield mockup.

5.4 Analysis of Gamma-Ray Spectra

As stated in previous sections, considerable disagreement was observed between measured and calculated gamma-ray spectra. Moreover, the large discrepancies were inconsistent with the good agreement that was observed for the *in situ* TLD data. Therefore, the spectral discrepancies were attributed to either problems with the spectrum measurements or problems with the calculation of the gamma-ray flux at the distant location of the spectrometer. The former explanation was, and still remains, a possibility since the NE-213 spectrometer had not been previously used

In a TSF experiment to measure gamma-ray spectra. However, the modestly successful investigation described below indicates that computational limitations combined with an experiment design which was not well suited for gamma-ray measurements appears to account for much of the disagreement.

Several possible explanations for the discrepancies were investigated using primarily one-dimensional calculations. Since preanalysis[4] indicated that the dominant source of observed gamma rays would be from neutron-induced photon production within the test slabs, most of the investigations focused on gamma-ray production mechanisms.

In addition to the search for a comprehensive solution, calculations were performed to quantify the effects of certain parameters which were not expected to contribute significantly to the problem, but were of some interest. One such study determined the effect on the calculated spectrum due to neutron-induced gamma-ray production in air, since the NE-213 spectrometer was located approximately 12 m behind the blanket and shield configurations. This effect was easily computed by including 12 m of air in 1D slab-geometry calculations of two typical configurations. In both cases, the flux in most energy groups decreased by 5-10% because attenuation of the neutron flux outweighed the

gamma-ray production. The gamma-ray flux in the 8-10 MeV group, however, did increase 15-20% with the maximum flux appearing approximately 5 m behind the configuration.

Another parametric study investigated the effect of the angular expansion of the cross sections on the calculated spectrum. To determine this effect, Config. II.B (UO_2 blanket followed by the reference inner shield) was calculated using a 1D slab gemometry and using macroscopic cross sections employing a P_8 angular expansion. The resulting gamma-ray spectrum showed no significant difference with respect to the spectrum calculated using a P_3 expansion. Hence, a P_3 expansion appears adequate for calculating the neutron and gamma-ray transport. This result could have been predicted, since most of the multigroup cross section data used in this analysis assume isotropic production of secondary gamma rays. This assumption may not be entirely accurate, but would not likely be a significant factor.

The most fruitful investigation of the observed discrepancies dealt with the collimation of the gamma-ray field incident on the NE-213 detector. The full geometry of the neutron and gamma-ray spectra measurements is shown in Fig. 27. Two large concrete collimators were used to restrict the angle of view of the spectrometer to the region including only the 1.5-m by 1.5-m test slabs and the

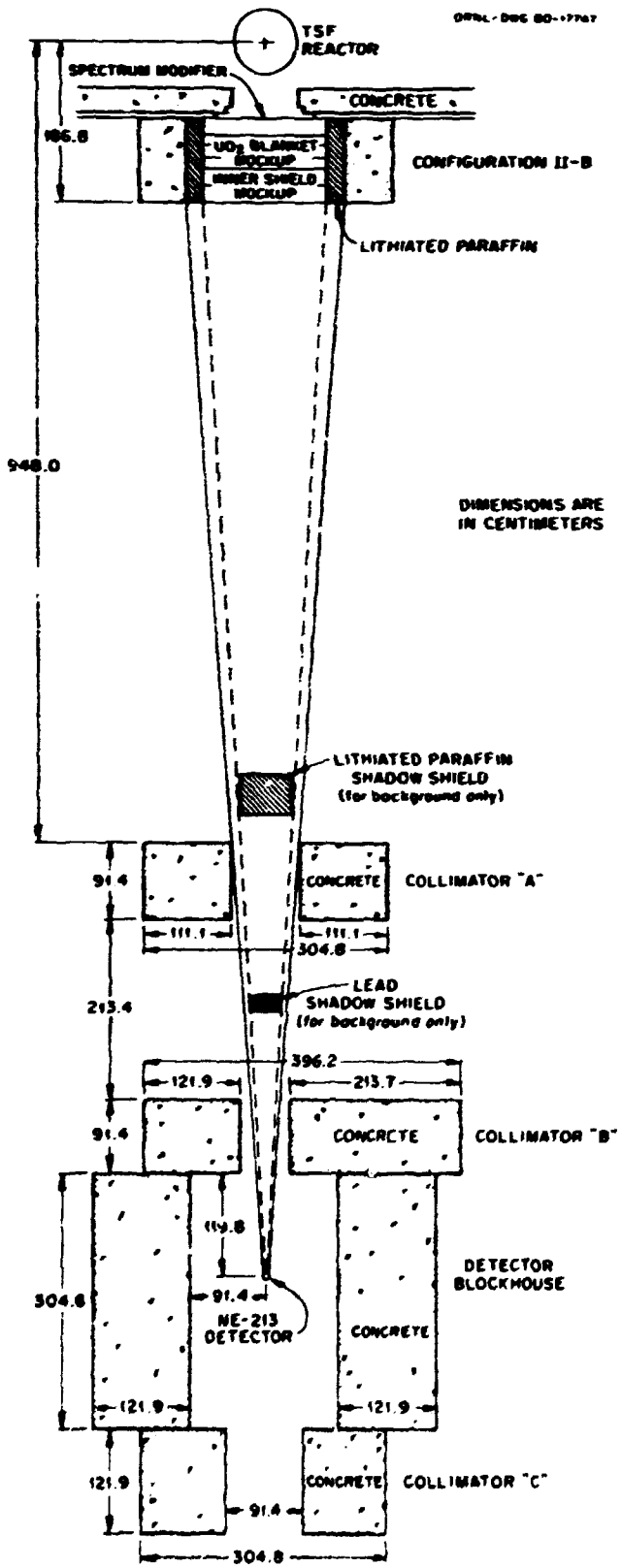

Fig. 27. Full geometry of spectrum measurements for Radial Blanket and Shield Experiment.

adjacent lithiated paraffin buffer zone. A background measurement was made with a two-part shadow shield placed in the beam such that only the region of the test slabs was obscured from the detector's view. Subtracting the background from the foreground then left a net spectrum which was attributed to the flux emanating from only the test assembly.

A similar collimation of the calculated spectrum was performed in the FALSTF calculations by defining specific limits for the angular integration of the scattering source. The analytic collimator was circular to correspond with the 2D cylindrical geometry, and subtended an appropriate solid angle so as to include only the test assembly, thus representing the same conditions as the net measured spectrum. The effect of removing the analytic collimator is shown in Figs. 28 and 29 for two similar shield configurations. In both cases, removing the collimator improved the agreement with the measured gamma-ray spectra, but had little effect on the calculated neutron spectra. In all the cases considered, removing the analytic collimator caused the calculated gamma-ray spectrum to approach the measured spectrum but never exceed the measurement. It should be noted, however, that removing the analytic collimator generally worsened the agreement between the spectral shape of the calculation and the measurement.

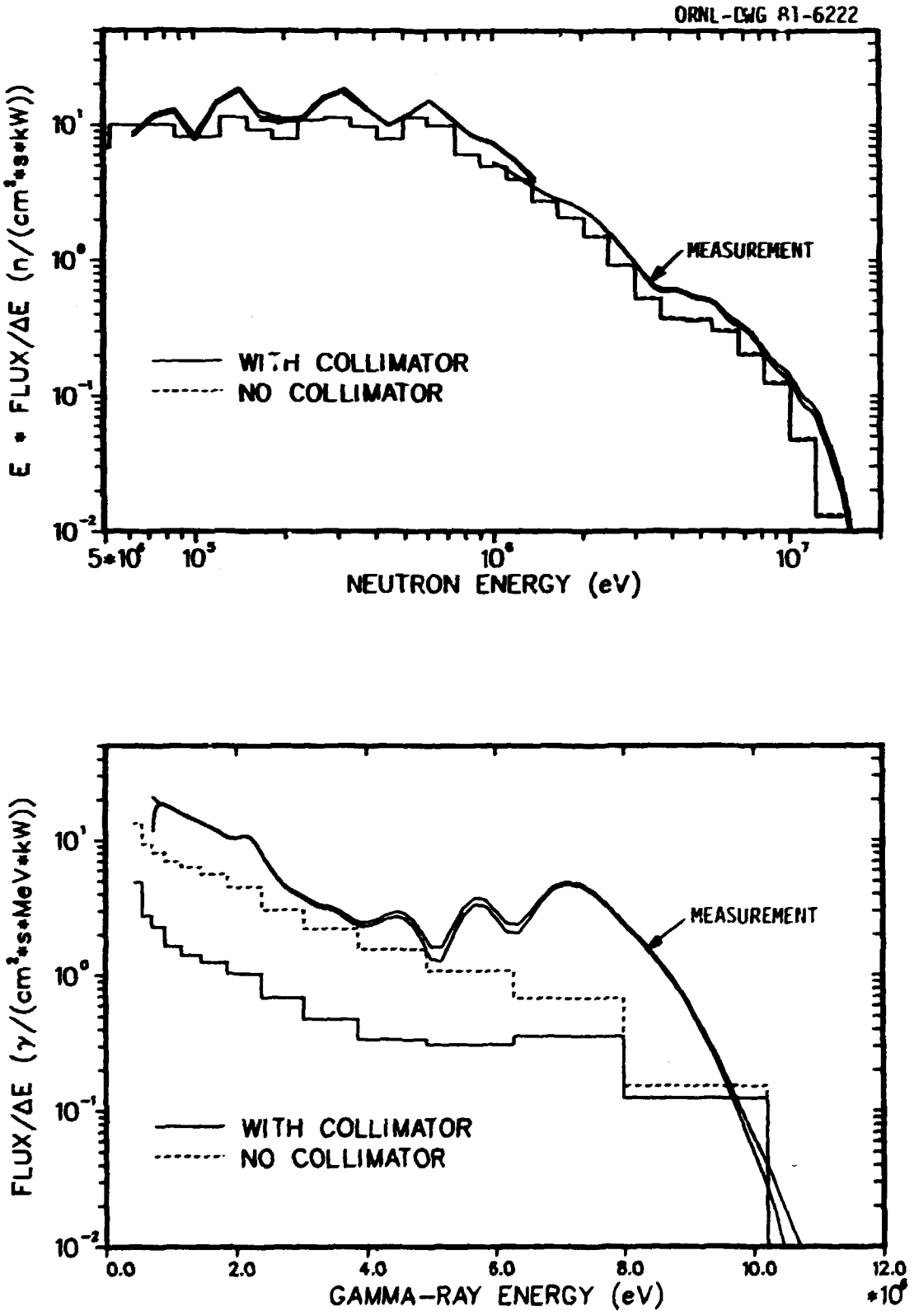

Fig. 28. Measured neutron (above) and gamma-ray (below) spectra compared to spectra calculated with and without an analytic collimator for the reference shield (Configuration II.B).

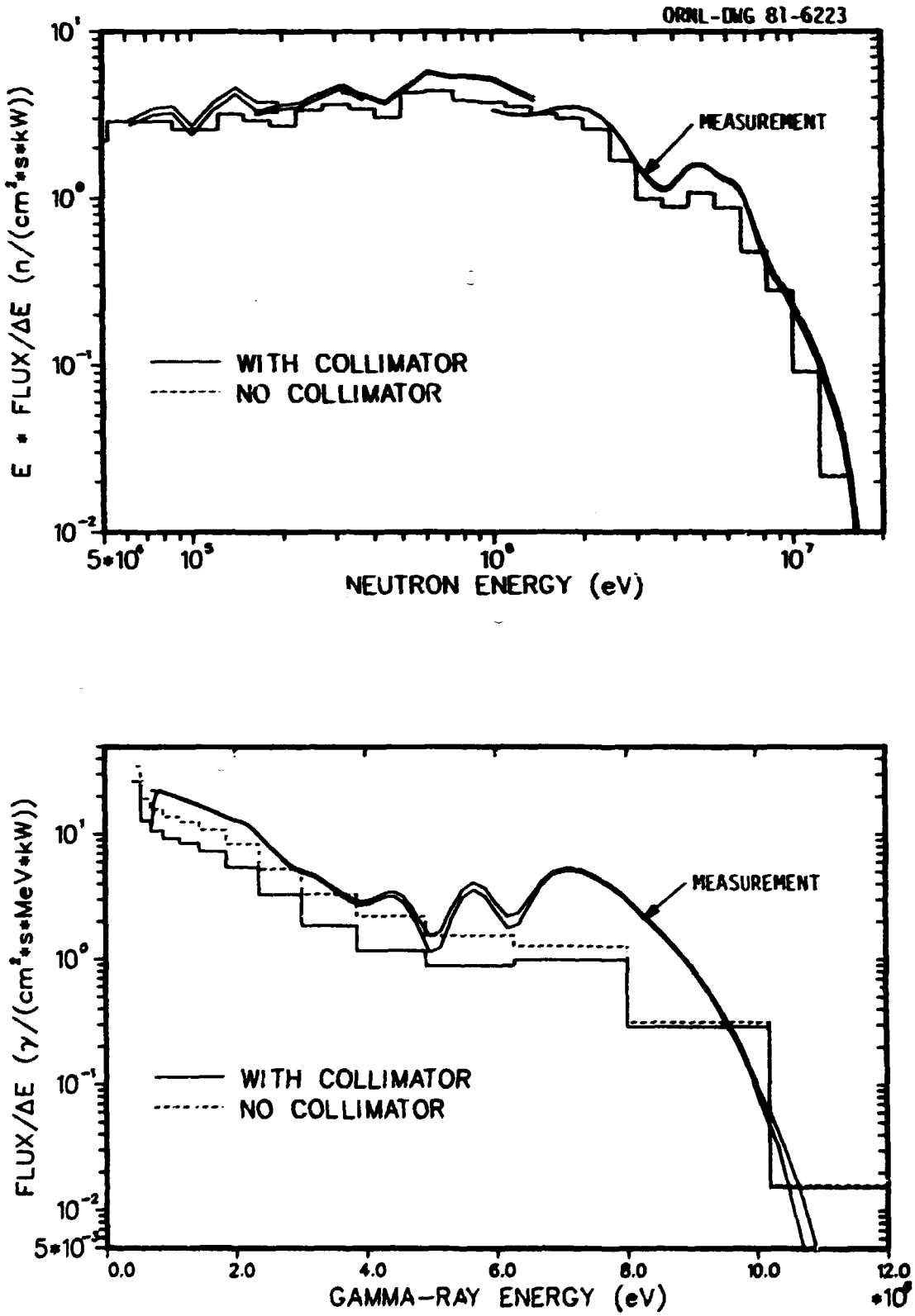

Fig. 29. Measured neutron (above) and gamma-ray (below) spectra compared to spectra calculated with and without an analytic collimator for UO_2 plus alternate inner shield (Configuration V.C).

The results shown in Figs. 28 and 29 suggest that the material regions outside the test slabs must contribute significantly to the observed gamma-ray flux. This is further demonstrated in Fig. 30 which gives an isoflux contour map for the gamma-ray flux above 1 MeV within Config. II.B. The gamma-ray flux appears to be channeled through the lithiated paraffin region resulting in a flux level at the exit of the configuration which competes with the flux emerging from the test slab. The same behavior was found to be true for other shield assemblies.

Since the angles defined by the analytic collimator are relatively precise, the observed diagreements appear to be due to the precision with which the collimator angles were defined in the experiment. Alignment of the detector collimators and shadow shields was difficult because of their size and weight and because of the large distances involved. Fortunately, this problem did not affect the neutron spectrum measurements since, for neutrons, the lithiated paraffin region appeared relatively black.

The concrete blockhouse which surrounded the spectrometer was also considered as a possible source of neutron-induced gamma rays. The importance of this contribution was estimated by performing a 1D calculation which modeled the blockhouse as an infinite annular cylinder. The source for the calculation was placed on the

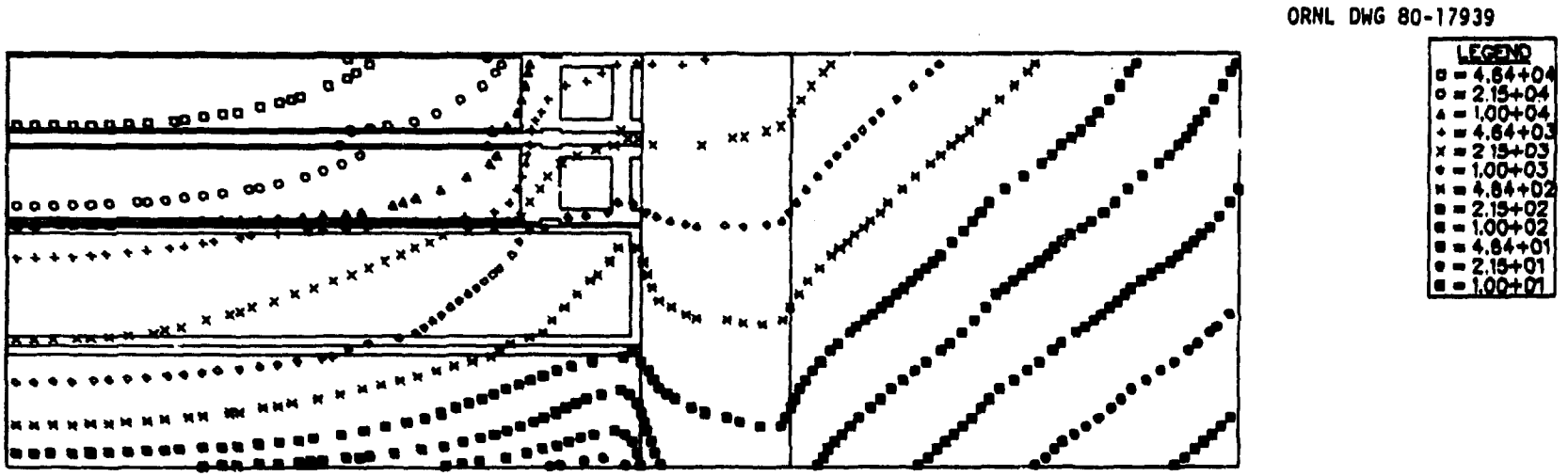

Fig. 30. Isoplot contours for the gamma-ray flux above 1 MeV within the UO_2 blanket + reference inner shield configuration (Configuration II.B).

axial centerline and was the neutron flux calculated at the detector position for Config. II.B. The calculation showed that the energy group which contained the 2.2 MeV hydrogen capture gamma ray increased 5% at the detector position, while most other groups increased less than 1%.

An additional contribution of similar magnitude was determined for neutron-induced photon production within the NE-213 detector itself. In this case, it was found that the 1.8-2.3 MeV group increased by 10-15% when detector-born gamma rays were accounted for, while most other groups increased by less than 5%. Therefore, it appears that the particular design of the experiment and the resulting difficulties in defining the precise solid angle viewed by the detector offer the best explanation to the discrepancies observed between the measured and calculated gamma-ray spectra.

6. CONCLUSIONS AND SUMMARY

Normally, the final phase in the analysis of this type of integral experiment involves expressing the results and conclusions in terms of their implications on the reactor shield design. However, prior to the completion of this analysis, the GCFR program was terminated in the United States. Furthermore, in the final year of the GCFR program, several design changes were made resulting in a significantly different shield arrangement. Therefore, a realistic interpretation of the data and analysis with respect to the GCFR has only academic value.

Fortunately, many conclusions which have generic value for fast reactor shield design can be made from the data. Firstly, it was observed that neutron transmission through UO_2 was generally underpredicted, but that for a typical blanket thickness, a maximum bias factor of only 1.3 was observed. On the other hand, neutron transmission through similar amounts of ThO_2 was predicted within the experimental uncertainties of 5-20%. The spectral characteristics of the transmitted neutron flux were predicted with comparable accuracy for the UO_2 and with somewhat lesser accuracy for the ThO_2. From the spectral comparisons, it was apparent that ENDF/B-V thorium data represented an improvement over ENDF/B-IV. Gamma-ray heating inside both the UO_2 and ThO_2 blankets was also predicted within the estimated uncertainties of 5-15%.

Secondly, it was discovered that the particular experiment design which had been successfully used for neutron measurements in many previous experiments was not appropriate for gamma-ray spectrum measurements. Specifically, the presence of the lithiated paraffin immediately adjacent to the test slabs and the method of detector collimation significantly affected the gamma-ray spectrum measurements. In future experiments requiring both neutron and gamma-ray data, the lithiated paraffin buffer zone should be replaced with a material which is compatible with both types of measurements, or a modified proceedure of detector collimation must be devised.

With respect to the shield configurations, it should be again noted that the experiment was not intended as a parametric study of shield materials, but was instead a study of specific shield designs for the GCFR. A conclusion which has generic value is that neutron transport through most of the the laminated shields was predicted to within 15%. This result is based on the integral data obtained directly behind (0.3-3 m) the shield configurations. The worst discrepancy for this data was less than 30%, while discrepancies at the 12-13 m distance generally ranged from 30 to 60%. Neutron attenuation for the individual shield assemblies was generally predicted within 15% of the integral measurements, except for one configuration where the data was likely in error. Analysis of the transmitted

neutron spectra showed that spectral differences between the calculated and measured data were generally consistent with the integral results. One exception to this was that calculations for shield configurations which included steel as the final material showed a substantial underprediction (factors of 0.5 to 2) of the neutron flux above 4 MeV.

The final conclusion with respect to the shield investigations is that the effectiveness of laminated shields which contain boron is dramatically affected by the spectral characteristics of the incident flux. This was observed for the full shield configuration which showed factors of 3 to 6 higher effectiveness for an incident blanket spectrum than for an incident core spectrum. Even for the two different blankets, a ThO_2-type spectrum resulted in a 5-15% higher shield effectiveness than a UO_2-type spectrum. This result emphasizes the importance of using a representative source spectrum for shielding-related studies, and also provides guidance toward optimizing shield designs.

The Radial Blanket and Shield Experiment and corresponding analysis benefitted the GCFR program by providing required verification of the adequacy of design methods and data. Specifically, it has shown that neutron transmission through UO_2 and ThO_2 blankets and through laminated shields containing steel, graphite, and boronated

graphite can be calculated well, even for large attenuations. It has also shown that gamma-ray heating within the blankets and shields can be calculated well. Although performed for the GCFR program, portions of the experiment and analysis have generic value for fast reactor shield design.

REFERENCES

1. General Atomic Company Project Staff, "300-MW(e) Gas-Cooled Fast Breeder Reactor Demonstration Plant," General Atomic Co. Report GA-A13045 (1974).

2. R. G. Perkins, C. J. Hamilton, and D. E. Bartine, "GCFR Shielding Design and Supporting Experimental Programs," Paper presented at Second Annual GCFR Program Technical Review, Rancho Bernardo, California, June 4-6, 1980.

3. R. G. Perkins, D. T. Ingersoll, C. J. Hamilton, "GCFR Radial Blanket and Shield Experiment Requirements," Unpublished report, General Atomic Company, February 28, 1979.

4. D. T. Ingersoll, D. E. Bartine, and F. J. Muckenthaler, "GCFR Radial Blanket and Shield Experiment: Objectives, Preanalysis, and Specifications," ORNL/TM-6956 (September 1979).

5. F. J. Muckenthaler, J. L. Hull, and J. J. Manning, "GCFR Radial Blanket and Shield Experiment," ORNL/TM-7237 (December 1980).

6. "Conceptual Shielding Configuration I," Letter to U. Gat from J. H. Broido, General Atomic Company, June 27, 1978.

7. R. W. Peelle, "Techniques Used at Oak Ridge National Laboratory for Unfolding Neutron and Gamma-Ray Pulse-Height Spectra," ORNL/TM-3463 (August 1971).

8. J. O. Johnson and D. T. Ingersoll, "User's Guide for the Revised SPEC-4 Neutron Spectrum Unfolding Code," ORNL/TM-7384 (August 1980).

9. W. A. Rhoades, D. B. Simpson, R. L. Childs, and W. W. Engle, Jr., "The DOT-IV Two-Dimensional Discrete Ordinates Transport Code with Space-Dependent Mesh and Quadrature," ORNL/TM-6529 (January 1979).

10. W. W. Engle, Jr., "A User's Manual for ANISN - A One-Dimensional Discrete Ordinates Transport Code with Anisotropic Scattering," ORGDP Report K-1693 (1967).

11. N. M. Greene, et al., "AMPX: A Modular Code System for Generating Coupled Multigroup Neutron-Gamma Libraries from ENDF/B," ORNL/TM-3706 (1976).

12. G. C. Haynes, "The AXMIX Program for Cross Section Mixing and Library Arrangement," ORNL Central Files Report 74-12-2 (December 1974).

13. R. L. Childs, "FALSTF User's Manual," draft report.

14. D. T. Ingersoll and C. O. Slater, "DOGS - A Collection of Graphics for Support of Discrete Ordinates Codes," ORNL/TM-7188 (March 1980).

15. R. E. Maerker, "Analyses of TSF Experiments on Radiation Heating in a Stainless Steel-Sodium CRBR Radial Shield Mockup Using a 32-Inch Diameter Collimated Beam Source," ORNL/TM-5992 (October 1977).

16. U. Gat and P. R. Kasten, "Gas-Cooled Fast Reactor Program Progress Report for January 1, 1974, Through June 30, 1975," ORNL-5119 (June 1976).

17. R. W. Roussin, et al., "The CTR Processed Multigroup Cross-Section Library for Neutronics Studies," ORNL/RSIC-37 (July 1980).

18. R. E. Maerker and F. J. Muckenthaler, "The Absolute Neutron Spectrum Emerging Through the Large Beam Collimator from the TSR-II Reactor at the Tower Shielding Facility," ORNL/TM-5183 (January 1976).

19. C. O. Slater, S. N. Cramer, and D. T. Ingersoll, "Analysis of the ORNL/TSF GCFR Grid-Plate Shield Design Confirmation Experiment," ORNL-5551 (August 1979).

20. R. E. Maerker, L. R. Williams, F. R. Mynatt, and N. M. Greene, "Response Functions for Bonner Ball Neutron Detectors," ORNL/TM-3451 (1971).

GCFR RADIAL BLANKET AND SHIELD EXPERIMENT (DATA PLAN)

I. ThO_2 Blanket Configurations (Priority 1A)

A. Spectrum Modifier (SM) (10.2-cm Fe + 8.9-cm Al + 2.54-cm Boral)

1. 3-, 6-, and 10-in. Bonner balls on centerline at 30.5 cm.
2. 3-, 6-, and 10-in. Bonner balls at 305 cm and NE213 or hydrogen counter location.
3. NE213 on centerline as close as feasible.
4. Hydrogen counters (1D) at NE213 location. (If NE213 run not feasible do hydrogen counters as close as feasible.)

B. Spectrum Modifier + 1.27-cm void + 6.76-cm ThO_2 slab

1. 3-, 6-, and 10-in. Bonner balls on centerline at 30.5 cm.
2. 3-, 6-, and 10-in. Bonner balls at on centerline at 305 cm.

C. Spectrum Modifier + 1.27-cm void + 7.62-cm ThO_2 + 1.27-cm void + 7.62-cm ThO_2

1. 3-, 6-, and 10-in. Bonner balls on centerline at 30.5 cm.
2. 3-, 6-, and 10-in. Bonner balls on centerline at 305 cm.

D. Spectrum Modifier + 1.27-cm void + 7.62-cm ThO_2 + 1.27-cm void + 7.62-cm ThO_2 + 1.27-cm void + 15.2-cm ThO_2

1. 3-, 6-, and 10-in. Bonner balls on centerline at 30.5 cm.
2. 3-, 6-, and 10-in. Bonner balls on centerline at 305 cm and at NE213 location.
3. NE213 on centerline as close as feasible.
4. Hydrogen counters (1D) at NE213 location.
5. TLD measurements on centerline in each void.

E. Spectrum Modifier + 1.27-cm void + 15.2-cm ThO_2 + 1.27-cm void + 7.62-cm ThO_2 + 1.27-cm void + 7.62-cm ThO_2 + 1.27-cm void + 15.2-cm ThO_2

1. 3-, 6-, and 10-in. Bonner balls on centerline at 30.5 cm.
2. 3-, 6-, and 10-in. Bonner balls on centerline at 305 cm and at NE213 location.
3. NE213 on centerline as close as feasible.
4. Hydrogen counters (1D) at NE213 location.
5. TLD measurements on centerline in each void.

F. Spectrum Modifier + 1.27-cm void + 15.2-cm ThO_2 + 1.27-cm void + 15.2-cm ThO_2 + 1.27-cm void + 7.62-cm ThO_2 + 1.27-cm void + 7.62-cm ThO_2 + 1.27-cm void + 25.4-cm Fe

1. TLD measurements on centerline in each void.

II. UO_2 Blanket Configuration (Priority 1A)

A. Spectrum Modifier + 1.27-cm void + 10.2-cm (UO_2 + Na) + 1.27-cm void + 10.2-cm (UO_2 + Na) + 1.27-cm void + 10.2-cm (UO_2 + Na)

1. 3-, 6-, and 10-in. Bonner balls on centerline at 30.5 cm.
2. 3-, 6-, and 10-in. Bonner balls on centerline at 305 cm and at NE213 location.
3. NE213 on centerline as close as feasible.
4. Hydrogen counters (ID) at NE213 location.
5. TLD measurements on centerline in each void.

B. Spectrum Modifier + 1.27-cm void + 10.2-cm (UO_2 + Na) + 1.27-cm void + 10.2-cm (UO_2 + Na) + 1.27-cm void + 10.2-cm (UO_2 + Na) + [0.95-cm SS + 12.7-cm (B_4C + C) + 1.27-cm SS] container + 15.2-cm SS

1. 3-, 6-, and 10-in. Bonner balls on centerline at 30.5 cm.
2. 3-, 6-, and 10-in. Bonner balls on centerline at 305 cm and at NE213 location.
3. NE213 on centerline as close as feasible.
4. Hydrogen counters (ID) at NE213 location.

III. Inner Radial Shield Configuration (Priority 1B)

A. Spectrum Modifier + 1.27-cm void + 15.2-cm ThO_2 + 1.27-cm void, + 7.62-cm ThO_2 + 1.27-cm void + 7.62-cm ThO_2 + 1.27-cm void + 15.2-cm ThO_2 + [0.95-cm SS + 12.7-cm (B_4C + C) + 1.27-cm SS] container

1. 3-, 6-, and 10-in. Bonner balls on centerline at 30.5 cm.
2. 3-, 6-, and 10-in. Bonner balls on centerline at 305 cm and at NE213 location.
3. NE213 on centerline as close as feasible.
4. Hydrogen counters (ID) at NE213 location.

B. Spectrum Modifier + 1.27-cm void + 15.2-cm ThO_2 + 1.27-cm void + 7.62-cm ThO_2 + 1.27-cm void + 7.62-cm ThO_2 + 1.27-cm void + 15.2-cm ThO_2 + [0.95-cm SS + 12.7-cm (B_4C + C) + 1.27-cm SS] container + 15.2-cm SS

1. 3-, 6-, and 10-in. Bonner balls on centerline at 30.5 cm.
2. 3-, 6-, and 10-in. Bonner balls on centerline at 305 cm and at NE213 location.
3. NE213 on centerline as close as feasible.
4. Hydrogen counters (ID) at NE213 location.

IV. Outer Radial Shield Configurations (Priority IC)

A. Spectrum Modifier + 1.27-cm void + 15.2-cm ThO_2 + 1.27-cm void + 7.62-cm ThO_2 + 1.27-cm void + 7.62-cm ThO_2 + 1.27-cm void + 15.2-cm ThO_2 + [0.95-cm SS + 12.7-cm (B_4C + C) + 1.27-cm SS] container + 1.27-cm void + 15.2-cm SS + 1.27-cm void + 4.45-cm SS + [0.952-cm SS + 5.1-cm (B_4C + C) + 0.8-cm SS] container

1. 3-, 6-, and 10-in. Bonner balls on centerline at 30.5 cm.
2. 3-, 6-, and 10-in. Bonner balls on centerline at 305 cm.

B. Spectrum Modifier + 1.27-cm void + 15.2-cm ThO_2 + 1.27-cm void + 7.62-cm ThO_2 + 1.27-cm void + 7.62-cm ThO_2 + 1.27-cm void + 15.2-cm ThO_2 + [0.95-cm SS + 12.7-cm (B_4C + C) + 1.27-cm SS] container + 1.27-cm void + 15.2-cm SS + 1.27-cm void + 4.45-cm SS + [0.952-cm SS + 5.1-cm (B_4C + C) + 0.8-cm SS] container + 22.9-cm graphite

1. 3-, 6-, and 10-in. Bonner balls on centerline at 30.5 cm.
2. 3-, 6-, and 10-in. Bonner balls on centerline at 305 cm.

C. Repeat B + [0.8-cm SS + 5.1-cm (B_4C + C) + 0.8-cm SS] container + 4.45-cm SS

1. 3-, 6-, and 10-in. Bonner balls on centerline at 18 cm and 30.5 cm.
2. 3-, 6-, and 10-in. Bonner balls on centerline at 305 cm and at NE213 location.
3. NE213 on centerline as close as feasible.

D. Repeat C + 35.6-cm void + 2.54-cm Fe + 61-cm concrete

1. 3-, 6-, and 10-in. Bonner balls on centerline in 35.6-cm void at 18 cm behind the SS.
2. TLD in front of 15.2-cm SS.
3. TLD behind 15.2-cm SS.
4. TLD in front of 2.54-cm Fe.

E. Spectrum Modifier + [0.95-cm SS + 12.7-cm (B_4C + C) + 1.27-cm SS] + 19.7-cm SS + [0.952-cm SS + 5.1-cm (B_4C + C) + 0.8-cm SS] + 22.9-cm graphite + [0.81-cm SS + 5.1-cm (B_4C + C) + 0.81-cm SS] + 4.45-cm SS

1. 3-, 6-, and 10-in. Bonner balls on centerline at 18 cm and 30.5 cm.
2. 3-, 6-, and 10-in. Bonner balls on centerline at 305 cm and at NE213 location.
3. NE213 on centerline as close as feasible.
4. Hydrogen counter (ID) at NE213 location.

V. Alternate Inner Radial Shield Configurations (Priority ID)

A. Spectrum Modifier + 1.27-cm void + 10.2-cm (UO_2 + Na) + 1.27-cm void + 10.2-cm (UO_2 + Na) + 1.27-cm void + 10.2-cm (UO_2 + Na)

1. 3-, 6-, and 10-in. Bonner balls on centerline at 30.5 cm.

B. Repeat A + 1.27-cm void + 15.2-cm graphite

1. 3-, 6-, and 10-in. Bonner balls on centerline at 30.5 cm and at 305 cm.
2. 3-, 6-, and 10-in. Bonner balls at NE123 location.
3. NE213 on centerline as close as feasible.
4. Hydrogen counter (ID) at NE213 location.

C. Repeat B + 1.27-cm void + [0.95-cm SS + 12.7-cm (B_4C + C) + 1.27-cm SS] container + 1.27-cm void + 4.45-cm SS

1. 3-, 6-, and 10-in. Bonner balls on centerline at 30.5 cm and 305 cm.
2. 3-, 6-, and 10-in. Bonner balls at NE213 location.
3. NE213 on centerline as close as feasible.
4. Hydrogen counter (ID) at NE213 location.
5. TLD on centerline in all voids following UO_2.

D. Repeat B + 1.27-cm void + [0.95-cm SS + 12.7-cm (B_4C + C) + 1.27 cm SS] container + 1.27-cm void + 15.2-cm SS + 1.27-cm void + 4.45-cm SS

1. 3-, 6-, and 10-in. Bonner balls on centerline at 30.5 cm and at 305 cm.
2. TLD on centerline in all voids following UO_2.

E. Spectrum Modifier + 1.27-cm void + 10.2-cm (UO_2 + Na) + 1.27-cm void + 10.2-cm (UO_2 + Na) + 1.27-cm void + [0.95-cm SS + 12.7-cm (B_4C + C) + 1.27-cm SS] container + 1.27-cm void + 4.45-cm SS

1. 3-, 6-, and 10-in. Bonner balls on centerline at 30.5 cm and at 305 cm.
2. TLD on centerline in all voids beyond UO_2 blanket.

VI. Reactor Source Measurement

A. 15.2-cm lead

1. NE213 on centerline as close as feasible.

B. 15.2-cm lead + spectrum modifier

1. NE213 on centerline as close as feasible.

C. 30.6-cm UO_2

1. NE213 on centerline as close as feasible.

D. 30.6-cm UO_2 + spectrum modifier

1. 3-, 6-, and 10-in. Bonner balls at same location as NE213.
2. NE213 on centerline as close as feasible.

APPENDIX B

Calculational Parameters

The significant input parameters used for a typical DOT-IV calculation are listed in Fig. B-1. The specific case presented is Configuration III.B which comprised the spectrum modifier, a 45-cm ThO_2 blanket mockup, and the reference inner shield mockup. The top boundary source had been previously computed as an internal boundary angular flux at the center of the ThO_2 blanket from the Configuration III.A calculation. Additionally, the boundary angular flux at the blanket/shield interface was saved in this case to be used as an external boundary source for subsequent shield calculations. The same radial mesh was used for all cases which included the ThO_2 blanket slabs, while the UO_2 cases used a somewhat different radial mesh. The same S_{10} angular quadrature was used for all calculations.

Input parameters for the corresponding FALSTF calculation are listed in Fig. B-2. The distributed source output tape from the previous DOT-IV calculation was used as the input tape for FALSTF and the same macroscopic cross sections were used for both the DOT-IV and FALSTF cases.

```
                    SN + 1D IN THO2 BLANKET + INNER SHIELD - BS TOP OF BLKT SECT 4

&1 $ $

MTPLX  =     0        PLOT GROSS INPUT UNIT IF .GT. 0
MTPOG  =    20        PLOT OUTPUT UNIT IF .GT. 0
MTSIG  =     9        CROSS SECTION UNIT
MTBSI  =    10        BOUNDARY SOURCE INPUT UNIT IF.GT.0
MTDSI  =     0        DISTRIBUTED SOURCE INPUT UNIT IF.GT.0 (SUPPLY SCRATCH IF INESRM.GT.0)

MTFCI  =     0        FIRST-COLLISION SOURCE INPUT UNIT IF.GT.0
MTIBI  =     0        INTERNAL BOUNDARY SOURCE INPUT  IF.GT.0
MTIBO  =    24        INTERNAL BOUNDARY FLUX OUTPUT IF.GT.0
MTMPP  =     0        LARGE-SCALE PRINT UNIT IF.GT.0
MTDIS  =     0        DIRECTIONAL FLUX OUTPUT UNIT IF.GT.0

10

MTDSO  =    22        DISTRIBUTED SOURCE OUTPUT UNIT IF.GT.0


&2 $ $

IADJ   =     0        0/1 = FORWARD/ADJOINT CALCULATION
ISCT   =     3        MAXIMUM ORDER OF SCATTERING
IZM    =    11        NUMBER OF MATERIAL ZONES
IM     =    50        NUMBER OF RADIAL INTERVALS (NEGATIVE INDICATES VARIABLE MESH IS USED)
JM     =    62        NUMBER OF AXIAL INTERVALS

IGM    =    76        NUMBER OF ENERGY GROUPS
IHT    =     5        POSITION OF TOTAL CROSS SECTION
IHS    =     6        POSITION OF SELF-SCATTER CROSS SECTION
IHM    =    91        CROSS SECTION TABLE LENGTH PER GROUP
MXX    =     0        MIXING TABLE LENGTH

10

MCR    =     0        RESERVED
MTP    =     0        NUMBER OF MATERIALS FROM MTSIG (0 IMPLIES MTM FROM MTSIG)
MTM    =    28        TOTAL NUMBER OF MATERIALS
IDPAC  =     0        0/1   NO DENS FACS/D(I,J) INPUT
MM     =    70        MAXIMUM NUMBER OF DIRECTIONS IN QUADRATURE     (NEGATIVE INDICATES VARIABLE QUADRATURE IS USED)

INGEOM =     1        0/1/2/3/4/5/6 = X-Y/R-Z/R-THETA/180-360 TRI/60 TRI/90 TRI/120 TRI  GEOMETRY
IBL    =     1        0 = VOID          4 = FXD BNDRY SRCE
IBR    =     0        1 = REFLECTED
IBB    =     0        2 = PERIODIC      5 = ALBEDO
IBT    =     4        3 = CYLINDRICAL

20

ISCM   =     2        SOURCE ITERATION MAXIMUM
IPXMI  =    -2        INITIAL FLUX ITERATION MAXIMUM PER GROUP   (NEGATIVE INDICATES LIMIT BY GROUP)
IPXMF  =     0        ALTERNATE FLUX ITERATION MAXIMUM PER GROUP (IP.GT.0)
MODE   =     3        0/1/2/3/4/5 = LIN-ZERO/ LINEAR/ STEP/ WEIGHTED/ LIN-THETA WEIGHTED/ THETA WEIGHTED
ITTPE  =     0        0/1/2/3/4 = FIXED SOURCE/K/DB2 SEARCH/CONCENTRATION SEARCH/DIMENSION SEARCH
```

Fig. B-1. Input parameters for typical DOT-IV calculation.

```
IACC   =     2        0/  2 = GROUPWISE REBALANCE/DIFFUSION ACCELERATION/PARTIAL FLOW REBALANCE (DEFAULT=2)
IALF   =     0        0/1 = STANDARD STABILIZATION/ALTERNATE
IGTYPE =     0        0/N = DISCRETE ORDINATES/THEORY SPECIFIED BY GROUP FOR N OUTERS, THEN PURE DISCRETE ORDINATES
INPFIN =     0        0/1/2/3 = FLUX 0 OR ON TAPE /F(IJ),G/FIJ(I,J)*FG(G)/FI(I)*FJ(J)*FG(G)
INPSRN =     0        DISTRIBUTED SOURCE INPUT, SAME AS INPFIN   (REQUIRES NTDSI.GT.0)

30

NJNTSR =     0        0/N = NO EFFECT/INTERIOR BOUNDARY SOURCE AT N J-BOUNDARIES INPUT FROM NTIBI
NINTSR =     0        0/N = NO EFFECT/INTERIOR BOUNDARY SOURCE AT N I-BOUNDARIES INPUT FROM NTIBI
NJNTFX =     1        0/N = NO EFFECT/INTERIOR BOUNDARY FLUX   AT N J-BOUNDARIES WRITTEN ON NTIBO
NINTFX =     0        0/N = NO EFFECT/INTERIOR BOUNDARY FLUX   AT N I-BOUNDARIES WRITTEN ON NTIBO
IACT   =     0        -N/N = CALCULATE N ZONEWISE ACTIVITIES/N ZONE AND POINT ACTIVITIES

IEED   =    11        0/N = NO EFFECT/CALCULATE N REGION EDITS
IED02  =     0        0/1/2/3 = NO EFFECT/PUNCH 1 D02 VALUE, IGM VALUES, IGM*IRED VALUES (NEG INDICATES NO BALANCE PRINT)
IFXDFT =     1        0/1/2 SCALAR FLUX PRINTED/NOT PRINTED/PRINTED AS CALCULATED
ICSPFT =     1        0/1 = CROSS SECTIONS PRINTED/NOT PRINTED
IDIOF  =     0        0/1/2 = DIRECTIONAL FLUX NOT SAVED/SAVED AND PRINTED/SAVED BUT NOT PRINTED

40

JDIPF  =     0        0/N = NO EFFECT/FIRST AXIAL INTERVAL FOR DIRECTIONAL FLUX OUTPUT
IDIPL  =     0        0/N = NO EFFECT/ LAST AXIAL INTERVAL FOR DIRECTIONAL FLUX OUTPUT
NBUF   =    40        SYSTEM BUFFER SPACE (IBM-DEFAULT=60K BYTES, UNIVAC-DEFAULT=2 K-WORDS, CDC-NO EFFECT)
IEPSBT =     0        0/1/11/21 = NO EFFECT/USE ZONE INPT. CONVG./1*PRINT CNVG./11*PRINT EVERY ITN
NINMJX =     0        MINIMUM J-BLOCKING (0=ALL GROUPS STORED IN MEMORY IF POSSIBLE, NV=0)

MAXMJF =     0        MAXIMUM J-BLOCKING (0 IMPLIES JM)
ISBT   =     1        I SET FOR BOUNDARIES        (DEFAULT=1)
NSBT   =     1        N SET FOR BOUNDARIES        (DEFAULT=1)
NSDM   =     1        N SET FOR DIMENSIONING      (DEFAULT=1)
IBFSCL =     1        NO. FLX ITNS BEFORE  REBALANCE (DEFAULT=1)

50

INISCL =     4        MIN NO. REBALANCE ITERATIONS (DEFAULT=4)
INTSCL =   100        MAX NO. REBALANCE ITERATIONS (DEFAULT=100)
NOFIS  =     1        0/1/2 NORMALIZED FISSION/UNNORMALIZED FISSION/NO FISSION
IFDF2S =     0        0/1 NO EFFECT/ED2 SUPPLIED BY GROUP, ZONE
ISWP   =     0        TYPE OF SWEEP(DIFFUSION THEORY, NV=4 OR 5)

NEYJN  =     1        J-INTERVAL FOR KEY FLUX OUTPUT (0 IGNORED)
NEYIN  =     1        I-INTERVAL FOR KEY FLUX OUTPUT (0 IGNORED)
NSIGTP =     0        0/1 NTSIG IS GIP FORMAT/ORDOSW FORMAT
NORPOS =     0        0/N = NO EFFECT/NORMALIZE TO POSITION N (NEG INDICATES APPLICABLE ZONES READ IN)
NORMAT =     0        0/N = NORMALIZE TO MACRO MATERIAL/NORMALIZE TO MATERIAL N (NEG INDICATES DO NOT APPLY DENSITY FACTOR)

60

MSTMAX =     0        MAXIMUM NUMBER OF M-SETS (0 IMPLIES MSTMAX=JM)
NEGFIX =     0        0/1 NO EFFECT/NEG SOURCE FIXUP (NV=0)
LOCOBJ =     0        FAST MEMORY OBJECTIVE (0 IMPLIES CDC- 38 K-WORDS, UNIVAC- 25 K-WORDS, IBM- RESERVED)
LCMOBJ =     0        SLOW MEMORY OBJECTIVE (0 IMPLIES CDC- 131 K-WORDS, OTHERS- NO EFFECT)
MKEYFX =     0        -N/N = LENGTH OF KEY FLUX ARRAY, IF ANY (NEGATIVE PRINTS ARRAY ONLY AT GROUP CONVERGENCE)
```

Fig. B-1. Cont'd

```
$3 * *

TMAX    = 1.500000E+02    MAXIMUM CPU TIME FOR THIS PROB(IGNORED IF 0)
SNF     = 0.0             SOURCE NORMALIZATION FACTOR (IGNORED IF 0)
EPS     = 0.0             EIGENVALUE CONVERGENCE CRITERION
EPP     = 1.000000E-03    POINTWISE FLUX CONVERGENCE CRITERION (NEGATIVE IMPLIES COARSE MESH CONVERGENCE)
EPV     = 0.0             VOLUMETRIC FLUX CONVERGENCE CRITERION

EPF     = 1.000000E-01    FISSION CONVERGENCE CRITERION
IKODJ   = 0.0             KEFF SOUGHT IN SEARCH (KTYPE.GT.1) OR INITIAL KEFF(KTYPE.EQ.1)  (DEFAULT=1.)
EVTH    = 0.0             KEFF CONVERGENCE RATIO (DEFAULT=0.2)
EVCHG   = 0.0             MAXIMUM EV CHANGE RATIO, EACH ITERATION  (DEFAULT=1.5)
EVMAX   = 0.0             MAXIMUM EV CHANGE RATIO, OVERALL         (DEFAULT=10.)

10

EVKMX   = 0.0             MAXIMUM ALLOWED KEFF-1 (DEFAULT=1.)
EVI     = 0.0             INITIAL EIGENVALUE (DEFAULT=1.)
DEVDFI  = 0.0             INITIAL EIGENVALUE SLOPE (DEFAULT=-1.)
EVDELX  = 0.0             INITIAL EIGENVALUE INCREMENT (DEFAULT=0.3)
SORMIN  = 0.0             MAXIMUM ERROR-MODE ADJUSTMENT RATIO (DEFAULT=1.2)

CONACC  = 1.000000E+00    REBALANCE ACCEPTANCE CRITERION (DEFAULT=1.0E10)
CONSCL  = 1.000000E-04    SPATIAL REBALANCE CONVERGENCE CRITERION (DEFAULT=1.0E-4)
CONFIX  = 0.0             FLUX FIXUP THRESHOLD (DEFAULT=0.3)
ASOLOI  = 0.0             REBALANCE MINIMUM DOMINANCE RATIO (RV=0.3)
ASOLIT  = 5.000000E-01    REBAL FLUX ITN COEF (DEFAULT=0.5)

20

ASOLCN  = 8.000000E+00    REBAL CONSTANT (DEFAULT=1.)
ORF     = 6.000000E-01    FLUX ACCELERATION FACTOR (DIFFUSION THEORY ONLY, DEFAULT=0.6)
FSNACC  = 0.0             FISSION ACCELERATION FACTOR (RV=0)
FLXMIN  = 1.000000E-60    MINIMUM FLUX FOR CONVERGENCE TESTS (DEFAULT=1.0E-60 (UNIVAC =1.0E-30) )
SMOOTH  = 0.0             RESERVED

EPO     = 0.0             SOURCE ITERATION FLUX CONVERGENCE CRITERION
EXTACV  = 1.000000E-01    EXTRAPOLATION CONVERGENCE CRITERION (DEFAULT=0.1)
THETA   = 5.000000E-01    THETA-WEIGHTED PARAMETER (DEFAULT=0.9 )
```

Fig. B-1. Cont'd

	VECTOR	NUCLIDE	DENSITY	MATERIAL	MATL/ZONE	PER INPT	CPI
1					-1		8.108008-04
2					-5		1.863608-03
3					-13		6.020698-03
4					-13		1.073508-02
5					-13		2.875608-02
6					-13		8.668608-02
7					-13		6.520698-02
8					-25		8.089898-02
9					-17		9.090398-02
10					-9		9.438298-02
11					-9		9.193098-02
12							8.503998-02
13							7.588998-02
14							6.671698-02
15							5.601608-02
16							8.609808-02
17							3.535708-02
18							2.793808-02
19							2.181608-02
20							1.687108-02
21							1.298508-02
22							9.868708-03
23							7.488198-03
24							5.651508-03
25							6.730608-03
26							5.258308-03
27							1.899408-03
28							1.033508-03
29							7.139308-04
30							8.926308-04
31							3.396208-04
32							5.059808-04
33							1.287908-04
34							3.609808-05
35							2.802408-05
36							1.706808-05
37							1.173508-05
38							0.0
39							0.0
40							0.0
41							0.0
42							0.0
43							0.0
44							0.0
45							0.0
46							0.0
47							0.0
48							0.0
49							0.0
50							0.0
51							0.0
52							0.0
53							0.0
54							0.0
55							0.0
56							0.0
57							0.0
58							0.0
59							0.0
60							0.0
61							0.0
62							0.0
63							0.0
64							0.0
65							0.0
66							0.0
67							0.0
68							0.0
69							0.0
70							0.0
71							0.0
72							0.0
73							0.0
74							0.0
75							0.0
76							0.0

Fig. B-1. Cont'd

SR CONSTANTS FOR DIRECTION SET 1

	WEIGHT	ETA	BETA	RO-RATE	ETA-RATE	LEVEL-RATE
1	0.0	-2.269469E-01	9.739067E-01	0.0	1	36	36
2	1.666780E-02	-1.888780E-01	9.739067E-01	1.888780E-01	1	37	36
3	1.666780E-02	1.888780E-01	9.739067E-01	1.888780E-01	2	38	36
4	0.0	-5.014662E-01	8.650631E-01	0.0	3	39	39
5	2.888180E-02	-8.333955E-01	8.650631E-01	8.333955E-01	0	00	39
6	1.292110E-02	-1.888780E-01	8.650631E-01	1.788520E+00	7	01	39
7	1.292110E-02	1.888780E-01	8.650631E-01	1.788510E+00	6	02	39
8	2.888180E-02	8.333955E-01	8.650631E-01	8.333940E-01	5	03	39
9	0.0	-7.337590E-01	6.790899E-01	0.0	15	00	00
10	2.701110E-02	-6.790899E-01	6.790899E-01	6.790899E-01	15	05	00
11	8.550360E-03	-8.333955E-01	6.790899E-01	8.726100E+00	10	06	00
12	1.921930E-02	-1.888780E-01	6.790899E-01	2.005260E+00	13	07	00
13	1.921930E-02	1.888780E-01	6.790899E-01	2.005260E+00	12	08	00
14	8.550960E-03	8.333955E-01	6.790899E-01	8.726130E+00	11	09	00
15	2.701110E-02	6.790899E-01	6.790899E-01	6.790860E-01	10	50	00
16	0.0	-9.012080E-01	8.333955E-01	0.0	25	51	51
17	2.888110E-02	-8.650631E-01	8.333955E-01	8.650631E-01	25	52	51
18	8.550860E-01	-6.790899E-01	8.333955E-01	5.625280E+00	23	53	51
19	2.706790E-02	-8.333955E-01	8.333955E-01	2.195880E+00	22	54	51
20	8.857870E-03	-1.888780E-01	8.333955E-01	1.108230E+01	21	55	51
21	8.857870E-03	1.888780E-01	8.333955E-01	1.108230E+01	20	56	51
22	2.706790E-02	8.333955E-01	8.333955E-01	2.195870E+00	19	57	51
23	8.550860E-03	6.790899E-01	8.333955E-01	5.625280E+00	18	58	51
24	2.888180E-02	8.650631E-01	8.333955E-01	8.650899E-01	17	59	51
25	0.0	-9.888560E-01	1.888780E-01	0.0	35	60	60
26	1.666780E-02	-9.739067E-01	1.888780E-01	9.739067E-01	35	61	60
27	1.292110E-02	-8.650631E-01	1.888780E-01	3.377670E+00	34	62	60
28	1.921930E-02	-6.790899E-01	1.888780E-01	1.533120E+00	33	63	60
29	8.857870E-03	-8.333955E-01	1.888780E-01	1.223490E+01	32	64	60
30	1.822870E-02	-1.888780E-01	1.888780E-01	8.915330E+00	31	65	60
31	1.822870E-02	1.888780E-01	1.888780E-01	8.915330E+00	30	66	60
32	8.857870E-03	8.333955E-01	1.888780E-01	1.223490E+01	29	67	60
33	1.921930E-02	6.790899E-01	1.888780E-01	3.533100E+00	28	68	60
34	1.292110E-02	8.650631E-01	1.888780E-01	3.377640E+00	27	69	60
35	1.666780E-02	9.739067E-01	1.888780E-01	9.738780E-01	26	70	60
36	0.0	-2.269469E-01	9.739067E-01	0.0	38	1	1
37	1.666780E-02	-1.888780E-01	9.739067E-01	1.888780E-01	39	2	1
38	1.666780E-02	1.888780E-01	9.739067E-01	1.888780E-01	37	1	1
39	0.0	-5.014662E-01	8.650631E-01	0.0	03	0	0
40	2.888180E-02	-8.333955E-01	8.650631E-01	8.333950E-01	03	5	0
41	1.292110E-02	-1.888780E-01	8.650631E-01	1.788520E+00	02	6	0
42	1.292110E-02	1.888780E-01	8.650631E-01	1.788510E+00	01	7	0
43	2.888180E-02	8.333955E-01	8.650631E-01	8.333940E-01	00	8	0
44	0.0	-7.337590E-01	6.790899E-01	0.0	50	9	9
45	2.701110E-02	-6.790899E-01	6.790899E-01	6.790899E-01	50	10	9
46	8.550360E-03	-8.333955E-01	6.790899E-01	8.726100E+00	49	11	9
47	1.921930E-02	-1.888780E-01	6.790899E-01	2.005260E+00	48	12	9
48	1.921930E-02	1.888780E-01	6.790899E-01	2.005260E+00	47	13	9
49	8.550960E-03	8.333950E-01	6.790899E-01	8.726110E+00	46	14	9
50	2.701110E-02	6.790899E-01	6.790899E-01	6.790860E-01	45	15	9
51	0.0	-9.012080E-01	8.333955E-01	0.0	59	16	16
52	2.888180E-02	-8.650631E-01	8.333955E-01	8.650631E-01	59	17	16
53	8.550360E-03	-6.790899E-01	8.333955E-01	5.625280E+00	58	18	16
54	2.706790E-02	-8.333955E-01	8.333955E-01	2.195880E+00	57	19	16
55	8.857870E-01	-1.888780E-01	8.333955E-01	1.108230E+01	56	20	16
56	8.857870E-01	1.888780E-01	8.333955E-01	1.108230E+01	55	21	16
57	2.706790E-02	8.333950E-01	8.333955E-01	2.195870E+00	54	22	16
58	8.550960E-01	6.790899E-01	8.333955E-01	5.625260E+00	53	23	16
59	2.888180E-02	8.650631E-01	8.333955E-01	9.650869E-01	52	24	16
60	0.0	-9.888560E-01	1.888780E-01	0.0	70	25	25
61	1.666780E-02	-9.739067E-01	1.888780E-01	9.739067E-01	70	26	25
62	1.292110E-02	-8.650631E-01	1.888780E-01	3.377670E+00	69	27	25
63	1.921930E-02	-6.790899E-01	1.888780E-01	1.533120E+00	68	28	25
64	8.857870E-01	-8.333955E-01	1.888780E-01	1.223490E+01	67	29	25
65	1.822870E-02	-1.888780E-01	1.888780E-01	8.915330E+00	66	30	25
66	1.822870E-02	1.888780E-01	1.888780E-01	8.915330E+00	65	31	25
67	8.857870E-01	8.333955E-01	1.888780E-01	1.223490E+01	64	32	25
68	1.921930E-02	6.790899E-01	1.888780E-01	3.533100E+00	63	33	25
69	1.292110E-02	8.650631E-01	1.888780E-01	1.377640E+00	62	34	25
70	1.666780E-02	9.739067E-01	1.888780E-01	9.738780E-01	61	35	25

Fig. B-1. Cont'd

INITIAL J-MESH

	HEIGHT	MIDPOINT	DELTA Z
1	-2.010000E+02	-2.006700E+02	6.600000E-01
2	-2.003400E+02	-2.000100E+02	6.600000E-01
3	-1.996800E+02	-1.993500E+02	6.600000E-01
4	-1.990200E+02	-1.986900E+02	6.599988E-01
5	-1.983600E+02	-1.980300E+02	6.600000E-01
6	-1.977000E+02	-1.973700E+02	6.600000E-01
7	-1.970400E+02	-1.967100E+02	6.600000E-01
8	-1.963800E+02	-1.960500E+02	6.599988E-01
9	-1.957200E+02	-1.953900E+02	6.600000E-01
10	-1.950600E+02	-1.947300E+02	6.600000E-01
11	-1.944000E+02	-1.940700E+02	6.600000E-01
12	-1.937400E+02	-1.934100E+02	6.600000E-01
13	-1.930800E+02	-1.927500E+02	6.600000E-01
14	-1.924200E+02	-1.920900E+02	6.600000E-01
15	-1.917600E+02	-1.914300E+02	6.600000E-01
16	-1.911000E+02	-1.907700E+02	6.600000E-01
17	-1.904400E+02	-1.901100E+02	6.600000E-01
18	-1.897800E+02	-1.894500E+02	6.600000E-01
19	-1.891200E+02	-1.887900E+02	6.600000E-01
20	-1.884600E+02	-1.881300E+02	6.600000E-01
21	-1.878000E+02	-1.874700E+02	6.600000E-01
22	-1.871400E+02	-1.868100E+02	6.600000E-01
23	-1.864800E+02	-1.861500E+02	6.600000E-01
24	-1.858200E+02	-1.854900E+02	6.600000E-01
25	-1.851600E+02	-1.848300E+02	6.600000E-01
26	-1.845000E+02	-1.841700E+02	6.600000E-01
27	-1.838400E+02	-1.835100E+02	6.600000E-01
28	-1.831800E+02	-1.828500E+02	6.600000E-01
29	-1.825200E+02	-1.821900E+02	6.600000E-01
30	-1.818600E+02	-1.815300E+02	6.600000E-01
31	-1.812000E+02	-1.808700E+02	6.600000E-01
32	-1.805400E+02	-1.802100E+02	6.600000E-01
33	-1.798800E+02	-1.795500E+02	6.600000E-01
34	-1.792200E+02	-1.788900E+02	6.600000E-01
35	-1.785600E+02	-1.782300E+02	6.600000E-01
36	-1.779000E+02	-1.775700E+02	6.600000E-01
37	-1.772400E+02	-1.769100E+02	6.600000E-01
38	-1.765800E+02	-1.762500E+02	6.600000E-01
39	-1.759200E+02	-1.755900E+02	6.600000E-01
40	-1.752600E+02	-1.749300E+02	6.600000E-01
41	-1.746000E+02	-1.742700E+02	6.600000E-01
42	-1.739400E+02	-1.736100E+02	6.600000E-01
43	-1.732800E+02	-1.729500E+02	6.600000E-01
44	-1.726200E+02	-1.722900E+02	6.600000E-01
45	-1.719600E+02	-1.716300E+02	6.600000E-01
46	-1.713000E+02	-1.709700E+02	6.600000E-01
47	-1.706400E+02	-1.703100E+02	6.600000E-01
48	-1.699800E+02	-1.696500E+02	6.600000E-01
49	-1.693200E+02	-1.689900E+02	6.600000E-01
50	-1.686600E+02	-1.683300E+02	6.600000E-01
51	-1.680000E+02	-1.676700E+02	6.600000E-01
52	-1.673400E+02	-1.670100E+02	6.600000E-01
53	-1.666800E+02	-1.663500E+02	6.600000E-01
54	-1.660200E+02	-1.656900E+02	6.600000E-01
55	-1.653600E+02	-1.650300E+02	6.600000E-01
56	-1.647000E+02	-1.643700E+02	6.600000E-01
57	-1.640400E+02	-1.637100E+02	6.600000E-01
58	-1.633800E+02	-1.630500E+02	6.600000E-01
59	-1.627200E+02	-1.623900E+02	6.600000E-01
60	-1.620600E+02	-1.617300E+02	6.600000E-01
61	-1.614000E+02	-1.610700E+02	6.600000E-01
62	-1.607400E+02	-1.604100E+02	6.600000E-01
63	-1.600800E+02		

INITIAL I-MESH ST? 1

	RATIOS	MIDPOINT	DELTA R
1	0.0	1.270000E+00	2.540000E+00
2	2.540000E+00	3.810000E+00	2.540000E+00
3	5.080000E+00	6.350000E+00	2.540000E+00
4	7.620000E+00	8.890000E+00	2.540000E+00
5	1.016000E+01	1.143000E+01	2.540000E+00
6	1.270000E+01	1.397000E+01	2.540000E+00
7	1.524000E+01	1.651000E+01	2.539999E+00
8	1.778000E+01	1.905000E+01	2.540001E+00
9	2.032000E+01	2.159000E+01	2.539999E+00
10	2.286000E+01	2.413000E+01	2.539999E+00
11	2.540000E+01	2.667000E+01	2.540001E+00
12	2.794000E+01	2.921000E+01	2.539999E+00
13	3.048000E+01	3.175000E+01	2.539999E+00
14	3.302000E+01	3.429000E+01	2.540001E+00
15	3.556000E+01	3.683000E+01	2.540001E+00
16	3.810000E+01	3.937000E+01	2.539999E+00
17	4.064000E+01	4.191000E+01	2.539999E+00
18	4.318000E+01	4.445000E+01	2.539999E+00
19	4.572000E+01	4.699000E+01	2.539999E+00
20	4.826000E+01	4.953000E+01	2.539999E+00
21	5.080000E+01	5.207000E+01	2.539999E+00
22	5.334000E+01	5.461000E+01	2.539999E+00
23	5.588000E+01	5.715000E+01	2.539999E+00
24	5.842000E+01	5.969000E+01	2.539999E+00
25	6.096000E+01	6.223000E+01	2.539999E+00
26	6.350000E+01	6.477000E+01	2.539999E+00
27	6.604000E+01	6.731000E+01	2.539999E+00
28	6.858000E+01	6.985000E+01	2.539999E+00
29	7.112000E+01	7.239000E+01	2.539999E+00
30	7.366000E+01	7.493000E+01	2.539999E+00
31	7.620000E+01	7.747000E+01	2.539999E+00
32	7.874000E+01	8.001000E+01	2.539999E+00
33	8.128000E+01	8.255000E+01	2.539999E+00
34	8.382000E+01	8.509000E+01	2.539999E+00
35	8.636000E+01	8.763000E+01	2.539999E+00
36	8.890000E+01	9.017000E+01	2.539999E+00
37	9.144000E+01	9.271000E+01	2.539999E+00
38	9.398000E+01	9.525000E+01	2.539999E+00
39	9.652000E+01	9.779000E+01	2.539999E+00
40	9.906000E+01	1.003300E+02	2.539999E+00
41	1.016000E+02	1.028700E+02	2.539999E+00
42	1.041400E+02	1.054100E+02	2.539999E+00
43	1.066800E+02	1.079500E+02	2.539999E+00
44	1.092200E+02	1.104900E+02	2.539999E+00
45	1.117600E+02	1.130300E+02	2.539999E+00
46	1.143000E+02	1.155700E+02	2.539999E+00
47	1.168400E+02	1.181100E+02	2.539999E+00
48	1.193800E+02	1.206500E+02	2.539999E+00
49	1.219200E+02	1.231900E+02	2.539999E+00
50	1.244600E+02	1.257300E+02	2.539999E+00
51	1.270000E+02		

Fig. B-1. Cont'd

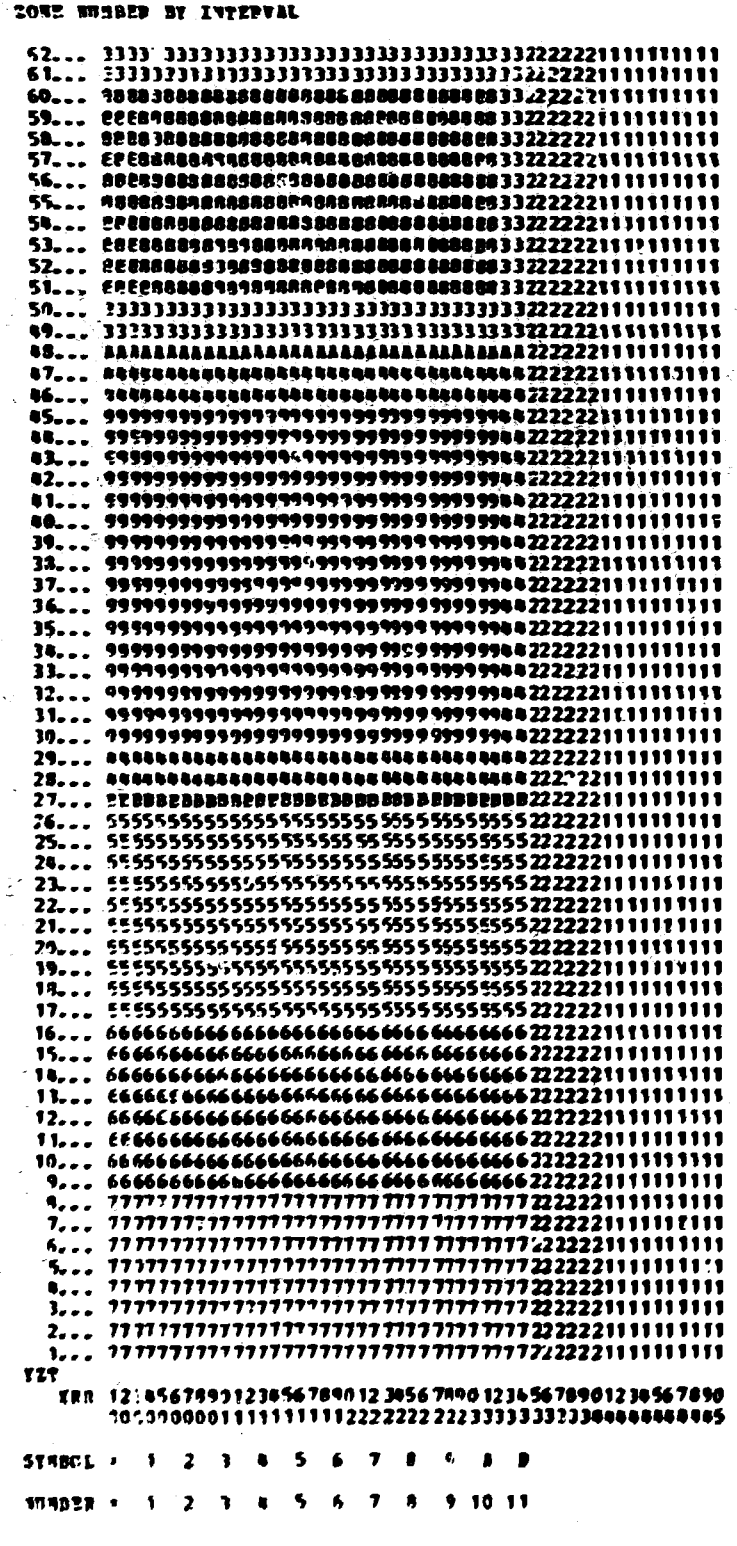

Fig. B-1. Cont'd

```
SN = 16 IN THO2 BLANKET + INNER SHIELD - BS TOP OF BLKT SECT 4

CONTROL PARAMETERS (1S)

    3   ISCT -- MAXIMUM ORDER OF SCATTERING (AO) IN DOT INPUT)
   11   IZM  -- NUMBER OF ZONES
   50   IM   -- NUMBER OF RADIAL INTERVALS
   62   JM   -- NUMBER OF AXIAL INTERVALS
   76   IGM  -- NUMBER OF ENERGY GROUPS
    5   INT  -- POSITION OF TOTAL CROSS SECTION IN C. S. TABLE
    6   IAS  -- POSITION OF SELF-SCATTER CROSS SECTION IN TABLE
   91   I1M  -- CROSS SECTION TABLE LENGTH (ITL IN DOT INPUT
    0   MS   -- CROSS SECTION MIXING TABLE LENGTH (MT1 IN DOT)
    0   NCR  -- NUMBER OF CROSS SECTION SETS FROM CARDS (1M)
   2M   NTP  -- NUMBER OF CROSS SECTION SETS FROM TAPE (NOM "SAC FOR IDAT1=2)
   2M   MT   -- TOTAL NUMBER OF CROSS SECTION SETS
    1   NOA  -- NUMBER OF POINTS FOR AZIMUTHAL ANGULAR INTEGRALS
    2   ICAT1-- 0/1/2  ALL IN CORE/ C.S. ON DISK / C.S. FROM GIP
    1   IPRTC-- 0/1  PRINT C.S./ DO NOT PRINT C.S.
    3   NDET -- NUMBER OF DETECTORS
    1   NACT -- NUMBER OF ACTIVITIES
    2   NREG -- NUMBER OF REGIONS (OUTPUTS CONTRIBUTION BY REG.)


CONTROL PARAMETERS (2S  IF ENTERED)

   10   NFSO -- INPUT UNIT FOR FALSTF INPUT TAPE
    1   NTYPE-- 0/1/2  NFSO CONTAINS  SCALAR FLUX TAPE / FINAL TOTAL SCATTERING SOURCE TAPE/ FIRST COLLISION SOURCE TAPE
    0   ITH  -- 0/1  FORWARD C.S. / ADJOINT C. S.
    1   NUM  -- 0/1  NO EFFECT / PUNCH 1 RESPONSE BY DETECTOR AND GROUP  ( W. A. MANNES MEMORIAL OPTION)
    1   NSH  --  RESPONSE TO BE PUNCHED (NUM.EQ.1)
10000   LBL  --  BLKSIZE IN FBSAM DD STATEMENT
   10   NBL  --  MAXIMUM NUMBER OF BLOCKS PER LOGICAL RECORD (FBSAM UNIT ONLY)
    1   NERC --  0/1 FOLLOW FBSAM ERROR PROCEDURES / IGNORE FBSAM I/O ERRORS


CONTROL PARAMETERS (1S  IF(ENTERED)

    0   NTRI -- NUMBER OF TRIANGLES (USED FOR LIMITED BOTTOM INTEGRATION)
    0   NPNT -- NUMBER OF POINTS (USED FOR TRIANGLE VERTICES)
    0   NBSO -- INCLUDE CONTRIBUTION OF TOP BOUNDARY SOURCE OR UNIT NBSO ( 0 MEANS NO EFFECT)
    0   IA04 -- NUMBER OF ANGLES IN DOT QUADRATURE FOR TOP BOUNDARY SOURCE (0 MEANS NO EFFECT)
    1   ICOLL-- 0/1  NO EFFECT / DETECTOR(S) WITH CIRCULAR COLLIMATOR(S)
    0   IBOT -- 0/1  NO EFFECT / DETECTOR(S) THAT SEE BOTTOM SURFACE ONLY
```

Fig. B-2. Input parameters for a typical FALSTF calculation.

	AXII	ADJ. SOURCE	RADII	REG. FOR B.S.	QUAD. PTS.	QUAD. DIP.	RATL./ ZONE	TAPE IDS
1	-2.01000E 02	1.000000E 00	0		1.000000E 00	1.000000E 00	-1	
2	-2.003400E 02	1.000000E 00	2.540000E 00				-5	
3	-1.996000E 02	1.000000E 00	5.080000E 00				-13	
4	-1.990200E 02	1.000000E 00	7.620000E 00				-13	
5	-1.983600E 02	1.000000E 00	1.016000E 01				-13	
6	-1.977000E 02	1.000000E 00	1.270000E 01				-13	
7	-1.970400E 02	1.000000E 00	1.524000E 01				-13	
8	-1.963800E 02	1.000000E 00	1.778000E 01				-25	
9	-1.957200E 02	1.000000E 00	2.032000E 01				-17	
10	-1.950760E 02	1.000000E 00	2.286000E 01				-9	
11	-1.944320E 02	1.000000E 00	2.540000E 01				-9	
12	-1.937880E 02	1.000000E 00	2.794000E 01					
13	-1.931440E 02	1.000000E 00	3.048000E 01					
14	-1.925010E 02	1.000000E 00	3.302000E 01					
15	-1.918570E 02	1.000000E 00	3.556000E 01					
16	-1.912140E 02	1.000000E 00	3.810000E 01					
17	-1.905700E 02	1.000000E 00	4.064000E 01					
18	-1.899550E 02	1.000000E 00	4.318000E 01					
19	-1.895400E 02	1.000000E 00	4.572000E 01					
20	-1.890250E 02	1.000000E 00	4.826000E 01					
21	-1.885100E 02	1.000000E 00	5.080000E 01					
22	-1.879950E 02	1.000000E 00	5.334000E 01					
23	-1.874800E 02	1.000000E 00	5.588000E 01					
24	-1.869650E 02	1.000000E 00	5.842000E 01					
25	-1.864500E 02	1.000000E 00	6.096000E 01					
26	-1.859350E 02	1.000000E 00	6.350000E 01					
27	-1.854200E 02	1.000000E 00	6.604000E 01					
28	-1.851000E 02	1.000000E 00	6.858000E 01					
29	-1.848000E 02	1.000000E 00	7.112000E 01					
30	-1.837000E 02	1.000000E 00	7.366000E 01					
31	-1.827970E 02	1.000000E 00	7.620000E 01					
32	-1.818540E 02	1.000000E 00	7.874000E 01					
33	-1.809910E 02	1.000000E 00	8.128000E 01					
34	-1.800870E 02	1.000000E 00	8.382000E 01					
35	-1.791840E 02	1.000000E 00	8.636000E 01					
36	-1.782810E 02	1.000000E 00	8.890000E 01					
37	-1.773780E 02	1.000000E 00	9.144000E 01					
38	-1.764750E 02	1.000000E 00	9.398000E 01					
39	-1.755720E 02	1.000000E 00	9.652000E 01					
40	-1.746690E 02	1.000000E 00	9.906000E 01					
41	-1.737660E 02	1.000000E 00	1.016000E 02					
42	-1.728620E 02	1.000000E 00	1.041400E 02					
43	-1.719590E 02	1.000000E 00	1.066800E 02					
44	-1.710560E 02	1.000000E 00	1.092200E 02					
45	-1.701530E 02	1.000000E 00	1.117600E 02					
46	-1.692500E 02	1.000000E 00	1.143000E 02					
47	-1.683470E 02	1.000000E 00	1.168400E 02					
48	-1.674440E 02	1.000000E 00	1.193800E 02					
49	-1.665400E 02	1.000000E 00	1.219200E 02					
50	-1.656370E 02	1.000000E 00	1.244600E 02					
51	-1.647340E 02	1.000000E 00	1.270000E 02					
52	-1.638310E 02	1.000000E 00						
53	-1.629280E 02	1.000000E 00						
54	-1.620250E 02	1.000000E 00						
55	-1.611220E 02	1.000000E 00						
56	-1.599990E 02	1.000000E 00						
57	-1.586670E 02	1.000000E 00						
58	-1.573330E 02	1.000000E 00						
59	-1.560000E 02	1.000000E 00						
60	-1.546670E 02	1.000000E 00						
61	-1.533330E 02	1.000000E 00						
62	-1.520000E 02	1.000000E 00						
63	-1.506670E 02	1.000000E 00						
64		1.000000E 00						
65		1.000000E 00						
66		1.000000E 00						
67		1.000000E 00						
68		1.000000E 00						
69		1.000000E 00						
70		1.000000E 00						
71		1.000000E 00						
72		1.000000E 00						
73		1.000000E 00						
74		1.000000E 00						
75		1.000000E 00						
76		1.000000E 00						

Fig. B-2. Cont'd

	MIXTURE	COMPONENT	NO. DENSITY	X OF DET.	Y OF DET.	Z OF DET.	PULT./ACT.	REGION/ZONE
1				0	0	-2.111500E 02	1.000000E 00	1
2				3	0	-9.058000E 02		1
3				0	0	-1.664000E 01		1
4								1
5								1
6								1
7								1
8								1
9								1
10								0
11								0

	COLL. ANG.	X DET. AXIS	Y DET. AXIS	Z DET. AXIS
1	3.360000E-01	0	0	-2.010000E 02
2	9.620000E-01	0	0	-2.010000E 02
3	9.980000E-01	0	0	-2.010000E 02

ACTIVITY FACTORS

GRP. ACT. 1
1 1.667000E 01
GRP. 2 THRU GRP. 76 SAME AS ABOVE

← Converts from $(min^{-1} \cdot W^{-1})$ to $(s^{-1} \cdot kW^{-1})$

Fig. B-2. Cont'd